Stockholm University

Master Thesis

Degree Project in Geology 60 hp

U-Pb zircon geochronology of metasedimentary rocks and modern sands from southern Brooks Range, Alaska

Henrik Tarras



Stockholm 2019

Department of Geological Sciences
Stockholm University
SE-106 91 Stockholm

Table of contents

ABSTRACT 1
1 INTRODUCTION 1
2 BACKGROUND 2
2.1 Tectonic setting 2
2.2 Regional geology 2
2.3 The Brooks Range 3
2.4 Sample information 6
2.5 U-Pb geochronology 6
3 METHODS 7
3.1 Mechanical processing 7
3.2 Cathodoluminescence imaging 7
3.3 Laser-Ablation Inductively Coupled Plasma Mass Spectrometry 8
3.4 Data reduction 8
3.5 Data visualization 9
4 RESULTS 9
4.1 Modern river sands 9
4.2 Detrital rocks 12
4.3 Comparative databases 15
5 DISCUSSION 16
5.1 Age correlations and provenance of modern river sands 16
5.2 Age correlations for 15JT10 17
5.3 Regional/tectonic implications from 15JT10 17
5.4 Age correlations for 15JT11 19
5.5 Regional/tectonic implications from 15JT11 19
6 CONCLUSIONS 19
7 REFERENCES 21
APPENDIX A – Analytical results 25
APPENDIX B – Concordia diagrams 46
APPENDIX C – Calculated sample ages 55

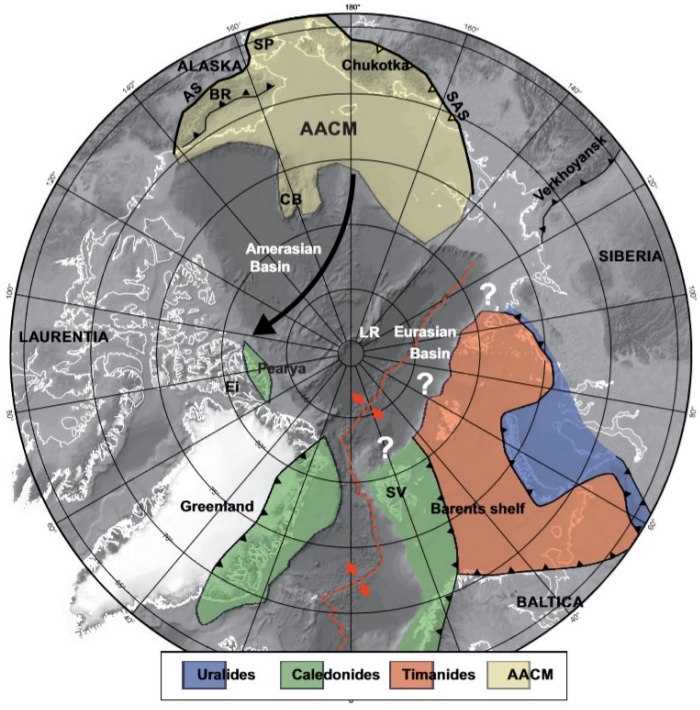
ABSTRACT

The Paleozoic to Mesozoic tectonic history of the Arctic is debated. The 'rotation' model suggests that the Arctic Alaska-Chukotka microplate (AACM) rotated counter-clockwise during the Mesozoic. This model predicts that, prior to rotation, the Timanian orogen extended from northern Europe (modern position) across the AACM. Thus, U-Pb zircon ages associated with Timanian orogenesis should be present in the Brooks Range of northern Alaska. While evidence for the occurrence of Timanian-aged zircons exist in the western Brooks Range, further geochronological studies across this vast area are needed, especially in the east. To address the shortage of data from the eastern Brooks Range and test this hypothesis, laser-ablation inductively coupled plasma mass spectrometry (LA-ICP-MS) U-Pb ages and cathodoluminescence (CL) images of zircons from *in-situ* detrital rocks samples along the North Fork of the Koyukuk River and from modern river sands along the Alatna River are presented. Results show that Timanian-age grains, albeit some with indications of metamorphic alteration, are present in detrital rocks as far east as the North Fork Koyukuk River, thus agreeing with the 'rotation' model of the AACM.

1 INTRODUCTION

Studies of the Arctic Alaska-Chukotka microplate (AACM) suggest counter-clockwise rotation from the modern-day Canadian Arctic margin (e.g. Grantz et al., 1990), therefore understanding the geochronology, paleogeography, stratigraphy and extent of orogenic signatures within this microplate is an important part of spatially and temporally linking together different crustal fragments now found distributed in the Arctic region. In this regard, the tectonic evolution of the AACM for the Paleozoic and its paleogeography during the Mesozoic is unresolved (Robinson et al., 2019).

According to some models (e.g.- Amato et al., 2009), the AACM should contain lithologies from the Timanian (Fig. 1), Caledonian and Uralian orogens and recent studies from Alaska's Brooks Range (Hoiland et al., 2017; Strauss et al., 2017; Moore et al., 2015; Till et al., 2014) provide some spatial constraints on these structures in the eastern parts of the AACM. Robinson et al. (2019) advocate the need for further high-quality geochronological data to unravel the complexities of these features in the Brooks Range.



U-Pb zircon geochronology reaches its full potential for determining

Fig. 1. Tectonic reconstruction of Arctic fragments and orogenies from Robinson et al. (2019). Rotational direction is represented by the black arrow. AACM – Arctic-Alaska Chukotka microplate; AS – Angayucham Suture; BR – Brooks Range: EI – Ellesmere Island; LR – Lomonosov Ridge; CB – Chukchi Borderland: SAS – South Anyui Suture; SV – Svalbard. Note the structural fabric of the Caledonian, Uralian, and Timanian orogens strike northwards across the Arctic.)

minimum and maximum ages of (meta)sedimentary strata when in-situ correlation to igneous rocks of known ages is possible (Fedo et al., 2003). This is facilitated by analyzing the uranium and lead isotopes in each zircon grain. Since the proportions of these depend on radioactive decay, an age can be determined. Uranium-lead ages of zircon from modern river sands can also aid in unraveling the geological history of a region by tracing the provenance of detritus to rocks of known ages (e.g. Campbell, 2005; Iizuka et al., 2013).

This study is intented to:

(1) test the correlations between known ages present in Brooks Range and ages in detrital rocks and modern river sands from this study;
(2) complement *in-situ* geochronological investigations of the Brooks Range by providing U-Pb age distributions of detrital zircons from modern sands along the Alatna river;
(3) investigate the presence and character of Timanian age zircons east of John River to constrain the eastward extent of Timanian input.

2 BACKGROUND

2.1 Tectonic setting

The Arctic Alaska part of the AACM has been identified to be a part of the North American Cordillera accretionary system (Miller et al., 2011; Beranek et al., 2013) which contains both allocthonous and autochtonous terranes (Robinson et al., 2019). Stratigraphic, geochronological and geophysical findings have been integrated into a 'rotation' model (Fig. 1) in which the AACM rifted from the Canadian Arctic Islands during the opening of the Amerasian basin in Late Jurassic to Early Cretaceous and thereafter rotated counterclockwise to its current position (Grantz et al., 1990; Shepherd et al., 2013; Gottlieb et al., 2014). According to this model, the present north American part of the AACM would have been closer to the Eurasian orogens (Pease, 2011) and zircon geochronology suggests a connection between the Canadian Arctic and eastern Arctic Alaska, as well as between western Alaska and Chukotka, and the Ural-Taimyr regions of Siberia before the opening of the Arctic Ocean in the Cretaceous (Miller et al., 2006; Amato et al., 2009; Miller at al., 2010, 2011; Till, 2016). One outstanding question is the spatial extent of the Timanian orogen in the Arctic region, which is important as the rotational model implies that the Brooks Range should contain Timanian elements, even though these signatures would be largely overprinted by Late Jurassic to Cenozoic deformation (Pease, 2011; Robinson et al., 2019). To date Timanian geochemical signatures in the eastern Brooks Range have been spatially constrained to east of the John River (Hoiland et al., 2017).

2.2 Regional geology

Arctic Alaska encompasses the east-west striking Brooks Range, positioned between ophiolites of the Angayucham terrane to the south and the North Slope subterrane to the north; to the west lies the Seward Peninsula (Fig. 2) (Moore et al., 1994). An Ellesmerian (Paleozoic) passive margin sequence overlies the North Slope subterrane and a pre-Mississippian angular unconformity occurs along the northern side of the Brooks Range (Robinson et al., 2019). The strata beneath the unconformity are less studied, but some of

these rocks are accessible as thrust sheets in the Brooks Range. They include Cambrian to Devonian metasedimentary and metavolcanic rocks (Oldow, 1987) and from Hf isotopic signatures have been argued to represent accreted island arc rocks (Moore, 1987; Julian & Oldow, 1998). According to Strauss et al. (2017) these rocks exhibit U-Pb zircon age peaks of 557 Ma (Ediacaran) to 410 Ma (Early Devonian), as well as lesser age peaks at 540, 477 and 441 Ma, and may correspond to the possible suture between non-Laurentian units of Arctic Alaska and the Laurentian units of the North Slope subterrane. In the Seward Peninsula, Neoproterozoic to early Paleozoic metasediments have detrital U-Pb zircon ages of 700-540 Ma, which is considered a Timanian signature (Amato et al., 2009, Robinson et al., 2019).

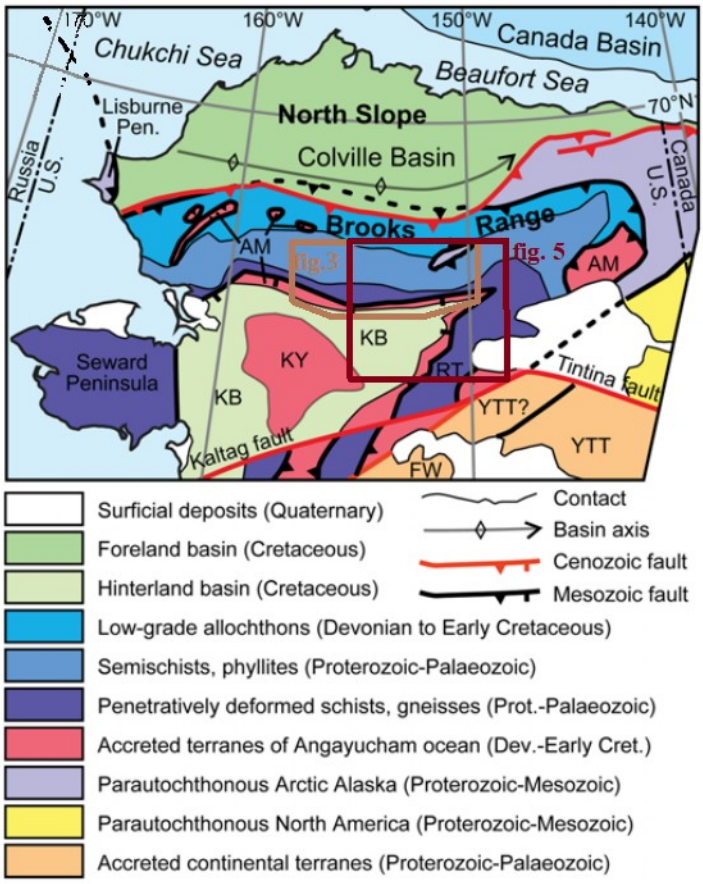


Fig. 2. Terranes of Arctic Alaska, modified from Hoiland et al. (2018). Brown square denotes the detrital rock study area and surrounding lithologies in the Wiseman quadrangle (Fig. 3), red square denotes area of sub-basins that drain to Allakaket (Fig. 5).

2.3 The Brooks Range

The bedrock in the Brooks Range is made of units which are related by their east-west trending structures, metamorphic signature, and stratigraphy (Robinson et al., 2019). The Doonerak antiform exposes the aforementioned pre-Mississippian unconformity in the northern Brooks Range (Dillon et al., 1986) and encompasses parts of the southern Central Belt and Schist Belt (Fig. 3). This antiform incorporates the allochthonous Endicott Mountains thrust sheets that contain the Endicott group (Moore et al., 1994), which is a section of Early Devonian clastic rocks suggested to originally have been deposited further south than its present position and later thrust over the Doonerak antiform (Oldow et al., 1987); it includes the Kanayut conglomerate, Hunt Fork shale and Noatak sandstone (Fig. 4). The Central Belt lies south of the Doonerak antiform (Fig. 3), which according to Robinson et al. (2019) is not well known in regards to age and tectonic origin. Cambrian to Middle Devonian rocks belonging to this terrane have been found in eastern Alaska that bear a resemblance to rocks in the western Brooks Range, Seward Peninsula and even as far west as the Russian Chukotka Peninsula (Robinson et al., 2019). The Schist belt lies on the southern flank of Brooks Range, south of the Central Belt (Fig. 3), and contains pre-mid-Palaeozoic strata characterized by high-strain penetrative deformation (Christiansen & Snee, 1994; Little et al., 1994). Normal faults put this unit in contact with the Greywacke-phyllite Belt which overlies it structurally (e.g. Till et al., 2016; Hoiland et al., 2017). Further south lies the oceanic Angayucham terrane and the Yukon-Koyukuk Basin (Fig. 3).

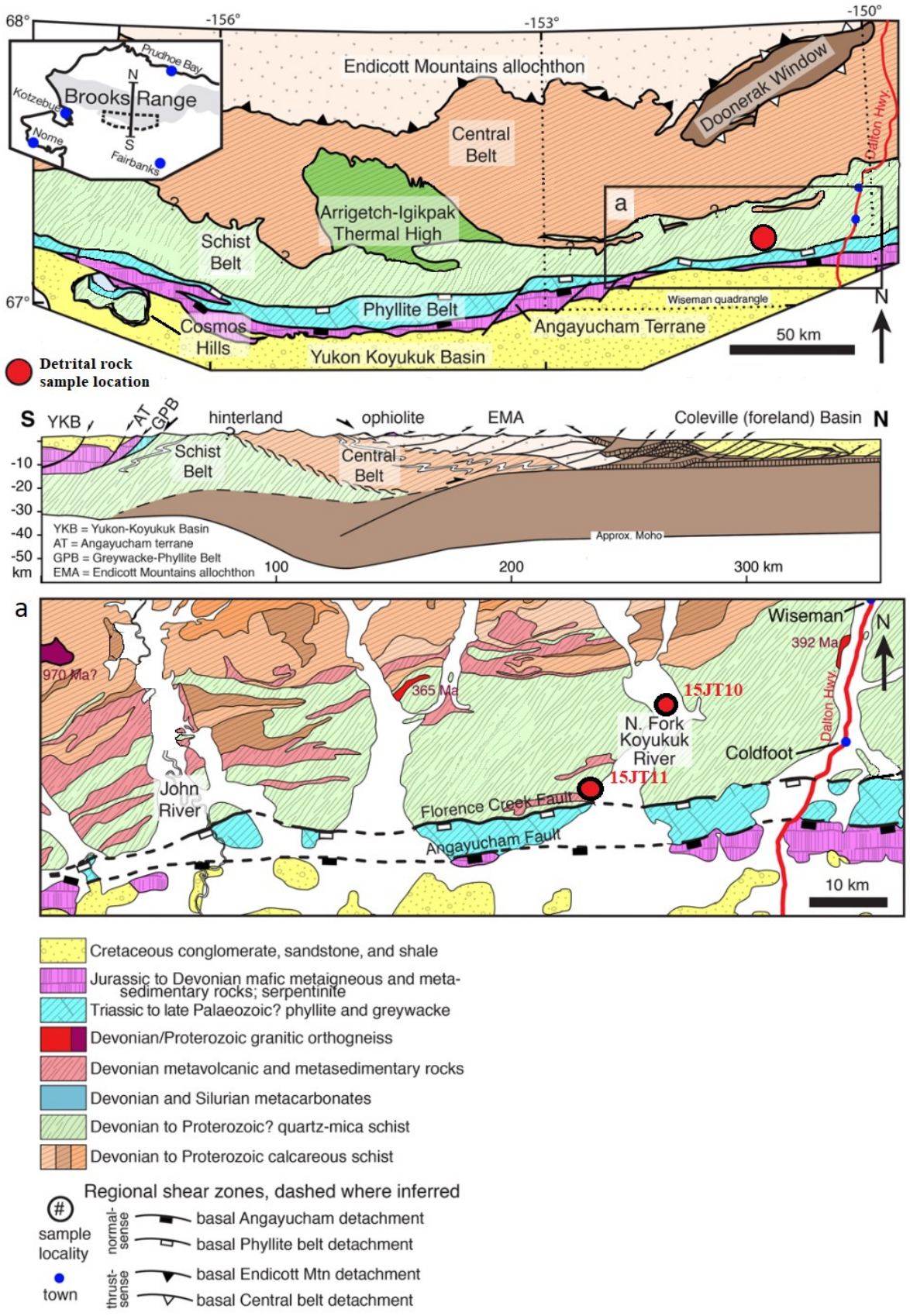


Fig. 3. Regional geological map of Arctic Alaska supplemented with structural relations along a north-south transect and a local map of detrital samples and their surrounding terranes. Modified from Hoiland et al. (2018).

In the central Brooks Range,sequences representing different metamorphic events with ages ranging from Neoproterozoic to Late Devonian (Dillon et al., 1986) have been interleaved during subsequent folding, faulting and low-grade metamorphism (Robinson et al., 2019). These can be subdivided into three major groups with regards to provenance and maximum depositional age: i) Mesoproterozoic provenance with a Neoproterozoic maximum depositional age, ii) Ordovician-Silurian provenance with an Early Devonian maximum depositional age, and iii) Paleozoic (with minor Proterozoic) provenance with a Middle Devonian maximum depositional age. Age peaks of 700-550 Ma are likely of Timanian origin, but may have been sedimentologically recycled (Robinson et al., 2019).

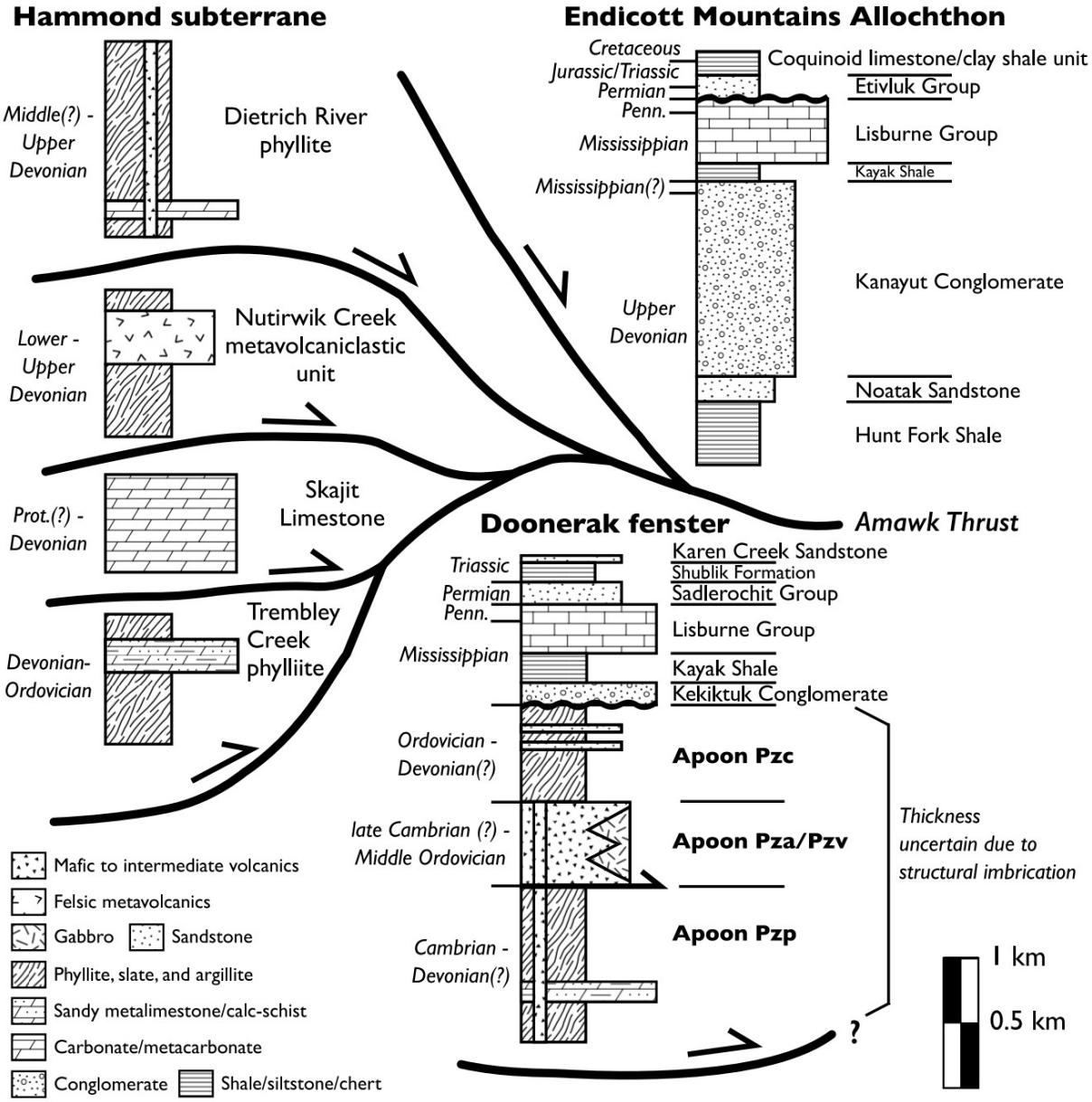


Fig. 4. Simplified stratigraphy of central Brooks Range by Strauss et al. (2017). The Endicott group, which contains the Kanayut conglomerate, is seen located on the north side of the Doonerak fenster.

2.4 Sample information

In-situ detrital rock samples were collected from Schist Belt lithologies near the North Fork of the Koyukuk River (Figs. 2, 3; Table 1) and modern river sands were sampled along the Alatna River and at Allakaket (Figs. 2, 5; Table 1).

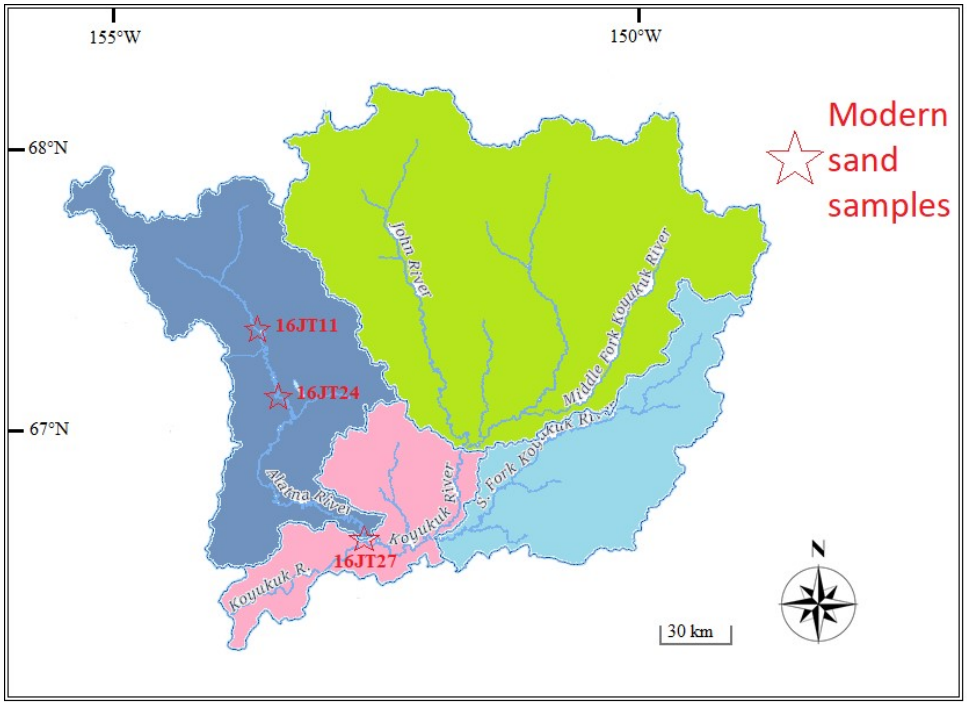


Fig. 5. The four sub-basins that drain to Allakaket, with sample locations of modern sands. Note: 16JT27 is the only sample with input from all four catchments. Retrieved and modified from: https://viewer.nationalmap.gov/advanced-viewer, 2019-03-10, The National Map, USGS.

Table 1. Sample locations, lithology and inferred stratigraphy.

Sample	Lithology	N. Latitude	W. Longitude	Stratigraphy/Location	Unit
15JT10	Conglomerate	67.297812	-150.689749	Endicott group	Kanayut Conglomerate
15JT11	Quartzite	67.210228	-150.868145	Apoon assemblage(?)	Pzp(?)
16JT11	River sand	67.365027	-153.651948	Alatna river	
16JT24	River sand	67.091952	-153.333487	Alatna river	
16JT27	River sand	66.563610	-152.656980	Allakaket	

Note: Pzp - dominantly fine-grained Paleozoic phyllite and slate, with minor calcareous and volcaniclastic strata.

2.5 U-Pb geochronology

The radiogenic decay of uranium and thorium to lead follows three schemes which make up the U-Th-Pb system (White, 2015):

1. $^{238}U \rightarrow {}^{234}U \rightarrow {}^{206}Pb\ (\lambda = 1.5512 \times 10^{-10}\alpha^{-1})$
2. $^{235}U \rightarrow {}^{207}Pb\ (\lambda = 9.8485 \times 10^{-10}\alpha^{-1})$
3. $^{232}\mathrm{Th} \rightarrow {}^{208}Pb\ (\lambda = 4.9475 \times 10^{-11}\alpha^{-1})$

where λ = half-life & α = decay constant.

Assuming homogeneity of isotope ratios after closure and that no parent or daughter isotopes have been added or removed (due to natural processes such as metamorphism or hydrothermal activity), the time taken for a daughter isotope to accumulate can be calculated for each individual decay scheme, a technique called *isochron* dating (Faure, 1986). Holding the previous assumptions to be true, the time-dependent evolution of the ratios of parent-daughter isotopes between the two uranium isochrons can be expressed as a *concordia curve*, and isochron ages that plot on this curve are said to be concordant (Faure, 1986). The uranogenic ratios from an analysis can be plotted over such a curve on a c*oncordia* diagram as *error ellipses*, their placement based on the weighted mean and the dimensions corresponding to errors (absolute and error correlation) (Faure, 1986). Combining the three uranogenic ratios of involved analyses yields a *concordia age,* which can yield very accurate age measurement (Ludwig, 1998). Since the two uranium isotopes have different half-lives and lead isotopes do not fractionate upon lead loss, disequilibrium events can alter the ratio between the isochron ages which causes their points of intersection to plot away from the concordia curve (Faure, 1986). This can also be caused by the internal migration of lead in zircon (Mezger and Krogstad, 1997; Cherniak and Watson, 2000). The degree of this offset is labeled *discordance*, and is often calculated as a percentage difference between the $^{206}Pb/^{238}U$ and $^{207}Pb/^{206}Pb$ or $^{206}Pb/^{238}U$ and $^{207}Pb/^{235}U$ ages (Spencer, 2016; Gehrels, 2014).

3 METHODS

3.1 Mechanical processing

A total of 34 samples were processed, whereof 29 (meta)sedimentary rocks did not yield zircon. Of the remaining five samples from which zircon was extracted, two were from metasedimentary outcrops (15JT10 and 15JT11) and three modern river sands (16JT11, 16JT24 and 16JT27). All *in-situ* rock samples were crushed and milled to sand size and the modern river sand samples were already the desired grain size. Heavy mineral fractions from all samples were extracted by means of density separation using a Wilfley table, and magnetic minerals of the heavy fraction were removed using magnet separation. The remaining high-density grains were soaked in ethanol and the zircons placed on a grain mount by hand-picking them under a binocular microscope.

3.2 Cathodoluminescence imaging

The grain mounts of the five samples that yielded zircon were embedded in epoxy and polished in order to expose the internal structure of the zircons at the Museum of Natural History, Stockholm. They were coated with gold to avoid luminescence quenching due to charging of particles (Habermann et al., 2000) prior to imaging with an ESEM FEI Quanta FEG 650 SEM with a cathodoluminescence (CL) sensor operating at a beam current of 15.0 kV and magnification of 150x. The emission from cathodoluminescence largely depends on crystallographic and chemical factors, thus resolving the internal textures and inclusions present in a mineral (Gucsik, 2009) and facilitating analytical location selection for LA-ICP-MS analyses. Classification of zircons was made based on the zircon CL features described in Corfu et al. (2003). CL images of all analyzed grains are available upon request to the author.

3.3 Laser-Ablation Inductively Coupled Plasma Mass Spectrometry

Mass spectrometry was performed using a New Wave Research-193 Excimer Laser coupled to a Thermo XSeriesTM II quadropole mass spectrometer at the Department of Geological Sciences, Stockholm University. The analytical conditions are given in table 2.

Table 2. LA-ICP-MS analytical conditions for all analyses in this study.

	Experiment 1	**Experiment 2**	**Experiment 3**	**Experiment 4**	**Experiment 5**	**Experiment 6**
Cones	REE, Zrn	REE, Zrn	REE, Zrn	REE, Zrn	REE, Zrn	REE, Zrn
Spot size	25 µm	25 µm	25 µm	25 µm	25 µm	25 µm
Energy density	7-8 J/cm2	7-7.4 J/cm2	6.7 J/cm2	7.1 J/cm2	6.6 J/cm2	7.5 J/cm2
Rep. rate	10 Hz	10 Hz	10 Hz	10 Hz	10 Hz	10 Hz
External standard	Plešovice	Plešovice	Plešovice	Plešovice	Plešovice	Plešovice
2nd standard	FC-5z	FC-5z	FC-5z	FC-5z	FC-5z	FC-5z
Nebulizer flow (Ar)	0.93 l/min	0.93 l/min	0.93 l/min	0.93 l/min	0.93 l/min	0.93 l/min
Aux	0.75	0.75	0.75	0.75	0.75	0.75
Cooling gas flow	13.0 l/min	13.0 l/min	13.0 l/min	13.0 l/min	13.0 l/min	13.0 l/min
Energy output	56%	56%	56%	56%	56%	56%
Fluency	7.6% J/cm^2	7.7 J/cm^2	7.7 J/cm2	7.7 J/cm^2	7.6 J/cm^2	6.65 J/cm^2

Vermeesch (2004) recommended 117 analyses for a detrital population to ensure that all provenance components present at the 5% level would have a 95% probability of being detected. To enhance the odds of achieving 117 acceptable analyses, 150 grains from each sample were analysed, and the 25 µm laser analytical locations were placed where there were no cracks or inclusions based on the cathodoluminescence images; a single exception was sample 16JT24 from which only 72 grains were analysed due to erratic behaviour of the LA-ICP-MS that was unresolved within the timeframe of the project.

The international zircon standard Plešovice (Sláma et al., 2008) was used as the external standard to tune the instrument, correct for downhole fractionation, baseline subtraction and instrument drift during data reduction. To ensure correct instrument behavior, the Duluth gabbro zircon (FC-5z) was employed as an 'internal' standard (Paces & Miller, 1993). A sample-standard bracketing scheme was used in which 4 Plešovice and 2 FC-5z initiated the run, followed by 12 unknowns and 1 Plešovice and 1 FC-5z, and finished with 4 Plešovice and 2 FC-5z.

3.4 Data reduction

The data was processed using Iolite on the IGOR Pro platform (Paton et al., 2011), which enables real-time visualization of time-resolved mass spectrometric data using the VizualAge (Petrus & Kamber, 2012) data reduction scheme. The latter performs downhole fractionation and long-term drift corrections, and enables on-demand visualization of ICP integrations and the selection of the most robust data output, e.g.- U-Pb data expressed as error ellipses (2σ) for the $^{206}Pb/^{238}U$ and $^{207}Pb/^{235}U$ ratios (Petrus & Kamber, 2012). The signal interval chosen for the integrations is adjusted to optimize concordant data (without

Pb-loss) and to encompass at least 10 seconds of data acquisition. The analyses which fulfilled this criteria were further filtered in Excel, retaining those with <10% discordance, <500 ^{204}Pb counts-per-second, a U/Th ratio <10, U (ppm) < 1500 and a 2σ mean age error <10%. Results of all analyses are available in Appendix A. Post-filtering, a ^{207}Pb/^{206}Pb or ^{206}Pb/^{238}U isochron age was chosen to represent the final age of each analysis. Because recent Pb-loss does not affect a Pb-Pb ratio as much as a U-Pb ratio (Faure, 1986), a cutoff was set at 1.2 Ga. The ^{207}Pb/^{206}Pb age was used for analyses >1.2 Ga and the ^{206}Pb/^{238}U age was used for analyses >1.2 Ga.

3.5 Data visualization

All results were plotted in Excel 2010 using Isoplot v. 4.1 (Ludwig, 2003), a macro 'add-in' designed for calculating and plotting radiogenic-isotope data for geochronological use. To visualize the age distributions, the acceptable analyses for each sample were plotted on separate histograms, which is a useful way to show age distributions of detrital zircon populations including those from modern river samples (e.g. Fielding et al., 2017; Campbell et al., 2005; Iizuka et al., 2013). The histograms were combined with probability density plots (PDP) which indicate the relative probablility of an age to occur within the dataset (Vermeesch, 2012). The adoption of kernel density estimation (KDE) plots within the field of geochronology is recommended by Vermeesch (2012), yet Robinson et al. (2019) states that most datasets from the Arctic use PDP, thus making the latter more compatible for comparisons to regional datasets. Consequently, age peaks from histograms were determined following the method of Robinson et al. (2019), i.e.- by taking the weighted average of ages in each peak and triming the data until an acceptable value for the mean square weighted deviation was achieved (MWSD $\leq$ 2). A uniform bin size of 35 Ma was used for all histograms. Additionally, concordia diagrams were constructed and are presented in Appendix B.

4 RESULTS

4.1 Modern river sands

Sample 16JT11. This sample represents the furthest upstream sample of the Alatna river (Fig. 5). Its zircons have a predominantly subhedral to anhedral crystal habit, with only three euhedral grains and zoning, when present, ranges from undeformed oscillatory to interrupted by recrystallization textures (Fig. 6). A total of 150 grains were analysed and 104 analyses were acceptable after the application of filtering criteria. An early- to mid-Devonian age peak of 405 ± 6 Ma (2σ, MSWD = 1.9, n=9) (Fig. 7; Appendix C) is evident and comprises 8.6% of the sample. Five of these grains feature oscillatory zoning and are 100-150 µm in size; one of these is an anhedral grain with a presumed metamorphic homogenous overgrowth around it (Fig. 6; Corfu et al., 2003). The remaining four grains in this age group range in size from 75 to 250 µm and are mainly subhedral (there is one anhedral grain) with a bright homogenous texture attributed to metamorphic alteration (Fig. 6; Corfu et al., 2003).

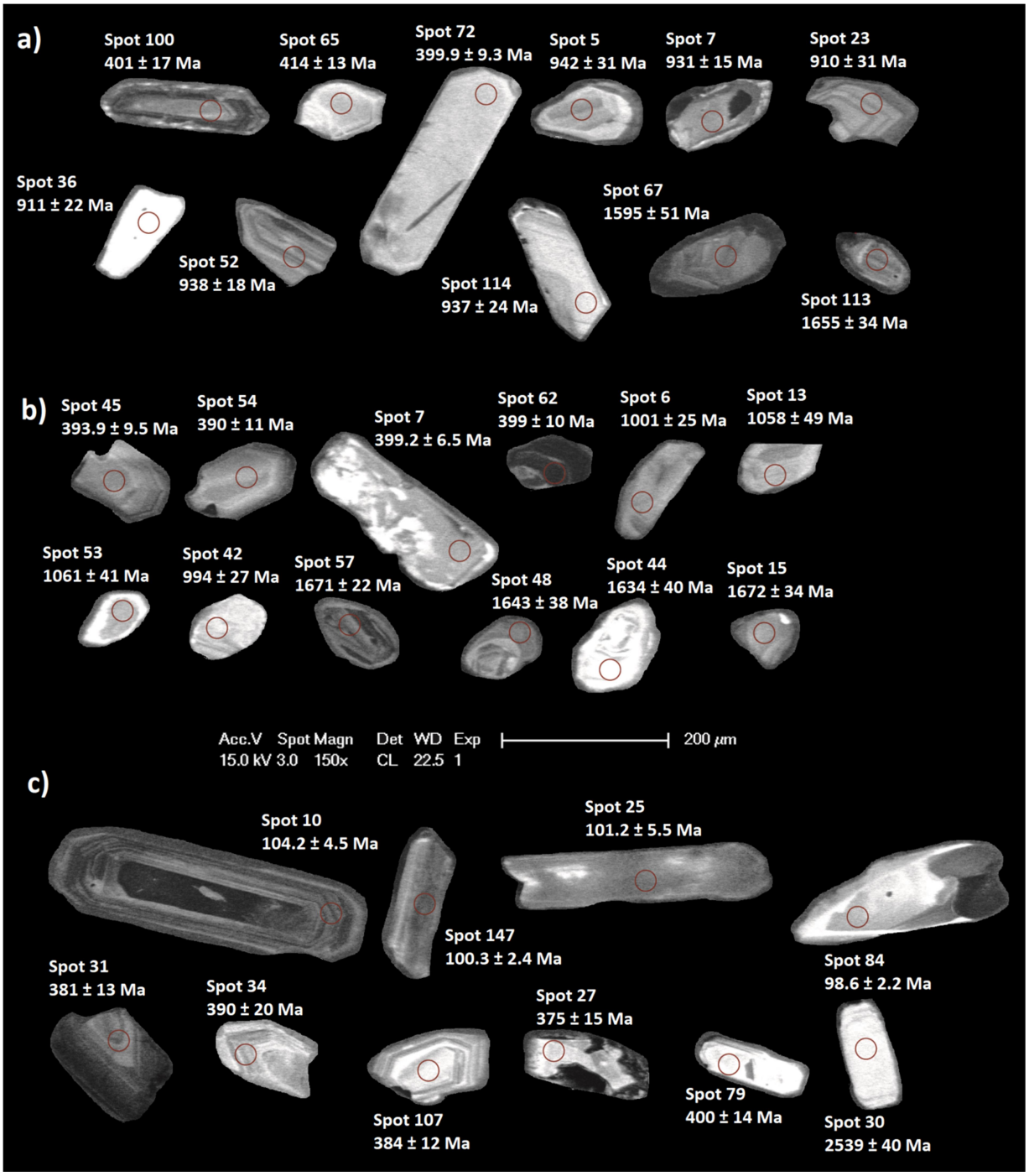


Fig. 6. Representative cathodoluminescence images of zircons from modern sand samples with a) zircons from sample 16JT11, b) zircons from sample 16JT24 and c) zircons from sample 16JT27.

The second largest peak is late Proterozoic, with a mean age of 938 ± 10 Ma (2σ, MSWD = 1.8, n=11) (Fig. 7; Appendix C), representing 10.6% of the accepted analyses. Three of these grains are igneous and subhedral, with lengths between 100–200 µm; they feature seemingly undisturbed oscillatory zones, with two having oscillatory bands <5 µm and 5-10 µm wide respectively and the third grain has broader, more diffuse zoning. Homogeneity from metamorphic alteration occurs in this age group (Fig. 6; Corfu et al., 2003).

The third most dominant age-group yields an Early- to Mid-Proterozoic wtd. mean age of c. 1620±23 Ma (2σ, MSWD = 1.8, n = 6) (Fig. 7; Appendix C) constituting 5.8% of the sample.

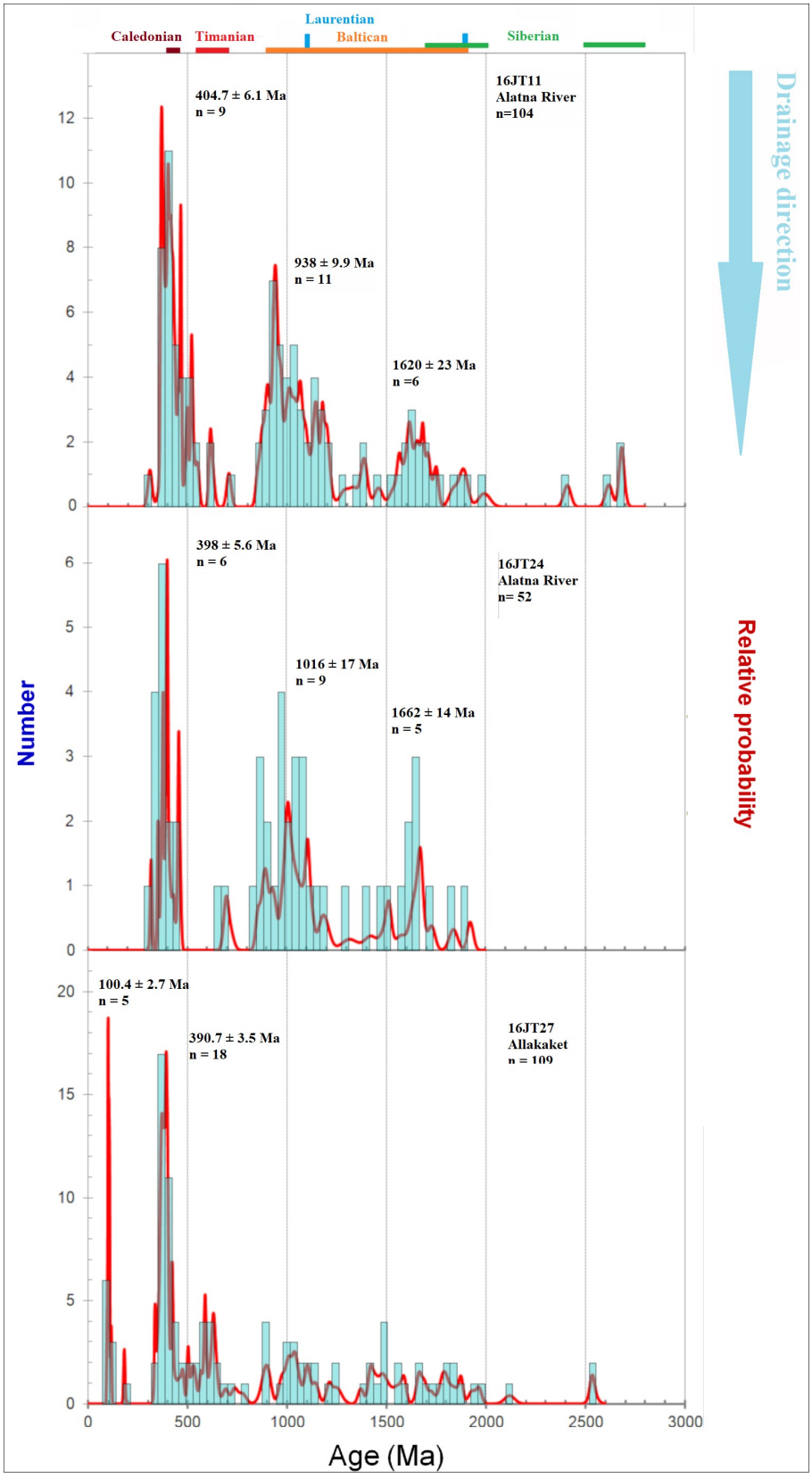


Fig. 7. Age histograms of modern river sands. Bin sizes are 35 Ma and errors 2σ.

A single c. 150 µm anhedral zircon in this group exhibits an oscillatory zonation with no transgressive textures while two anhedral grains, c. 100 and 150 µm in length show signs of recrystallization (Fig. 6; Corfu et al., 2003).

The remaining 3.8% (n=4) of the analyses in this sample yield ages older than 2 Ga from relatively large crystals (c. 100-150 µm) (Fig. 6). Three anhedral grains have >2.5 Ga (Archean) ages and two of these exhibit diffuse oscillatory zoning, while the other is homogenous (Fig. 6).

Sample 16JT24. This is the southernmost sample along the Alatna river. None of the zircon grains are euhedral and 15.5% (n=11) are subhedral, and the remainder are anhedral (Fig. 6). There are indications of alteration in as much as 32% of the grains, such as overgrowths, inclusions, and in one grain a spongy texture which can be a sign of hydrothermal alteration, but no metamictisation is visible and the remaining grains (26.7%, n=19) are igneous with no signs of alteration (Fig. 6). Of the 71 analyses, 52 are of acceptable quality after the application of filtering criteria. A major early- to mid-Devonian

peak of c. 398 ± 6 Ma (2σ, MSWD = 1.3, n=6) (Fig. 7; Appendix C) is made up of 11.5% of the sample. Two 125 µm grains are igneous, one being subhedral with <5 µm oscillatory bands and was analysed in the interior portion, while the other is anhedral with a more faint, dark oscillatory zonation (Fig. 6). One 175 µm subhedral zircon shows signs of metamorphic alteration as evident by irregular homogenous zones and grain boundary alteration (Fig. 6; Corfu et al., 2003).

The second most prominent age peak yields a late Proterozoic wtd. mean age of c. 1016 ± 17 Ma (2σ, MSWD=1.9, n=9) (Fig. 7, Appendix C) based on 17.3% of the analyses. Two igneous grains are present in this age group, a subhedral 125 µm zircon with <5 µm oscillatory bands and a 150 µm anhedral grain with slightly less discernible growth stages (Fig. 6). Seven grains between 100-150 µm in size are interpreted as having experienced postmagmatic recrystallization or low-grade metamorphism based on interrupted zoning and/or inclusions (Fig. 6).

The oldest calculated age population has an early- to mid-Proterozoic wtd. mean age of c. 1662 ± 14 Ma (2σ, MSWD = 1.02, n=5) (Fig. 7, Appendix C) and represents 9.6% of analyses. Three grains in this group are interpreted as igneous on the basis of having a faint but undeformed oscillatory growth-zoning; one grain is subhedral and 100 µm long, while the others are smaller (75 µm in length) and anhedral (Fig. 6). Two grains 125 µm and 100 µm long are metamorphic with homogenous or irregular, interrupted textures (Fig. 6; Corfu et al., 2003).

Sample 16JT27. This sample is from the Allakaket river and is the only modern river sample draining all sub-basins. Aside from one euhedral igneous grain, this sample has 65% anhedral grains (n=97), 35% subhedral grains (n=52) and CL imaging indicates that 56 grains (37%) have signs of post-magmatic recrystallization such as patches of local recrystallization over (in some grains) intact oscillatory zones (Fig. 6; Corfu et al., 2003). After application of the data filtering criteria, 109 of 150 analyses are of acceptable quality. The youngest population has a mid-Cretaceous (Cenomanian) mean age of c. 100 ± 3 Ma (2σ, MSWD = 1.9, n=5) (Fig. 7; Appendix C), constituting c. 5% of the sample. One large (c. 375 µm) subhedral igneous grain is present which has <5 µm magmatic oscillatory growth-zoning and four analyzed zircons c. 100-250 µm in length are metamorphic, as evident by anhedral crystal habit and entirely homogenous or irregular textures in CL (Fig. 6; Corfu et al., 2003).

A mid-Devonian peak at 391 ± 4 Ma (2σ, MSWD = 1.5, n=18) (Fig. 7, Appendix C) was derived from 16.5% of the analyses. This age group contains two igneous grains c. 100 µm in size, featuring well-defined oscillatory growth-zoning with bands up to 10 µm wide (Fig. 6; Corfu et al., 2003). Remaining grains grains are metamorphic based on their bright homogenous or very irregular textures (Corfu et al., 2003) and anhedral habit, with sizes 75-200 µm (Fig. 6). Chronologically unrelated to this age population is one bleached subhedral grain which yields a late Archean age of 2539 ± 40 Ma (2σ) in the core (Fig. 6).

4.2 Detrital rocks

Sample 15JT10. This *in-situ* sample is from an outcrop exposed along the North Fork of the Koyukuk River and is the northernmost detrital rock sample in this study (Fig. 3). It is thought to represent the Kanayut Conglomerate, which is part of the Endicott Group. The zircon

grains from this sample are predominantly anhedral (84%) and the remainder are subhedral and 17 grains show signs of metamorphic alteration (Fig. 8). After application of filtering criteria, 110/149 analyses were of acceptable quality. A major early- to mid-Devonian age population includes 16% of the analyses and yields a mean age of c. 400 ± 3 Ma (MSWD = 2.0, n=18) (Fig. 9; Appendix C). Eight of these analyses are from igneous grains between 100 – 200 µm in size and generally have undisturbed, regular magmatic growth-zones of 5-10 µm width and is made up of three subhedral grains and five anhedral ones (Fig. 8). The analyses were performed on the outer portion of three grains and in the core of another, while the other four analyses were placed in mixed regions. Within the age group, nine other grains are anhedral and metamorphic, varying in size from c. 75-175 µm (Fig. 8).

Zircons older than 500 Ma constitute 16% of the sample (n=18/110). These analyses yield ages too diverse to produce a reliable mean age. The oldest anhedral, 100 µm long crystal is Archean, 2706 ± 56 Ma (2σ), but its cathodoluminescence has the bright, bleached appearance which is typical of metamorphic alteration (Fig. 8; Corfu et al., 2003). The oldest igneous grain is dated at 2694 ± 20 Ma and is c. 125 µm and subhedral with c. 5-10 µm-wide oscillatory growth-zones (Fig. 8).

The majority of the analysed zircons (n=76/110) are younger than 500 Ma and close to the observed Devonian age peak (Fig. 9), but their ages are too disparate to generate a well-constrained mean age (e.g., to achieve a low MSWD). Their presence nevertheless indicates a strong Devonian to early Carboniferous (Mississippian) signature. The maximum depositional age of c. 365 ± 2 (2σ) (Fig. 9; Addendum C) in this sample is from the weighted average of 20 of the 25 youngest grains since the five youngest analyses suggest Pb-loss as evident by a younging of ages (Fig. 10).

Sample 15JT11. This sample is also from an in-situ outcrop exposed along the North Fork of the Koyukuk River (Fig. 3). It is thought to represent a quartzite from the Pzp unit of the Apoon assemblage. Seven zircons are euhedral and seventy-two are subhedral (Fig. 8).

Of the 150 grains analysed, 129 were of acceptable quality. Of the 129 analyses, 14% combine to yield an early- to mid-Devonian age peak of c. 400 ± 3 Ma (MSWD = 1.9, n=18) (Fig. 9, Appendix C). Nine zircons in this age group are igneous and subhedral to anhedral, sizing between 100 and 175 µm with clearly defined oscillatory bands of both <5 µm and c. 5-10 µm width depending on the grain, other grains feature patchy textures indicating post-magmatic recrystallization (Fig. 8; Corfu et al., 2003).

Analyses older than 500 Ma make up 29% of the sample (n=38), with the two oldest grains being 2324 ± 19 and 2404 ± 42 Ma (2σ) (Archean). Both of these are anhedral, c. 80-150 µm in length, and exhibit local recrystallization with patchy zoning (Fig. 8). Geochronologically, there is a gap of c. 500 m.y. between the Archean grains and the next oldest grain of 1816 ± 32 Ma (2σ). Thirteen analyses are present in a broad age range from 909 to 1143 Ma (2σ) (Neoproterozoic), while another continuous band of fifteen analyses range in age from 1353 to 1653 Ma (2σ) (Mesoproterozoic).

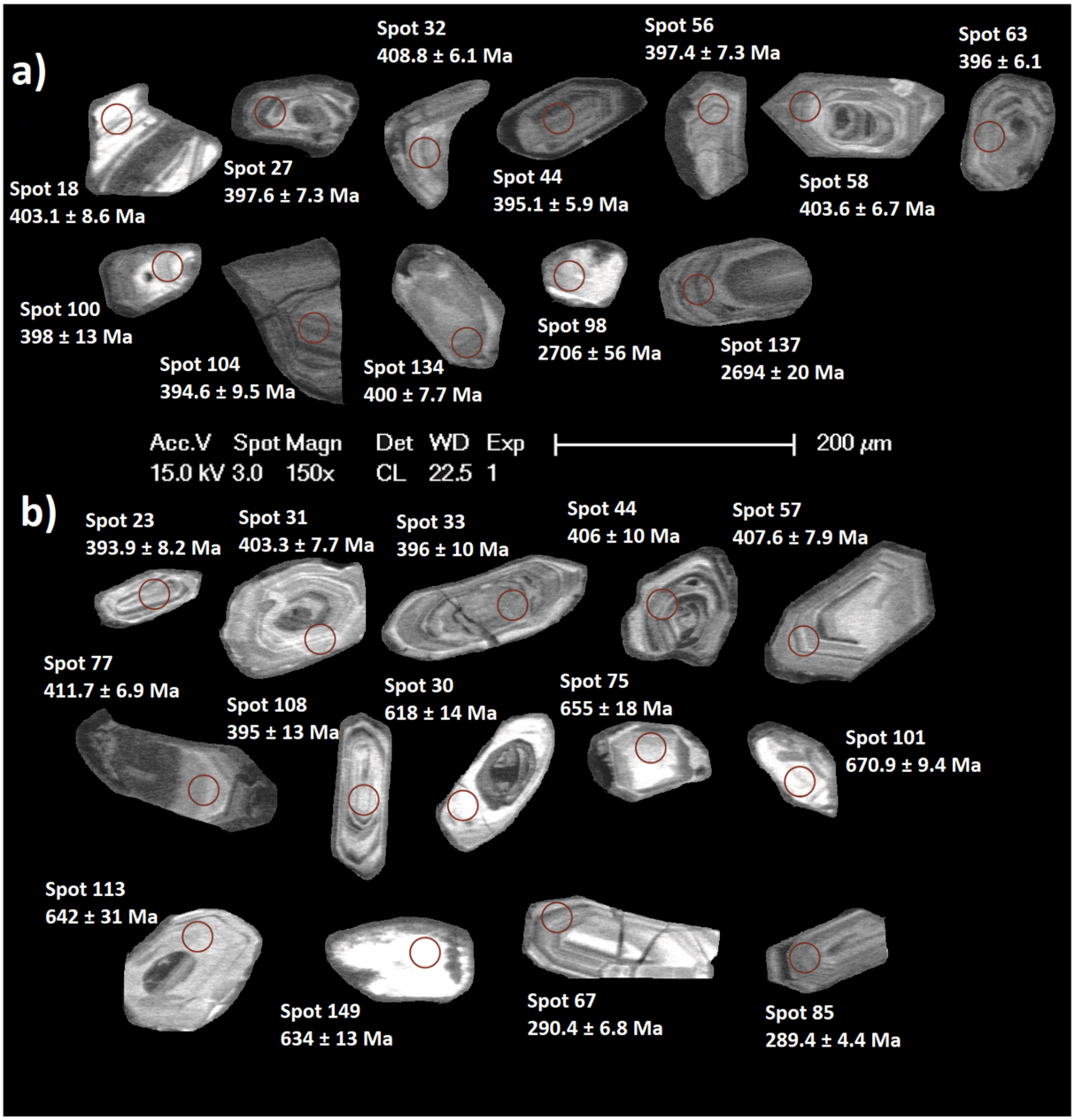


Fig. 8. Representative cathodoluminescence images of zircons from detrital rock samples from North Fork Koyukuk River with a) zircons from sample 15JT10 and b) zircons from sample 15JT11.

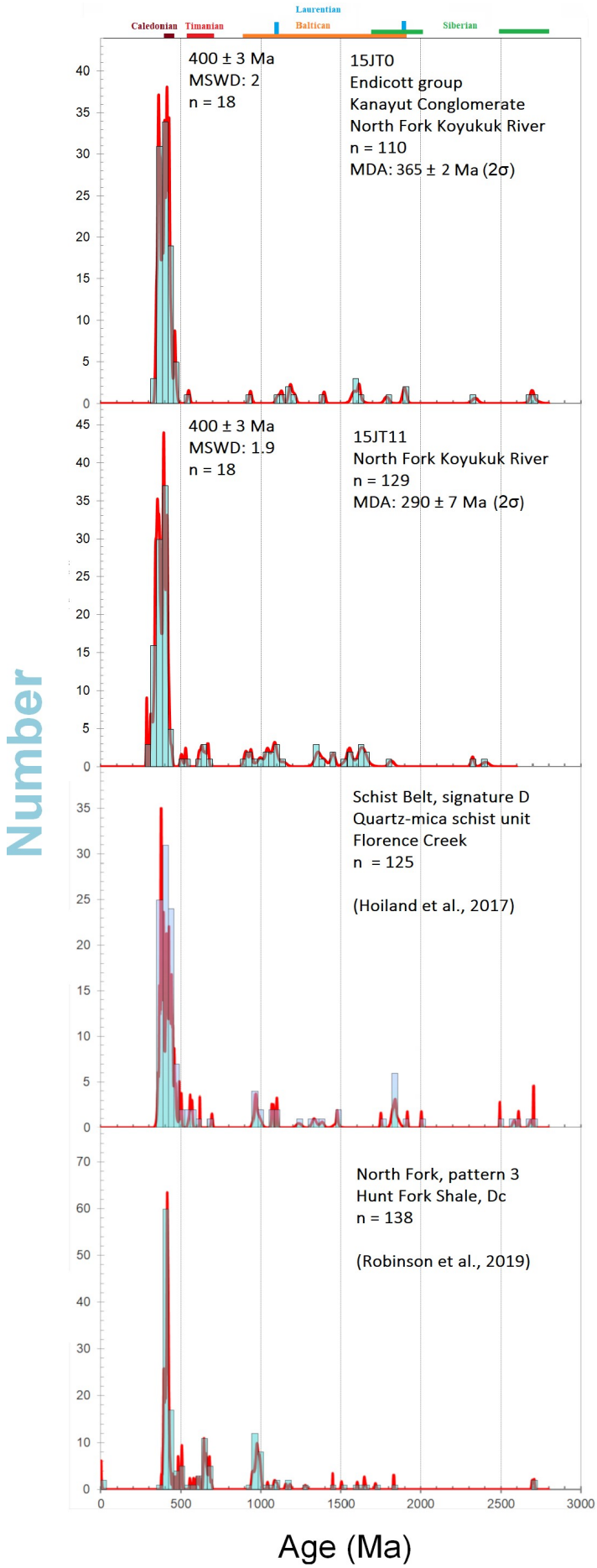
Neither of these semi-continuous age groups can generate a weighted mean age with a satisfactory MSWD (≤2). The remaining <500 Ma analyses comprise 56.6% (n=73) of the population. Five sub- to anhedral grains with apparent ages similar to the Timanian orogeny signature are present and four of these feature igneous oscillatory zoning whereof two have varying degrees of bright homogeneity, which can be suggestive of metamorphic alteration (Corfu et al., 2003) while the fifth is entirely brightly homogenous (Fig. 8). A maximum depositional age of c. 290 ± 4 Ma (2σ) for this sample is based on the concordia age of two subhedral igneous zircons (Figs. 8, 9, Addendum C).

Fig. 9 (below)**.** Age histograms of detrital rocks from the North Fork of the Koyukuk River (this study) juxtaposed to similar lithologies from the region identified by Robinson et al. (2019) to share a common age population.

4.3 Comparative databases

U-Pb detrital zircon age data from Hoiland et al. (2017) comprises a north-to-south transect of the Schist Belt and Greywacke-Phyllite Belt of Brooks Range and the Yukon-Koyukuk Basin. These units are similar to the two outcrop samples from the North Fork Koyukuk River presented here (Fig. 11) and provide a spatially and temporally broad framework for correlation of the different geological formations across the region. The second comparative dataset is from Robinson et al. (2019) and comprises both metamorphic and non-metamorphic sedimentary rocks from the North Koyukuk river. These combined datasets provide (1) a sample of the unit Pzw of the Apoon assemblage, structurally related to the Pzp unit sample in this study, (2) a distribution of ages from younger units which may be relevant to the modern river sands, and (3) a detrital signature pattern from the Hunt Fork shale (Dhf) and the chloritic and carbonate rocks (DC) identified by Robinson et al. (2019) which have been correlated with the Schist Belt data from Hoiland et al. (2017). The Hoiland et al. (2017) data was filtered with the same criteria as in this study, while that of Robinson et al. (2019) used the same filtering except for a stricter U (ppm) < 1000 limit.

In order to compare the results with orogenic signatures, definitions from Hoiland et al. (2017) have been used in which Caledonian age signatures are 450-400 Ma, Timanian 700-550 Ma, Baltican 1900-900 Ma, and Siberian 2000-1700 Ma and 2800-2500 Ma.



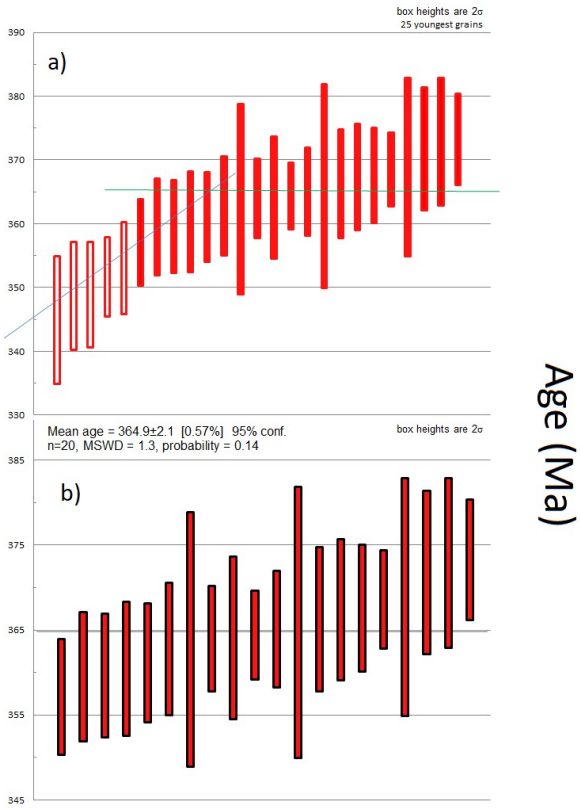


Fig. 10. MSWD plot of the 25 youngest grains in sample 15JT11. Blue line denotes sloping trend indicative of Pb-loss. Green horizontal line shows where errors are within range of each other.

In contrast, the Laurentian age signatures consists of two diagnostic age peaks at 1.9 and 1.1 Ga (Robinson et al., 2019). Age signatures indicative of Uralian orogeny are 340-320 Ma in the southern Urals and 320-280 Ma in the Polar Urals/Taimyr region (Pease, 2011). Age signatures corresponding to Uralian-Taimyrian cooling are 200-310 Ma (Moore et al., 2015; Zhang et al., 2017).

5 DISCUSSION

5.1 Age correlations and provenance of modern river sands

The Alatna river sands (16JT11 and 16JT24) exhibit similar age distributions and dominant age peaks (Fig. 7). Timanian-aged grains are present in the upstream sample (16JT11) but not in the downstream one (16JT24) (Fig. 7). This absence is partly interpreted as a function of hydrodynamics and partly as a function of sampling since 16JT24 is half the sample weight of 16JT11, i.e. lower sampling volume may decrease the provenance components present.

The following results (Figs. 7, 11) suggest that age distributions from strata in the Wiseman quadrangle along the John River (Hoiland et al., 2017) and the North Fork of the Koyukuk River (Robinson et al., 2019) are represented in these Alatna river sands:

(1) Data from the Hunt Fork Shale (Dhf) and Chloritic and carbonate rocks (Dc) in Robinson et al. (2019), as well as samples in Hoiland et al. (2017) from the quartz-mica schist of the Schist belt, share a dominant Devonian age peak.

(2) Late Mesoproterozoic to early-Neoproterozoic ages are the next most dominant population in samples 16JT11 and 16JT24. Similar age foci are present in the Dbcw (calcereous chloritic wacke), Dhf (Hunt Fork Shale), Dc (Chloritic and carbonate rock) and Hunt Fork Schist from the northern Koyukuk River (Robinson et al., 2019), and also in the calcareous schist unit (13-CH-BR04), quartz-mica schist unit (90LL71) in the Schist belt of Hoiland et al. (2017).

(3) A late Paleozoic age peak is shared by both Alatna river samples, as well as in Dhf, Dbcw, Dc, Hunt Fork Schist of Robinson et al. (2019) and the calcareous schist unit in the Schist belt (Hoiland et al., 2017).

The downstream sample 16JT27 is situated at a river junction in the Yukon-Koyukuk Basin where all four subbasins drain (Fig. 5). This vast area includes the Yukon-Koyukuk Basin, Phyllite Belt, Schist Belt and Central Belt terranes (Fig. 2). An increased Timanian signature may be present in this sample (Fig. 7) but this is tentative as only seven grains are present. Axelsson et al. (2018, 2019) noted minor Timanian peaks from rock samples along the Alatna River, which would be a potential source for these grains in the modern river sands. The overall age distribution in 16JT27 is similar to the other Alatna River samples, but with the addition of mid-Cretaceous ages (Fig. 7). Sample 16JT27 represents the first mid-Cretaceous input seen in the modern river sands, mixed with Devonian-Proterozoic ages that may be derived mainly from known sources in the Survey Pass and Wiseman quadrangles (Fig. 11).

Five grains combine to give a mean wtd. average age of c. 100.4 ± 2.7 Ma (Cenomanian-Late Albian); two of these grains have visible igneous oscillatory zoning, while the other three show signs of alteration (bleached appearance) indicative of a metamorphic source (Corfu et al., 2003; Fig. 6). U-Pb ages from the Shungnak conglomerate in the Yukon-Koyukuk Basin define a similar peak (Fig. 11) (Hoiland et al., 2017) and it also has several older age peaks (Fig. 11). Additionally, O'Brien et al. (2018) reported Albian metamorphic ages from southern Brooks Range lithologies.

5.2 Age correlations for 15JT10

The age distribution in sample 15JT10 is similar to the quartz-mica schist of the Schist belt (Fig. 9) and with published data on the Kanayut Conglomerate. The Kanayut conglomerate has major age peaks at 400-430 Ma, minor Proterozoic input, and the youngest maximum depositional age (MDA) of 365 Ma. The MDA slightly predates a 330 Ma plant fossil finding from the upper part of the conglomerate (Moore, 2004; Moore et al., 1994).

5.3 Regional/tectonic implications from 15JT10

It has previously been suggested that the Endicott group was deposited far south of its current position and that during early Cenozoic crustal shortening was thrust north of the Doonerak antiform (Oldow, 1987; Moore et al., 2016). Robinson et al. (2019) recognized greenschist facies metamorphism 20 km south of the Doonerak antiform in the Hunt Fork shale, a basal member of the Endicott group.

The age similarities between 15JT10, the quartz mica schist and the Kanayut conglomerate, along with the spatial relationship between 15JT10 and the quartz mica schist (Figs. 3, 9, 11) implies a tectonic and/or depositional connection between the Schist belt and Endicott group, in agreement with a more southerly depositional origin for the latter.

The Kanayut conglomerate likely incorporated Devonian detritus from the same protolith(s) as the older Hunt Fork shale, but with additional Proterozoic sources as unroofing progressed. Furthermore, since the Kanayut formation is underlain by the Noatak sandstone north of the Doonerak antiform (Fig. 4) it is possible that the quartz-mica schist in the southern Brooks Range is the metamorphosed correlative of this unit, the micaceous component likely due to the Noatak Sandstone interfingering the overlying basal marine shale member of the Kanayut formation, as well as having a gradational contact with the Hunt Fork shale (Brosgé, 1988).

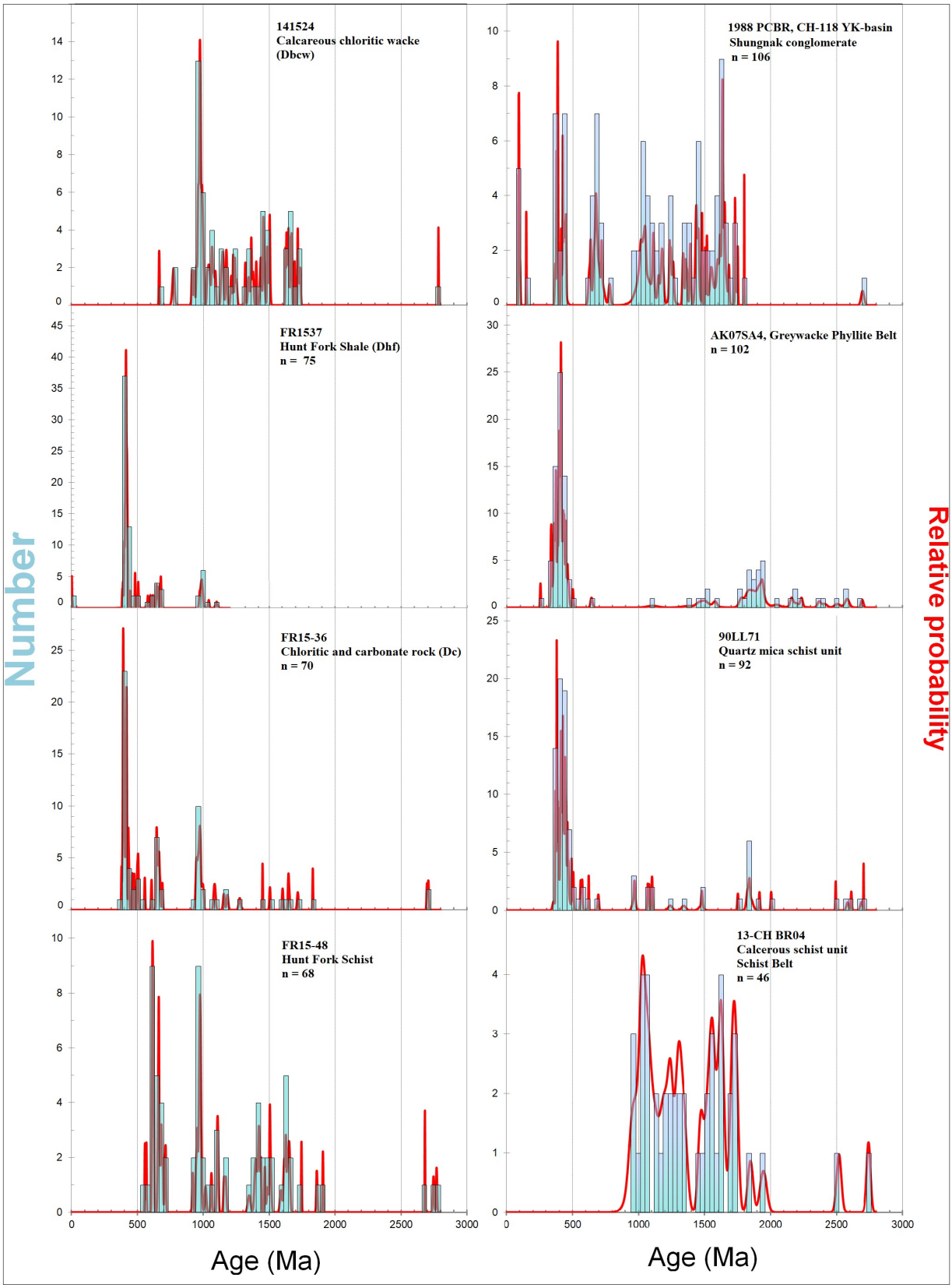


Fig. 11. Age histograms of detrital rock samples juxtaposed to ages from the quartz-mica schist of the Schist belt and the Hunt Fork Shale, Dc samples from the Doonerak antiform, identified by Robinson et al. (2019) as sharing a similar age signature.

5.4 Age correlations for 15JT11

Sample 15JT11 exhibits an age peak and MDA not compatible with the Pzp unit of the Apoon assemblage, for which Strauss et al., 2017 reported unimodal 441 and 490 Ma age populations and an early Devonian maximum depositional age, but acknowledged substantial Pb-loss for the youngest zircon grains and therefore was conservative with his MDA estimate. Nevertheless, considering the age group discrepancies it is not plausible that this sample represents the Pzp unit. The age peak of 400 Ma and the general distribution of minor age groups closely resemble those of the quartz-mica schist unit (Fig. 9), but the maximum depositional age of 290 Ma (Appendix C) is significantly younger than the schist unit age of 353 Ma (Hoiland et al., 2017). The MDA of 15JT11 is more similar to the proximal Phyllite belt, which has a depositional age as young as Mississippian based on outliers and conodont assemblages (Hoiland et al., 2017).

5.5 Regional/tectonic implications from 15JT11

The sample is from a section of the Schist belt classified by Hoiland et al. (2017) as a Devonian to Proterozoic(?) quartz-mica schist. The outcrop is located close to the Florence Creek fault which juxtaposes these rocks with Triassic to late Paleozoic(?) phyllite and greywacke of the Phyllite belt, and Devonian metavolcanic and metasedimentary rocks are also in near proximity (Fig. 3). The Phyllite belt (Slate Creek terrane) is in normal fault contact with the Schist belt (Coldfoot terrane) and constitutes the hanging wall (Till et al., 2016, Hoiland et al., 2017). Little et al. (1994) identified the Florence Creek fault as a ductile shear-zone. Given the structural complexity in the area and the age distributions indicating a mainly Schist Belt signature but with a Phyllite Belt depositional age, it is likely that sample 15JT11 consists of mainly Schist Belt detritus with input from the previously higher Phyllite Belt strata to which it is syn- to post-depositional.

Timanian ages suggests that zircons from this orogen may be present in outcrops along the North Fork of Koyukuk River, yet the majority of these grains show signs of metamorphic alteration in CL images. This location is further east than the John River where Hoiland et al. (2017) also identified a Timanian signature and potentially extends the 'Timanian suture' further east.

6 CONCLUSIONS

Detrital zircon U-Pb ages from sedimentary rocks along the North Koyukuk River and in modern river sands from the Alatna and Allakaket Rivers have been compared with existing datasets from the Wiseman quadrangle (Hoiland et al., 2017; Robinson et al., 2019). The zircon age distributions seen in Alatna River sands represents a mixture of Schist Belt and Central Belt strata, and indicate that the upstream sections of their drainage sub-basin are not statistically likely to host any outcrops with novel ages compared to previous studies. The occurrence of Devonian-Proterozoic ages in the Allakaket sample (16JT27) is in agreement with age profiles from rocks in the Wiseman quadrangle (e.g. Hoiland et al., 2017, Robinson et al., 2019). The additional mid-Cretaceous (Cenomanian) zircon ages constitute an additional provenance component which is not present in the upstream

modern sand samples and has a probable origin from lithologies in the southern Brooks Range or the Yukon-Koyukuk Basin.

The zircon age distribution of sedimentary rock sample 15JT10 (classified as Kanayut conglomerate in the field) indicates a tectonic or depositional relationship between the quartz-mica schist unit (Fig. 11) and the Kanayut formation. This supports the suggestion that the allochtonous Endicott group, now best preserved to the north of the Doonerak antiform, was originally deposited in a basin that was more southerly (Oldow, 1987).

Sedimentary rock sample 15JT11, a quartzite classified in the field as belonging to the Pzp unit of the Apoon assemblage, has a late Devonian age peak and a maximum depositional age of 290 Ma; the sample is clearly too young to represent Pzp (Strauss et al., 2017). Since the sample location is structurally complex, it is possible that the sample may represent a different unit and is classified incorrectly. Both sedimentary rock age distributions from this study show an affinity with pattern 3 of Robinson et al. (2019), therein suggested to indicate a post-accretionary phase during which nearby detritus accumulated in rift-related basins. Furthermore, sample 15JT11 confirms previous suggestions that Timanian ages might be found east of the John River (Hoiland et al., 2017).

Acknowledgements

I wish to extend a near infinite amount of thanks to my main supervisor Victoria Pease and secondary supervisor Emelie Axelsson at the Department of Geological Sciences, Stockholm University, for guiding me in the ways of geochronology. Many thanks also goes to researchers Carl Hoiland and Frank Robinson for sharing their data from Brooks Range and to Kerstin Lindén at the Museum of Natural History, Stockholm, who assisted with grain mount treatment and cathodoluminescence imaging.

7 REFERENCES

Amato, J.M., Toro, J., Miller, E.L., Gehrels, G.E., Farmer, G.L., Gottlieb, E.S., and Till, A.B., 2009. Late Proterozoic–Paleozoic evolution of the Arctic Alaska–Chukotka terrane based on U-Pb igneous and detrital zircon ages: Implications for Neoproterozoic paleogeographic reconstructions: Geological Society of America Bulletin, v. 121, p. 1219–1235, https://doi.org/ 10.1130/B26510.1.

Axelsson, E., Pease, V., Toro, J., Miller, E., Pearcey, S., 2018. Zircon provenance studies along the Alatna River in the Brooks Range, Alaska. ICAM VIII electronic abstract volume.

Axelsson, E., Pease, V., Toro, J., Miller, E., Pearcey, S., 2019. A synthesis of detrital zircon data across 250 km of the Central and Schist belts of the Brooks Range, Alaska: Implications for Arctic tectonic sutures. Geological Society of America *Abstracts with Programs.* Vol. 51, No. 4 doi: 10.1130/abs/2019CD-329240

Beranek, L.P., Van Staal, C.R., McClelland, W.C., Israel, S., and Mihalynuk, M.G., 2013. Baltican crustal provenance for Cambrian-Ordovician sandstones of the Alexander terrane, North American Cordillera: Evidence from detrital zircon U-Pb geochronology and Hf iso- tope geochemistry: Journal of the Geological Society, v. 170, p. 7–18, https://doi.org/10.1144/jgs2012-028.

Brosgé, W. P., Nilsen, T. H., Moore, T. E., & Dutro Jr., J. T., 1988. Geology of the Upper Devonian and Lower Mississippian(?) Kanayut Conglomerate in the central and eastern Brooks Range. Geology and Exploration of the National Petroleum Reserve in Alaska, 1974 to 1982, (September), 299–316.

Campbell, I.H., Reiners, P.W., Allen, C.M., Nicolescu, S., and Upadhyay, R., 2005. He-Pb double dating of detrital zircons from the Ganges and Indus Rivers: Implication for quantifying sediment recycling and provenance studies: Earth and Planetary Science Letters, v. 237, p. 402–432, doi:10.1016/j.epsl.2005.06.043.

Cherniak, D.J., Watson, E.B., 2000. Pb diffusion in zircon, Chemical Geology 172, 5-24.

Christiansen, P.P., and Snee, L.W., 1994. Structure, metamorphism, and geochronology of the Cosmos Hills and Ruby Ridge, Brooks Range schist belt, Alaska: Tectonics, v. 13, p. 193–213, doi: 10.1029 /93TC01545.

Corfu, F., Hanchar, J.M., Hoskin, P.W.O., Kinny, P., 2003. Atlas of Zircon Textures: Reviews in Mineralogy and Geochemistry, 53 (1), p. 469–500, doi: https://doi.org/10.2113/0530469.

Dillon, J.T., Brosge, W.P., and Dutro, J.T., Jr., 1986. Generalized Geologic Map of the Wiseman Quadrangle, Alaska: U.S. Geological Survey Open-File Report 86–219, scale 1:250,000.

Faure, G., 1986. Principles of Isotope Geology, 2nd edn, New York: John Wiley & Sons.

Fedo, C.M., Sircombe, K.N., Rainbird, R.H., 2003. Detrital Zircon Analysis of the Sedimentary Record: Reviews in Mineralogy and Geochemistry 53 (1), p. 277-303, doi: https://doi.org/10.2113/0530277.

Fielding, L., Najman, Y., Millar, I., Butterworth, P., Ando, S., Padoan, M., Barfod, D., and Kneller, B., 2017. A detrital record of the Nile River and its catchment: Journal of the Geological Society, v. 174, p. 301–317, doi:10.1144/jgs2016-075.

Gehrels, G., 2014. Detrital zircon U-Pb geochronology applied to tectonics. Annual Review of Earth and Planetary Sciences 42, 127e149. http://dx.doi.org/10.1146/

Gottlieb, E.S., Meisling, K.E., Miller, E.L., and Mull, C.G., 2014. Closing the Canada Basin: Detrital zircon geochronology relationships between the North Slope of Arctic Alaska and the Franklinian mobile belt of Arctic Canada: Geosphere, v. 10, p. 1366–1384, https://doi .org/10.1130/GES01027.1.

Grantz, A., May, S.D., Taylor, P.T., and Lawver, L.A., 1990. Canada Basin, in Grantz, A., Johnson, L., and Sweeney, J.F., eds., The Arctic Ocean Region: Boulder, Colorado, USA, Geological Society of America, The Geology of North America, v. L, p. 379–402, https:// doi.org/10.1130/DNAG-GNA-L.379.

Gucsik, A., 2009. Cathodoluminescence and its Application in the Planetary Sciences: Berlin, Springer-Verlag, p. 1-5.

Habermann, D., Neuser, R.D., Richter, D.K., 2000. Quantitative High Resolution Spectral Analysis of Mn2+ in Sedimentary Calcite, *in* Pagel, M., Barbin, V., Blanc, P., Ohnenstetter, D., eds., Cathodoluminescence in Geosciences: An Introduction: Berlin, Springer-Verlag, p. 345.

Hoiland, C.W., Miller, E.L., Pease, V., and Hourigan, J.K., 2017. Detrital zircon U-Pb geochronology and Hf isotope geochemistry of metasedimentary strata in the southern Brooks Range: Constraints on Neoproterozoic Cretaceous evolution of Arctic Alaska, in Pease, V., and Coakley, B., eds., Circum-Arctic Lithosphere Evolution: Geological Society of London, Special Publication 460, p. 121–158.

Iizuka, T., Campbell, I.H., Allen, C.M., Gill, J.B., Maruyama, S., and Makoka, F., 2013. Evolution of the African continental crust as recorded by U-Pb, Lu-Hf and O isotopes in detrital zircons from modern rivers: Geochimica et Cosmochimica Acta, v. 107, p. 96–120, doi:10.1016/j.gca.2012.12.028.

Julian, F.E., and Oldow, J., 1998. Structure and lithology of the lower Paleozoic Apoon assemblage, eastern Doonerak Window, central Brooks Range, Alaska, in Oldow, J.S., and Avé Lallemant, H.G., eds., Architecture of the Central Brooks Range Fold and Thrust Belt, Arctic Alaska: Geological Society of America Special Paper 324, p. 65–80, https://doi.org/ 10.1130/0-8137-2324-8.65.

Little, T.A., Miller, E.L., Lee, J., and Law, R.D., 1994. Extensional origin of ductile fabrics in the Schist Belt, central Brooks Range, Alaska—I. Geologic and structural studies: Journal of Structural Geology, v. 16, p. 899–918, doi: 10 .1016 /0191 -8141(94)90075 -2.

Ludwig, K. R., 1998. On the treatment of concordant uranium-lead ages. Geochimica et Cosmochimica Acta, 62(4), 665–676. https://doi.org/10.1016/S0016-7037(98)00059-3

Ludwig, K.R., 2003. Isoplot/Ex 3.00: A geochronological toolkit for Microsoft Excel: Berkeley Geochronology Centre, p. 1–72, doi:10.1139/e2012-058.

Mezger, K., Krogstad, E.J., 1997. Interpretation of discordant U-Pb zircon ages: an evaluation. Journal of Metamorphic Geology 15 (1), 127-140. http://dx.doi.org/ 10.1111/j.1525-1314.1997.00008.x

Miller, E.L., Toro, J., Gehrels, G., Amato, J.M., Prokopiev, A., Tuchkova, M., Akinin, V.V., Dumitru, T.A., Moore, T.E., and Cecile, M.P., 2006. New insights into Arctic paleogeography and tectonics from U-Pb detrital zircon geochronology: Tectonics, v. 25, TC3013, doi: 10 .1029 /2005TC001830.

Miller, E.L., Gehrels, G.E., Pease, V., and Sokolov, S., 2010a. Stratigraphy and U-Pb detrital zircon geochronology of Wrangel Island, Russia: Implications for Arctic paleogeography: American Association of Petroleum Geologists Bulletin, v. 94, no. 5, p. 665–692, doi: 10 .1306 /10200909036.

Miller, E.L., Kuznetsov, N., Soboleva, A., Udoratina, O., Grove, M.J., and Gehrels, G., 2011. Baltica in the Cordillera?: Geology, v. 39, p. 791–794, https://doi.org/ 10.1130/G31910.1.

Moore, T.E., 1987, Geochemistry and tectonic setting of some volcanic rocks of the Franklinian Assemblage, central and eastern Brooks Range, in Tailluer, I.L., and Weimer, P., eds., Field Trip Guidebook-Pacific Section: Society of Economic Paleontologists and Mineralo- gists 50, p. 691–710.

Moore, T.E., Wallace, W.K., Bird, K.J., Karl, S.M., Mull, C.G., and Dillon, J.T., 1994. Geology of northern Alaska, in Plafker, G., and Berg, H.C., eds., The Geology of Alaska: Boulder, Colorado, USA, Geological Society of America, Geology of North America, v. G-1, p. 49–140.

Moore, Thomas & Wallace, W.K. & Bird, Kenneth & Karl, S.M. & Mull, C.G. & Dillon, J.T., 1994. Geology of northern Alaska. The Geology of Alaska. The Geology of North America. G-1. 49-140. 10.1130/DNAG-GNA-G1.49.

Moore, T.E., O'Sullivan, P.B., Potter, C.J. & Donelick, R.A., 2015. Provenance and detrital zircon evolution of early Brookian foreland basin deposits of the western Brooks Range, Alaska, and implications for early Brookian tectonism. Geosphere, 11, 93–122.

Moore, T.E., and Box, S.E., 2016. Age, distribution and style of deformation in Alaska north of 60°N: Implications for assembly of Alaska: Tectonophysics, v. 691, p. 133–170, doi:10.1016/j.tecto.2016.06.025.

O'Brien, T. M., Miller, E. L., Pease, V., Hayden, L. A., Fisher, C. M., Hourigan, J. K., & Vervoort, J. D., 2018. Provenance, U-Pb detrital zircon geochronology, Hf isotopic analyses, and Cr-spinel geochemistry of the northeast Yukon-Koyukuk Basin: Implications for interior basin development and sedimentation in Alaska. Bulletin of the Geological Society of America, 130(5–6), 825–847. https://doi.org/10.1130/B31825.1

Oldow, J.S., Seidenstecker, C.M., Phelps, J.C., Julian, F.E., Gott- schalk, R.R., Boler, K.W., Handschy, J.W., and Avé Lallement, H.G., 1987. Balanced Cross-Sections through the Central Brooks Range and North Slope, Arctic Alaska: Tulsa, Oklahoma, American Association of Petroleum Geologists Special Publication, 19 p., 8 plates, scale 1:200,000.

Paces, J.B., Miller, J.D., 1993. Precise U–Pb ages of Duluth Complex and related mafic intrusions, northeastern Minnesota — geochronological insights to physical, petrogenetic, paleomagnetic, and tectonomagmatic processes associated with the 1.1 Ga midcontinent rift system. J. Geophys. Res. 98 (B8), 13997–14013.

Paton, C., Hellstrom, J., Paul, B., Woodhead, J., & Hergt, J., 2011. Iolite: Freeware for the Visualisation and Processing of Mass Spectrometric Data. Journal of Analytical Atomic Spectrometry, 26(12), 2508-2518.

Pease, V., 2011. Chapter 20 Eurasian orogens and Arctic tectonics: an overview: Geological Society, London, Memoirs, v. 35, p. 311–324, doi:10.1144/m35.20.

Petrus, J., & Kamber, B., 2012. VizualAge: A Novel Approach to Laser Ablation ICP-MS U-Pb Geochronology Data Reduction. Geostandards and Geoanalytical Research, 1-24.

Robinson, F.A., Toro, J., and Pease, V., 2019. U-Pb and oxygen isotope characteristics of Timanian- and Caledonian-age detrital zircons from the Brooks Range, Arctic Alaska , USA: , p. 1–21.

Robinson, F.A., Toro, J., and Pease, V., 2019. U-Pb and oxygen isotope characteristics of Timanian- and Caledonian-age detrital zircons from the Brooks Range, Arctic Alaska , USA: , p. 1–21.

Shepherd, G.E., Muller, R.D., and Seton, M., 2013. The tectonic evolution of the Arctic since Pangea breakup: Integrating constraints from surface geology and geophysics with mantle structure: Earth-Science Reviews, v. 124, p. 143–183.

Sláma, J., Košler, J., Condon, D.J., Crowley, J.L., Gerdes, A., Hanchar, J.M., Horstwood, M.S.A., Morris, G.A., Nasdala, L., Norberg, N., Schaltegger, U., Schoene, B., Tubrett, M.N., Whitehouse, M.J., 2008. Plešovice zircon — a new natural reference material for U– Pb and Hf isotopic microanalysis. Chem. Geol. 249, 1–35.

Spencer, C.J., Kirkland, C.L., and Taylor, R.J.M., 2016. Strategies towards statistically robust interpretations of in situ U-Pb zircon geochronology: Geoscience Frontiers, v. 7, p. 581–589, doi:10.1016/j.gsf.2015.11.006.

Strauss, J.V., Hoiland, C.W., Ward, W.P., Johnson, B.G., Lyle, L.L., and McClelland, W.C., 2017. Orogen transplant: Taconic-Caledonian arc magmatism in the central Brooks Range of Alaska: Geological Society of America Bulletin, v. 129, p. 649–676, https://doi .org/10.1130/B31593.1.

Till, A.B., Amato, J.M., Aleinikoff, J.N., and Bleick, H.A., 2014. U-Pb detrital zircon geochronology as evidence for the origin of the Nome Complex, northern Alaska, and implications for regional and trans-Arctic correlations, in Dumoulin, J.A., and Till, A.B., eds., Reconstruction of a Late Proterozoic to Devonian Continental Margin Sequence, Northern Alaska: Its Paleogeographic Significance and Contained Base-Metal Sulfide Deposits: Geological Society of America Special Paper 506, p. 111–131, https://doi.org/ 10.1130/2014.2506(04).

Till, A.B., 2016. A synthesis of Jurassic and Early Creta-ceous crustal evolution along the southern margin of the Arctic Alaska-Chukotka microplate and implications for defining tectonic boundaries active during opening of Arctic Ocean basins: Lithosphere, v. 8, p. 219–237, https://doi.org/10.1130/L471.1.

Vermeesch, P., 2012. On the visualisation of detrital age distributions: Chemical Geology, v. 312–313, p. 190–194, doi:10.1016/j.chemgeo.2012.04.021.

White, W., 2015. Isotope Geochemistry. Singapore: C.O.S. Printers Pte Ltd.

Zhang, X., Pease, V., Carter, A., Kostuychenkko, S., Suleymanov, A., Scott, R., 2017. Timing of exhumation and deformation across the Taimyr fold-thrust belt: Insights from apatite fission track dating and balanced cross-sections. IN Pease, V., Coakley, B. (eds), Circum-Arctic Lithosphere Evolution. Geological Society (London) Special Publication 460, DOI 10.1144/SP460.3

APPENDIX A - Analytical results

					Pb-uncorrected ratios							Pb-uncorrected ages								
Analysis	U (ppm)	Pb (ppm)	Th (ppm)	U/Th	207Pb/206Pb	±2σ abs.	207Pb/235U	±2σ abs.	206Pb/238U	±2σ abs.	error corr.	238U/206Pb	±2σ abs.	206Pb/238U	±2σ abs.	207Pb/235U	±2σ abs.	207Pb/206Pb	Error ±2σ abs.	Disc.[1] %	Disc.[2] %
Sample 16JT27, experiment 1																					
16JT27-1	332	b.d.	b.d.	1	0.05	0.003	0.4	0.03	0.05	0	0.1	18.519	0.75446	339	14	352	17	344	69	3.7	1.5
16JT27-2	132	b.d.	b.d.	2	0.07	0.004	2	0.07	0.18	0.01	-0.3	5.6433	0.22293	1051	38	1043	25	1051	49	-0.8	0.0
16JT27-5	170	b.d.	b.d.	1	0.1	0.004	5	0.1	0.32	0.01	0.4	3.1546	0.12937	1772	63	1774	21	1786	54	0.1	0.8
16JT27-6	91	b.d.	b.d.	1	0.1	0.006	5	0.2	0.3	0.02	0.1	3.3113	0.16447	1701	75	1769	34	1842	58	3.8	7.7
16JT27-9	266	b.d.	b.d.	4	0.06	0.004	0.5	0.03	0.07	0	0.0	14.245	0.62905	437	18	443	22	543	85	1.4	19.5
16JT27-10	1254	b.d.	b.d.	2	0.05	0.004	0.1	0.01	0.02	0	-0.1	61.387	2.67560	104	5	104	5	340	100	-0.4	69.4
16JT27-13	527	388	297	2	0.07	0.003	1	0.03	0.15	0.01	0.0	6.7843	0.25775	886	31	887	14	922	48	0.1	3.9
16JT27-14	562	119	197	2	0.05	0.003	0.5	0.02	0.06	0	0.2	15.748	0.64480	397	16	398	12	441	53	0.3	10.0
16JT27-15	234	134	99	2	0.07	0.003	1	0.06	0.15	0.01	0.2	6.6445	0.25607	904	33	904	24	925	51	0.0	2.3
16JT27-16	224	106	62	3	0.08	0.004	2	0.08	0.21	0.01	0.2	4.7801	0.18965	1224	44	1226	25	1247	51	0.2	1.8
16JT27-17	207	265	115	1	0.1	0.005	3	0.2	0.27	0.01	0.2	3.7313	0.13923	1531	51	1530	32	1543	57	-0.1	0.8
16JT27-18	435	120	210	2	0.06	0.004	0.5	0.02	0.06	0	0.1	16.475	0.70566	382	15	383	16	493	56	0.3	22.5
16JT27-19	395	92	186	2	0.05	0.003	0.4	0.02	0.06	0	0.1	17.731	0.69162	354	14	357	13	424	54	0.8	16.5
16JT27-20	997	76	107	9	0.07	0.003	1	0.05	0.13	0.01	0.7	7.8431	0.43060	773	40	787	26	943	43	1.8	18.0
16JT27-21	114	43	60	2	0.06	0.007	0.7	0.05	0.08	0.01	-0.3	11.933	0.64080	518	27	520	32	540	130	0.4	4.1
16JT27-24	246	406	173	1	0.1	0.005	5	0.1	0.31	0.01	0.1	3.1949	0.12249	1754	61	1757	20	1780	34	0.2	1.5
16JT27-25	1069	173	1283	1	0.05	0.004	0.1	0.01	0.02	0	0.3	63.211	3.47620	101	6	101	8	220	130	-0.6	54.0
16JT27-27	571	51	97	7	0.06	0.003	0.4	0.02	0.06	0	0.3	16.779	0.70380	375	15	374	11	501	52	-0.3	25.1
16JT27-28	959	338	678	2	0.05	0.002	0.5	0.01	0.06	0	0.2	16.367	0.61609	382	14	382	9	373	51	0.0	-2.4
16JT27-29	1394	486	388	4	0.07	0.003	1	0.02	0.15	0.01	0.3	6.6269	0.25032	906	32	912	8	1004	39	0.6	9.8
16JT27-30	87	364	101	1	0.2	0.007	10	0.3	0.46	0.02	0.5	2.1692	0.08470	2442	80	2448	28	2539	40	0.2	3.8
16JT27-31	902	304	563	2	0.06	0.002	0.5	0.01	0.06	0	0.1	16.447	0.59514	381	13	382	8	435	49	0.3	12.4
16JT27-32	276	422	170	2	0.1	0.005	5	0.2	0.31	0.01	0.5	3.2051	0.13355	1751	62	1763	27	1794	34	0.7	2.4
16JT27-34	529	279	509	1	0.06	0.004	0.5	0.02	0.06	0	0.2	16.026	0.87319	390	20	392	16	530	82	0.5	26.4
16JT27-35	667	97	637	1	0.05	0.003	0.1	0.01	0.02	0	0.3	61.767	2.67060	104	5	102	6	228	66	-1.3	54.6
16JT27-36	365	42	257	1	0.05	0.006	0.1	0.01	0.02	0	0.1	60.827	3.18200	105	6	107	10	604	97	1.8	82.6
16JT27-38	233	134	80	2	0.07	0.004	2	0.06	0.17	0.01	0.1	5.8005	0.27253	1025	44	1004	24	973	58	-2.1	-5.3

Analysis	U	Pb	Th	U	207Pb		207Pb		206Pb		error	238U		206Pb		207Pb		207Pb	Error	Disc.[1]	Disc.[2]
	(ppm)	(ppm)	(ppm)	Th	206Pb	±2σ abs.	235U	±2σ abs.	238U	±2σ abs.	corr.	206Pb	±2σ abs.	238U	±2σ abs.	235U	±2σ abs.	206Pb	±2σ abs.	%	%
16JT27-39	829	200	332	2	0.05	0.002	0.4	0.01	0.06	0	0.1	17.731	0.66018	354	13	354	8	412	51	-0.1	14.1
16JT27-40	360	338	343	1	0.06	0.003	0.8	0.03	0.1	0	0.5	10.06	0.41496	611	24	615	15	683	47	0.7	10.5
16JT27-41	864	914	860	1	0.06	0.003	0.9	0.03	0.1	0.01	0.4	9.7752	0.42999	628	26	633	15	609	59	0.8	-3.1
16JT27-43	461	409	328	1	0.07	0.003	1	0.04	0.12	0.01	0.3	8.285	0.34321	734	29	738	18	835	60	0.5	12.1
16JT27-44	144	20	27	4	0.06	0.003	0.6	0.03	0.07	0	0.4	13.569	0.55231	458	18	465	21	460	69	1.5	0.4
16JT27-45	76	90	26	2	0.1	0.007	6	0.2	0.35	0.02	0.1	2.8653	0.13136	1928	78	1944	30	2118	51	0.8	9.0
16JT27-47	141	135	49	2	0.1	0.004	4	0.1	0.29	0.01	0.3	3.4965	0.14671	1621	58	1664	20	1721	34	2.6	5.8
16JT27-48	325	359	200	1	0.08	0.004	2	0.05	0.19	0.01	0.4	5.2274	0.24320	1128	48	1139	18	1268	51	1.0	11.0
16JT27-55	167	288	b.d.	3	0.06	0.004	0.4	0.03	0.06	0	0.0	16.949	0.66073	370	14	373	18	438	88	0.8	15.5
16JT27-56	114	165	b.d.	2	0.06	0.004	0.5	0.03	0.06	0	0.3	16	0.66560	391	16	389	20	450	63	-0.5	13.1
16JT27-57	29	61	457	2	0.07	0.007	1	0.1	0.15	0.01	-0.1	6.8729	0.34010	875	41	874	56	890	100	-0.1	1.7
16JT27-58	305	308	330	6	0.09	0.004	3	0.06	0.24	0.01	0.3	4.207	0.15929	1375	47	1391	15	1471	35	1.2	6.5
16JT27-60	243	248	379	1	0.06	0.003	0.7	0.02	0.09	0	0.1	11.628	0.47323	532	21	534	14	617	55	0.4	13.8
16JT27-62	244	6	17	3	0.05	0.004	0.2	0.02	0.03	0	0.3	35.088	1.47740	181	8	187	14	320	100	3.2	43.4
16JT27-68	1128	18	96	2	0.05	0.003	0.1	0.01	0.02	0	0.4	67.34	3.44640	95	5	96	5	240	72	1.1	60.4
16JT27-70	314	8	10	6	0.05	0.003	0.5	0.02	0.06	0	0.2	15.748	0.64480	397	16	400	14	366	73	0.7	-8.5
16JT27-71	26	1	1	4	0.06	0.006	0.5	0.05	0.06	0	0.1	15.625	0.80566	400	20	415	32	632	95	3.6	36.7
16JT27-72	106	15	20	1	0.06	0.003	0.5	0.02	0.06	0	0.2	16.584	0.66005	378	14	388	16	514	61	2.6	26.5
16JT27, experiment 2																					
16JT27-73	793	324	228	3	0.06	0.004	0.9	0.04	0.11	0	0.1	9.4967	0.37878	645	24	670	19	734	49	3.7	12.1
16JT27-74	490	457	110	4	0.1	0.003	5	0.1	0.33	0.01	0.4	3.0488	0.06135	1828	32	1844	18	1874	20	0.9	2.5
16JT27-75	236	222	56	4	0.1	0.007	5	0.2	0.33	0.02	0.2	3.0488	0.15802	1827	81	1868	36	1893	49	2.2	3.5
16JT27-76	710	70	300	2	0.05	0.003	0.1	0.01	0.02	0	0.5	59.312	1.75900	108	3	107	7	286	69	-0.5	62.3
16JT27-77	110	196	94	1	0.08	0.003	2	0.08	0.17	0.01	0.4	5.7372	0.15141	1035	25	1063	27	1124	53	2.6	7.9
16JT27-78	698	115	119	6	0.06	0.002	0.6	0.03	0.08	0	0.5	13.072	0.39301	475	14	472	16	527	45	-0.6	9.9
16JT27-79	186	38	48	3	0.05	0.005	0.5	0.04	0.06	0	0.1	15.625	0.53711	400	14	402	29	380	110	0.5	-5.3
16JT27-80	88	194	49	1	0.1	0.003	6	0.1	0.36	0.01	0.3	2.8019	0.04632	1966	28	1957	19	1964	27	-0.5	-0.1
16JT27-81	182	56	83	2	0.05	0.005	0.4	0.04	0.06	0	0.1	17.094	0.46753	366	10	363	27	400	89	-0.9	8.4
16JT27-82	985	364	351	3	0.06	0.002	0.8	0.03	0.1	0	0.3	10.482	0.15383	587	8	600	16	651	34	2.2	9.8
16JT27-83	947	591	172	5	0.1	0.005	6	0.1	0.34	0.01	0.3	2.9155	0.10200	1900	57	1916	23	1929	33	0.8	1.5
16JT27-84	818	26	120	7	0.05	0.004	0.1	0.01	0.02	0	0.0	64.893	1.43180	99	2	101	9	293	98	2.0	66.3
16JT27-87	436	169	75	7	0.1	0.006	4	0.1	0.28	0.01	0.0	3.5336	0.14983	1603	59	1630	26	1660	33	1.7	3.4

Analysis	U	Pb	Th	U	207Pb		207Pb		206Pb		error	238U		206Pb		207Pb		207Pb	Error	Disc.[1]	Disc.[2]
	(ppm)	(ppm)	(ppm)	Th	206Pb	±2σ abs.	235U	±2σ abs.	238U	±2σ abs.	corr.	206Pb	±2σ abs.	238U	±2σ abs.	235U	±2σ abs.	206Pb	±2σ abs.	%	%
16JT27-88	359	20	38	#	0.05	0.003	0.5	0.02	0.06	0	-0.1	16.34	0.50728	383	12	382	15	322	61	-0.3	-18.9
16JT27-89	223	157	83	3	0.09	0.004	3	0.1	0.26	0.01	0.3	3.8911	0.15140	1472	53	1466	23	1423	32	-0.4	-3.4
16JT27-92	189	67	77	3	0.06	0.005	1	0.07	0.11	0.01	0.1	8.8496	0.37591	690	28	689	35	679	82	-0.1	-1.6
16JT27-93	616	206	450	1	0.05	0.002	0.4	0.01	0.05	0	0.1	18.741	0.34419	335	6	344	11	378	59	2.6	11.3
16JT27-94	177	166	87	2	0.08	0.004	3	0.1	0.23	0.01	0.2	4.3725	0.15104	1327	41	1322	29	1247	51	-0.4	-6.4
16JT27-95	491	189	339	2	0.05	0.002	0.4	0.02	0.06	0	0.4	16.835	0.48181	372	10	375	11	389	46	0.8	4.4
16JT27-96	130	28	43	3	0.06	0.004	0.5	0.04	0.07	0	0.0	14.728	0.39042	424	11	428	26	457	85	0.9	7.2
16JT27-97	605	176	249	3	0.06	0.003	0.7	0.08	0.09	0.01	0.8	11.588	1.12790	532	50	531	52	537	80	-0.2	0.9
16JT27-98	47	29	19	2	0.07	0.005	2	0.09	0.16	0.01	-0.2	6.0643	0.23536	983	35	977	34	937	78	-0.6	-4.9
16JT27-99	510	268	297	2	0.06	0.002	0.8	0.03	0.09	0	0.3	10.87	0.27174	567	14	579	14	618	36	2.1	8.3
16JT27-100	162	242	139	1	0.08	0.005	2	0.1	0.18	0.01	0.1	5.618	0.21778	1055	38	1058	38	1074	98	0.3	1.8
16JT27-101	94	91	48	2	0.07	0.006	2	0.1	0.17	0.01	0.0	5.7274	0.20010	1037	33	1035	47	1104	76	-0.2	6.1
16JT27-102	297	180	283	1	0.05	0.002	0.5	0.02	0.06	0	0.0	15.974	0.33174	391	8	389	12	392	52	-0.6	0.2
16JT27-103	1166	331	503	2	0.06	0.004	0.5	0.01	0.06	0	-0.1	15.576	0.89770	401	22	401	8	428	56	-0.1	6.3
16JT27-104	519	551	247	2	0.09	0.006	3	0.07	0.25	0.01	0.0	4.065	0.23134	1415	70	1457	17	1489	43	2.9	5.0
16JT27-105	445	225	97	4	0.1	0.006	3	0.09	0.25	0.01	0.1	4.0486	0.19669	1420	60	1472	23	1567	39	3.5	9.4
16JT27-106	43	43	18	2	0.1	0.007	3	0.2	0.24	0.01	0.0	4.1754	0.17259	1383	51	1433	59	1497	93	3.5	7.6
16JT27-107	142	55	80	2	0.06	0.006	0.5	0.05	0.06	0	0.3	16.26	0.52879	384	12	387	33	598	85	0.8	35.8
16JT27-108	830	244	383	2	0.05	0.002	0.5	0.01	0.06	0	0.1	15.974	0.28070	391	6	389	8	359	35	-0.5	-8.9
16JT27-109	195	176	92	2	0.09	0.003	3	0.08	0.23	0.01	0.2	4.3253	0.08793	1340	25	1346	21	1370	28	0.4	2.2
16JT27-110	326	503	274	1	0.09	0.002	3	0.05	0.24	0	0.2	4.1494	0.06887	1395	20	1398	13	1417	21	0.2	1.6
16JT27-111	472	913	413	1	0.1	0.002	4	0.06	0.28	0	0.1	3.5651	0.05211	1594	20	1596	12	1588	22	0.1	-0.4
16JT27-112	344	152	187	2	0.06	0.002	0.9	0.03	0.1	0	0.2	9.6432	0.25108	636	16	636	16	677	36	0.0	6.1
16JT27-114	730	675	845	1	0.06	0.002	0.8	0.03	0.1	0	0.1	10.406	0.19491	592	11	591	15	570	40	-0.2	-3.9
16JT27-115	704	280	329	2	0.06	0.003	0.8	0.03	0.1	0.01	0.4	9.8425	0.46500	624	28	621	17	669	88	-0.5	6.7
16JT27-116	209	176	114	2	0.08	0.003	2	0.08	0.19	0	0.2	5.3419	0.11700	1106	22	1102	26	1101	53	-0.4	-0.5
16JT27-117	159	152	68	3	0.1	0.002	4	0.09	0.3	0.01	0.2	3.3818	0.05833	1669	25	1669	17	1664	23	0.0	-0.3
16JT27-118	262	112	248	1	0.05	0.004	0.4	0.03	0.06	0	0.1	16.863	0.48344	371	11	370	21	405	68	-0.3	8.4
16JT27-120	162	179	95	2	0.09	0.002	3	0.09	0.25	0.01	0.5	3.9793	0.08076	1444	26	1445	21	1441	28	0.1	-0.2
16JT27-121	446	76	64	6	0.06	0.002	0.9	0.02	0.1	0	0.0	9.7943	0.21104	627	13	624	12	655	36	-0.5	4.3
16JT27-123	164	41	59	2	0.05	0.004	0.4	0.03	0.06	0	0.3	16.978	0.63415	369	14	369	23	467	66	0.0	21.0
16JT27-124	242	234	120	2	0.07	0.003	2	0.04	0.17	0	0.0	5.8928	0.12848	1010	21	1013	13	1034	37	0.3	2.3
16JT27-125	910	329	422	2	0.06	0.002	0.5	0.02	0.06	0	0.2	15.723	0.27194	397	7	394	11	416	49	-0.9	4.5

Analysis	U (ppm)	Pb (ppm)	Th (ppm)	U Th	207Pb 206Pb	±2σ abs.	207Pb 235U	±2σ abs.	206Pb 238U	±2σ abs.	error corr.	238U 206Pb	±2σ abs.	206Pb 238U	±2σ abs.	207Pb 235U	±2σ abs.	207Pb 206Pb	Error ±2σ abs.	Disc.[1] %	Disc.[2] %
16JT27-126	66	61	30	2	0.07	0.006	2	0.1	0.17	0.01	0.3	5.9844	0.16832	996	26	997	53	1026	87	0.1	2.9
16JT27-129	626	180	254	2	0.05	0.003	0.4	0.02	0.06	0	0.0	17.123	0.43981	366	9	368	15	373	52	0.6	1.9
16JT27-130	431	119	147	3	0.05	0.004	0.4	0.03	0.06	0	0.4	17.575	1.26640	357	25	357	22	427	84	0.0	16.4
16JT27-131	502	189	162	3	0.06	0.002	0.8	0.02	0.1	0	0.2	10.56	0.21186	583	11	583	12	620	40	0.0	6.0
16JT27-133	1200	85	b.d.	1	0.05	0.005	0.1	0.01	0.02	0	0.1	55.525	2.52810	115	5	118	10	351	69	2.6	67.2
16JT27-135	134	113	b.d.	1	0.09	0.005	3	0.2	0.26	0.01	0.3	3.7879	0.17218	1507	59	1501	50	1492	66	-0.4	-1.0
16JT27-137	336	71	b.d.	1	0.06	0.004	0.5	0.03	0.07	0	0.1	14.793	0.32824	421	9	423	22	480	100	0.4	12.2
16JT27-138	855	225	b.d.	1	0.06	0.002	0.6	0.02	0.08	0	0.0	12.361	0.22919	502	9	498	14	495	41	-0.7	-1.3
16JT27-139	253	38	b.d.	2	0.06	0.005	0.5	0.04	0.07	0	0.1	14.837	0.28617	421	8	417	27	555	87	-0.9	24.2
16JT27-141	1024	656	b.d.	2	0.1	0.002	4	0.09	0.3	0.01	0.3	3.3898	0.06665	1666	29	1668	18	1689	23	0.1	1.4
16JT27-142	1147	309	b.d.	1	0.05	0.003	0.4	0.02	0.06	0	0.0	17.301	0.50885	362	10	361	12	320	62	-0.3	-13.1
16JT27-144	123	39	b.d.	2	0.08	0.006	2	0.2	0.19	0	0.4	5.3996	0.12828	1095	24	1090	53	1128	67	-0.5	2.9
16JT27-145	71	516	23	2	0.2	0.005	10	0.2	0.48	0.01	0.3	2.1008	0.04414	2510	46	2511	18	2533	22	0.0	0.9
16JT27-146	152	151	47	2	0.06	0.004	0.5	0.04	0.06	0	0.3	15.748	0.39680	397	10	395	26	457	63	-0.5	13.2
16JT27-147	495	179	215	2	0.05	0.004	0.1	0.01	0.02	0	0.1	64.185	1.40070	100	2	104	7	271	76	3.1	63.0
16JT27-148	140	293	30	3	0.08	0.004	2	0.09	0.19	0.01	0.2	5.184	0.15587	1143	30	1143	33	1156	54	0.0	1.1
16JT27-149	133	356	36	3	0.08	0.003	2	0.06	0.21	0.01	0.1	4.8426	0.11256	1209	26	1209	20	1205	37	0.0	-0.3
16JT27-150	231	93	11	#	0.07	0.002	2	0.04	0.16	0.01	0.3	6.1728	0.17528	968	26	966	17	941	38	-0.2	-2.9
15JT10, experiment 3																					
15JT10-1	290	81	274	2	0.05	0.002	0.5	0.02	0.06	0	-0.2	16.311	0.24209	384	6	380	11	383	39	-0.9	-0.2
15JT10-2	106	56	140	1	0.06	0.006	0.5	0.05	0.07	0	0.5	15.175	0.46053	411	12	411	37	469	86	0.0	12.4
15JT10-3	99	21	45	2	0.06	0.003	0.5	0.03	0.07	0	-0.1	14.006	0.35308	444	11	446	19	530	82	0.4	16.2
15JT10-4	194	32	61	3	0.06	0.003	0.6	0.03	0.08	0	0.3	13.175	0.45133	472	16	471	18	432	79	-0.2	-9.3
15JT10-5	216	37	60	3	0.05	0.003	0.5	0.03	0.07	0	0.2	14.205	0.30265	439	9	437	16	406	49	-0.3	-8.0
15JT10-6	348	125	218	2	0.05	0.003	0.4	0.02	0.06	0	-0.1	17.153	0.32364	365	7	368	13	409	66	0.8	10.7
15JT10-7	142	38	53	2	0.06	0.004	0.6	0.05	0.07	0	0.3	13.532	0.47609	459	15	457	31	456	96	-0.4	-0.7
15JT10-8	149	31	45	3	0.06	0.005	0.5	0.04	0.06	0	0.5	16.639	0.52602	376	11	376	26	448	79	0.0	16.1
15JT10-9	590	641	754	1	0.06	0.002	0.5	0.01	0.06	0	0.2	16.208	0.39402	386	9	388	10	438	46	0.5	11.9
15JT10-10	254	63	62	3	0.06	0.003	0.5	0.02	0.07	0	0.2	14.556	0.27544	428	8	426	15	447	46	-0.5	4.3
15JT10-11	640	364	377	2	0.07	0.003	0.5	0.02	0.06	0	0.2	17.953	0.45125	349	8	405	10	822	72	13.7	57.5
15JT10-12	427	109	99	3	0.06	0.002	0.5	0.02	0.06	0	0.5	16.639	0.52602	376	11	378	13	465	58	0.5	19.1
15JT10-13	313	158	122	2	0.05	0.002	0.5	0.02	0.07	0	0.3	15.04	0.20584	415	6	413	10	389	31	-0.5	-6.7

Analysis	U	Pb	Th	U	207Pb		207Pb		206Pb		error	238U		206Pb		207Pb		207Pb	Error	Disc.[1]	Disc.[2]
	(ppm)	(ppm)	(ppm)	Th	206Pb	±2σ abs.	235U	±2σ abs.	238U	±2σ abs.	corr.	206Pb	±2σ abs.	238U	±2σ abs.	235U	±2σ abs.	206Pb	±2σ abs.	%	%
15JT10-15	169	63	55	2	0.05	0.003	0.4	0.02	0.06	0	0.0	16.722	0.26566	376	6	374	14	411	51	-0.5	8.6
15JT10-16	618	399	331	1	0.05	0.001	0.5	0.01	0.07	0	0.4	14.643	0.19942	426	6	423	9	391	26	-0.6	-8.9
15JT10-17	301	77	68	3	0.05	0.004	0.5	0.03	0.07	0	-0.1	14.663	0.23650	425	7	423	20	428	86	-0.5	0.7
15JT10-18	155	42	34	3	0.06	0.003	0.5	0.03	0.07	0	0.0	15.504	0.33652	403	9	405	19	466	65	0.5	13.5
15JT10-19	116	34	32	3	0.05	0.005	0.5	0.05	0.07	0	0.1	15.456	0.74055	404	19	401	35	430	110	-0.7	6.0
15JT10-20	98	28	31	2	0.05	0.003	0.4	0.02	0.06	0	0.1	16.779	0.33782	373	7	371	18	488	76	-0.6	23.5
15JT10-21	360	410	114	2	0.09	0.001	3	0.06	0.24	0.01	0.7	4.1305	0.07678	1397	23	1397	17	1396	17	0.0	-0.1
15JT10-22	399	746	198	2	0.1	0.001	4	0.07	0.28	0	0.6	3.5162	0.05069	1613	20	1618	14	1614	15	0.3	0.1
15JT10-23	427	153	199	2	0.05	0.002	0.4	0.01	0.06	0	0.1	17.212	0.29624	364	6	368	10	405	49	1.1	10.1
15JT10-24	453	206	251	1	0.06	0.003	0.5	0.04	0.07	0	0.3	14.599	0.34099	427	10	432	23	409	67	1.1	-4.4
15JT10-25	232	92	199	1	0.05	0.003	0.4	0.02	0.06	0	-0.1	17.422	0.36421	360	7	364	17	416	66	1.2	13.5
15JT10-26	544	119	98	6	0.07	0.002	2	0.03	0.16	0	0.4	6.3857	0.11825	938	16	938	13	882	36	0.0	-6.3
15JT10-27	847	193	385	2	0.06	0.002	0.5	0.02	0.06	0	0.3	15.723	0.29667	398	7	405	13	432	50	1.8	8.0
15JT10-29	155	296	111	1	0.1	0.002	4	0.09	0.27	0.01	0.4	3.6644	0.06714	1561	25	1564	20	1581	31	0.2	1.3
15JT10-30	107	30	35	3	0.06	0.005	0.6	0.05	0.08	0	0.2	13.405	0.35938	464	12	468	32	550	130	0.9	15.6
15JT10-31	380	75	94	4	0.05	0.003	0.5	0.03	0.07	0	0.1	14.43	0.33316	432	10	435	22	430	67	0.8	-0.4
15JT10-32	289	113	154	2	0.06	0.002	0.5	0.02	0.07	0	0.2	15.267	0.23309	409	6	409	13	449	44	0.0	9.0
15JT10-33	113	75	102	1	0.06	0.005	0.5	0.04	0.07	0	0.2	15.504	0.33652	403	9	405	29	561	98	0.6	28.2
15JT10-34	443	135	217	2	0.05	0.003	0.4	0.02	0.06	0	0.2	17.094	0.40909	366	9	368	14	377	67	0.4	2.8
15JT10-35	176	79	64	2	0.06	0.004	0.7	0.05	0.09	0	0.1	11.198	0.31350	551	15	552	28	576	85	0.2	4.3
15JT10-36	609	140	177	3	0.05	0.002	0.4	0.02	0.06	0	0.3	16.75	0.28058	374	6	373	10	391	48	-0.2	4.4
15JT10-38	421	266	347	1	0.06	0.002	0.5	0.01	0.06	0	0.3	15.576	0.26688	401	6	402	10	425	42	0.2	5.6
15JT10-39	216	137	59	4	0.08	0.002	2	0.05	0.21	0	0.4	4.8426	0.09380	1212	22	1213	16	1259	26	0.1	3.7
15JT10-40	72	43	20	3	0.08	0.004	2	0.1	0.19	0.01	0.5	5.322	0.13312	1109	26	1111	33	1114	47	0.2	0.4
15JT10-41	252	69	109	2	0.05	0.003	0.4	0.02	0.06	0	0.3	17.361	0.33155	361	7	364	15	377	58	0.8	4.2
15JT10-42	194	50	84	2	0.05	0.004	0.4	0.03	0.06	0	0.1	17.036	0.34826	368	8	366	20	406	70	-0.5	9.4
15JT10-43	215	62	104	2	0.05	0.005	0.4	0.03	0.06	0	-0.1	17.422	0.36421	360	8	366	22	427	72	1.7	15.8
15JT10-44	289	90	140	2	0.05	0.002	0.5	0.02	0.06	0	0.3	15.82	0.24277	395	6	392	12	418	52	-0.8	5.5
15JT10-46	558	140	228	2	0.05	0.002	0.5	0.02	0.07	0	0.1	14.793	0.28448	422	8	421	13	423	55	-0.1	0.3
15JT10-47	173	57	86	2	0.06	0.002	0.5	0.02	0.07	0	0.2	14.535	0.31689	429	9	432	15	469	43	0.7	8.5
15JT10-51	527	266	558	1	0.05	0.002	0.5	0.02	0.06	0	0.3	16.287	0.47746	384	11	386	14	322	53	0.5	-19.3
15JT10-52	142	35	69	2	0.05	0.003	0.4	0.03	0.06	0	0.2	17.212	0.71098	364	15	365	19	385	67	0.3	5.5
15JT10-53	290	147	264	1	0.05	0.002	0.5	0.02	0.07	0	0.1	15.129	0.32042	413	8	409	14	430	50	-0.9	4.0

Analysis	U	Pb	Th	U	207Pb		207Pb		206Pb		error	238U		206Pb		207Pb		207Pb	Error	Disc.[1]	Disc.[2]
	(ppm)	(ppm)	(ppm)	Th	206Pb	±2σ abs.	235U	±2σ abs.	238U	±2σ abs.	corr.	206Pb	±2σ abs.	238U	±2σ abs.	235U	±2σ abs.	206Pb	±2σ abs.	%	%
15JT10-55	199	86	151	1	0.06	0.003	0.5	0.03	0.07	0	0.1	15.129	0.34331	413	9	416	16	434	61	0.8	4.9
15JT10-56	235	75	140	2	0.06	0.002	0.5	0.02	0.06	0	-0.2	15.723	0.29667	397	7	401	12	439	47	0.9	9.5
15JT10-58	358	169	321	1	0.05	0.002	0.5	0.02	0.07	0	-0.1	15.48	0.26359	404	7	404	13	431	45	0.1	6.4
15JT10-59	531	148	310	2	0.06	0.002	0.5	0.02	0.06	0	0.1	16.695	0.30658	375	7	394	13	441	43	4.8	14.9
15JT10-61	59	13	21	3	0.06	0.004	0.5	0.04	0.07	0	0.2	14.859	0.37533	421	11	421	27	533	86	0.0	21.0
15JT10-63	529	141	264	2	0.05	0.002	0.5	0.02	0.06	0	0.3	15.773	0.24878	396	6	398	15	406	56	0.5	2.5
15JT10-66	233	54	104	2	0.05	0.002	0.4	0.02	0.06	0	0.1	16.987	0.27123	369	6	366	12	367	47	-0.7	-0.5
15JT10-67	59	180	53	1	0.1	0.007	9	0.3	0.43	0.01	-0.1	2.3474	0.06061	2287	50	2289	32	2340	39	0.1	2.3
15JT10-68	240	76	156	1	0.05	0.002	0.4	0.02	0.06	0	0.1	17.271	0.38778	363	8	364	12	435	41	0.3	16.6
15JT10-69	968	452	880	1	0.06	0.003	0.5	0.02	0.06	0	0.2	16.287	0.66314	384	15	399	13	411	71	3.8	6.6
15JT10-70	266	56	98	2	0.06	0.002	0.5	0.02	0.07	0	0.0	14.663	0.25800	425	7	427	13	462	48	0.4	8.0
15JT10-71	162	103	67	2	0.08	0.002	2	0.04	0.19	0	0.2	5.2083	0.08681	1132	18	1129	15	1170	24	-0.3	3.2
15JT10-72	144	251	102	1	0.1	0.004	5	0.2	0.33	0.01	0.3	3.0285	0.06787	1838	36	1883	25	1900	25	2.4	3.3
15JT10-75	127	28	59	2	0.06	0.003	0.5	0.03	0.07	0	0.1	14.993	0.26973	417	7	410	17	442	49	-1.7	5.7
15JT10-76	848	133	306	3	0.05	0.002	0.4	0.01	0.06	0	0.3	17.188	0.25111	365	5	363	9	374	30	-0.3	2.5
15JT10-77	93	21	51	2	0.05	0.005	0.4	0.03	0.06	0	-0.1	17.094	0.67207	369	14	365	22	460	110	-1.1	19.8
15JT10-78	207	50	105	2	0.06	0.003	0.5	0.02	0.07	0	-0.1	15.175	0.27632	411	7	414	16	430	48	0.6	4.3
15JT10-79	295	51	105	3	0.05	0.003	0.5	0.03	0.07	0	0.2	14.065	0.33629	443	10	442	18	399	58	-0.2	-11.0
15JT10-80	171	32	69	3	0.05	0.004	0.5	0.05	0.07	0	0.2	14.577	0.48874	428	14	431	30	420	100	0.7	-1.9
15JT10-81	328	61	137	3	0.05	0.002	0.5	0.02	0.07	0	-0.1	15.244	0.27885	409	7	411	14	405	56	0.4	-1.1
15JT10-85	206	46	88	3	0.05	0.003	0.5	0.02	0.07	0	0.2	14.451	0.25059	431	7	426	16	440	59	-1.2	2.0
15JT10-86	704	180	377	2	0.05	0.002	0.5	0.02	0.07	0	0.4	15.015	0.24800	416	7	418	13	390	36	0.6	-6.6
15JT10-87	370	103	177	2	0.06	0.002	0.5	0.02	0.07	0	0.4	14.493	0.33606	432	10	432	14	507	45	0.0	14.8
15JT10-89	735	120	253	3	0.05	0.002	0.4	0.01	0.06	0	0.3	17.544	0.33857	357	7	360	9	400	39	0.9	10.7
15JT10-90	118	24	43	3	0.05	0.003	0.5	0.02	0.07	0	0.1	15.038	0.33919	415	9	413	16	460	61	-0.5	9.8
15JT10-91	273	119	266	1	0.05	0.004	0.4	0.03	0.06	0	0.1	18.182	0.52893	345	10	347	23	414	93	0.6	16.7
15JT10-92	200	61	125	2	0.05	0.004	0.4	0.03	0.06	0	0.2	17.391	0.39319	361	8	353	19	440	72	-2.1	18.1
15JT10-94	244	105	182	1	0.06	0.002	0.5	0.02	0.07	0	0.2	15.152	0.25253	412	7	413	13	484	51	0.2	14.9
15JT10-95	422	137	246	2	0.06	0.002	0.5	0.02	0.06	0	0.2	15.576	0.29115	401	7	404	12	468	54	0.7	14.3
15JT10-96	187	88	152	1	0.05	0.003	0.5	0.03	0.07	0	0.0	14.993	0.22478	416	6	413	19	449	61	-0.8	7.3
15JT10-97	173	42	58	2	0.06	0.003	0.5	0.03	0.07	0	0.0	14.184	0.26156	440	8	443	18	485	58	0.7	9.3
15JT10-98	82	85	22	3	0.2	0.009	10	0.5	0.52	0.02	-0.3	1.9157	0.05872	2704	70	2734	36	2706	56	1.1	0.1
15JT10-100	161	68	113	1	0.06	0.005	0.5	0.04	0.06	0	0.2	15.699	0.54218	398	13	409	29	530	120	2.7	24.9

Analysis	U (ppm)	Pb (ppm)	Th (ppm)	U Th	207Pb 206Pb	±2σ abs.	207Pb 235U	±2σ abs.	206Pb 238U	±2σ abs.	error corr.	238U 206Pb	±2σ abs.	206Pb 238U	±2σ abs.	207Pb 235U	±2σ abs.	207Pb 206Pb	Error ±2σ abs.	Disc.[1] %	Disc.[2] %
15JT10-101	825	142	186	4	0.06	0.002	0.5	0.02	0.07	0	0.0	14.514	0.27385	429	8	433	11	478	52	0.9	10.2
15JT10-102	126	30	45	2	0.06	0.004	0.5	0.03	0.07	0	0.0	14.925	0.40098	418	11	418	23	454	68	0.0	7.9
15JT10-103	123	119	62	2	0.08	0.004	2	0.1	0.2	0	0.2	4.9383	0.08291	1188	18	1193	44	1169	65	0.4	-1.6
15JT10-104	604	289	462	1	0.06	0.003	0.5	0.02	0.06	0	-0.3	15.848	0.40185	395	10	399	13	472	59	1.1	16.4
15JT10-105	111	21	31	3	0.06	0.005	0.6	0.06	0.08	0	0.5	13.405	0.44922	464	15	471	38	605	98	1.5	23.3
15JT10-106	181	90	139	1	0.06	0.003	0.5	0.03	0.07	0	0.0	15.106	0.22818	413	6	417	17	479	68	1.0	13.8
15JT10-107	114	303	113	1	0.1	0.004	4	0.2	0.28	0.01	0.6	3.635	0.09117	1566	35	1567	34	1609	54	0.1	2.7
15JT10-108	956	189	316	2	0.05	0.002	0.5	0.01	0.06	0	0.4	16.223	0.22371	386	5	389	9	411	29	0.8	6.2
15JT10-109	338	126	239	1	0.05	0.002	0.5	0.02	0.06	0	0.0	16.067	0.23749	389	6	395	12	404	40	1.5	3.7
15JT10-111	424	285	517	1	0.06	0.002	0.5	0.02	0.06	0	-0.1	15.528	0.26523	402	7	406	13	462	48	1.0	13.0
15JT10-112	333	267	118	2	0.1	0.003	5	0.1	0.32	0.01	0.2	3.1546	0.07066	1775	35	1799	20	1788	31	1.3	0.7
15JT10-114	94	21	35	2	0.06	0.008	0.5	0.07	0.07	0	0.1	14.925	0.53464	418	14	417	47	560	130	-0.2	25.4
15JT10-115	447	106	180	2	0.06	0.002	0.6	0.02	0.08	0	0.2	13.423	0.21621	463	7	466	11	468	39	0.6	1.0
15JT10-116	444	130	275	2	0.05	0.003	0.4	0.02	0.06	0	-0.1	17.986	0.45288	349	9	350	16	297	63	0.3	-17.4
15JT10-117	102	16	26	4	0.06	0.004	0.5	0.04	0.07	0	-0.1	14.577	0.25500	428	7	433	24	658	66	1.2	35.0
15JT10-118	256	143	282	1	0.06	0.003	0.5	0.02	0.06	0	0.1	16.835	0.45347	372	10	376	15	416	60	1.1	10.6
15JT10-121	207	70	127	2	0.06	0.005	0.5	0.05	0.07	0	0.3	14.62	0.36336	426	11	431	33	450	100	1.2	5.3
15JT10-122	298	68	151	2	0.05	0.004	0.5	0.04	0.06	0	0.2	16.779	0.47858	373	10	376	25	443	93	0.8	15.8
15JT10-124	115	34	68	2	0.05	0.003	0.5	0.03	0.06	0	0.1	16.026	0.28250	391	7	394	19	500	64	0.7	21.8
15JT10-125	259	56	125	2	0.05	0.003	0.4	0.02	0.06	0	0.0	17.825	0.31774	352	6	351	13	426	56	-0.2	17.4
15JT10-129	381	94	197	2	0.05	0.002	0.5	0.02	0.06	0	0.3	16.327	0.22124	384	5	387	12	401	48	0.8	4.3
15JT10-132	38	93	45	1	0.1	0.005	4	0.2	0.27	0.01	0.4	3.663	0.13149	1555	50	1554	49	1590	50	-0.1	2.2
15JT10-134	266	78	198	1	0.05	0.002	0.5	0.02	0.06	0	0.4	15.625	0.31738	400	8	406	13	446	41	1.5	10.3
15JT10-137	93	238	79	1	0.2	0.005	10	0.3	0.52	0.01	0.5	1.9268	0.04455	2693	52	2686	23	2694	20	-0.3	0.0
15JT10-138	126	29	72	2	0.05	0.005	0.4	0.04	0.06	0	0.1	17.123	0.76234	366	16	373	30	403	76	1.9	9.2
15JT10-140	271	116	264	1	0.06	0.002	0.5	0.02	0.06	0	0.2	15.674	0.27024	399	7	407	14	501	39	2.1	20.5
15JT10-142	395	99	228	1	0.05	0.002	0.4	0.02	0.06	0	0.3	17.762	0.37859	353	7	352	12	386	45	-0.3	8.5
15JT10-144	98	62	39	2	0.08	0.003	2	0.08	0.2	0.01	-0.2	4.9603	0.11072	1184	24	1186	26	1179	66	0.2	-0.4
15JT10-146	332	70	65	2	0.05	0.003	0.4	0.03	0.06	0	0.2	17.212	0.47399	364	10	362	20	407	72	-0.6	10.5
15JT10-147	102	422	69	0	0.1	0.002	5	0.1	0.34	0.01	0.4	2.9542	0.05586	1878	31	1886	17	1895	24	0.4	0.9
15JT10-148	179	43	36	2	0.05	0.002	0.4	0.02	0.06	0	0.2	17.036	0.40630	368	8	371	13	407	51	0.9	9.7

15JT11, experiment 4

Analysis	U	Pb	Th	U	207Pb		207Pb		206Pb		error	238U		206Pb		207Pb		207Pb	Error	Disc.[1]	Disc.[2]
	(ppm)	(ppm)	(ppm)	Th	206Pb	±2σ abs.	235U	±2σ abs.	238U	±2σ abs.	corr.	206Pb	±2σ abs.	238U	±2σ abs.	235U	±2σ abs.	206Pb	±2σ abs.	%	%
15JT11-1	160	51	95	2	0.06	0.003	0.5	0.02	0.07	0	0.2	14.97	0.35856	417	10	417	15	465	54	0.1	10.4
15JT11-4	700	168	439	2	0.05	0.002	0.4	0.02	0.06	0	0.6	18.083	0.91560	347	17	351	16	374	41	1.1	7.2
15JT11-5	51	40	26	2	0.09	0.004	3	0.1	0.23	0.01	0.3	4.4072	0.10100	1317	27	1322	30	1353	50	0.4	2.7
15JT11-6	83	154	84	1	0.09	0.004	3	0.2	0.26	0.01	0.4	3.8506	0.12306	1487	42	1489	35	1529	41	0.1	2.7
15JT11-8	102	98	48	2	0.1	0.003	4	0.1	0.28	0.01	0.5	3.5436	0.08037	1602	32	1620	30	1630	37	1.1	1.7
15JT11-9	573	98	214	3	0.05	0.002	0.4	0.02	0.06	0	0.3	17.575	0.37064	357	7	357	12	326	40	0.1	-9.4
15JT11-10	440	127	317	2	0.05	0.002	0.4	0.01	0.06	0	0.2	16.961	0.27616	369	6	371	11	363	45	0.5	-1.7
15JT11-11	93	41	35	3	0.08	0.005	2	0.07	0.17	0.01	0.1	5.7703	0.22309	1030	37	1067	27	1138	67	3.5	9.5
15JT11-13	953	237	484	2	0.06	0.002	0.5	0.02	0.07	0	0.3	14.948	0.67030	417	18	424	11	456	44	1.7	8.6
15JT11-14	128	138	76	2	0.1	0.005	4	0.2	0.27	0.01	0.3	3.7679	0.11216	1517	40	1582	40	1663	56	4.1	8.8
15JT11-15	345	87	196	2	0.05	0.003	0.4	0.02	0.06	0	0.1	16.722	0.36353	374	8	378	12	343	57	1.0	-9.1
15JT11-16	236	17	33	8	0.05	0.004	0.4	0.02	0.05	0	0.1	19.92	0.63491	315	10	320	18	418	98	1.4	24.5
15JT11-17	347	61	155	2	0.05	0.003	0.4	0.02	0.06	0	-0.1	17.953	0.48348	349	9	348	15	331	58	-0.3	-5.5
15JT11-18	375	147	291	1	0.06	0.003	0.5	0.02	0.06	0	0.6	16.155	0.54807	387	13	392	16	516	54	1.3	25.0
15JT11-20	131	33	59	3	0.06	0.005	0.5	0.04	0.07	0	0.2	14.881	0.62004	419	17	419	30	484	91	0.0	13.4
15JT11-22	96	27	51	2	0.06	0.006	0.5	0.05	0.06	0	0.2	15.949	0.58505	392	14	402	30	460	110	2.5	14.8
15JT11-23	205	90	190	1	0.05	0.003	0.5	0.02	0.06	0	0.1	15.873	0.32754	394	8	397	15	397	69	0.8	0.8
15JT11-24	628	177	369	2	0.05	0.002	0.4	0.01	0.06	0	0.2	17.153	0.29421	365	6	366	9	386	39	0.2	5.4
15JT11-26	713	131	266	3	0.05	0.002	0.4	0.01	0.06	0	0.4	17.731	0.34581	354	7	356	7	379	28	0.7	6.7
15JT11-27	227	67	116	2	0.06	0.004	0.5	0.04	0.07	0	0.0	14.514	0.56876	429	16	432	25	481	89	0.7	10.8
15JT11-28	225	73	138	2	0.05	0.003	0.4	0.03	0.06	0	0.0	16.835	0.39678	372	8	372	19	382	95	0.0	2.6
15JT11-29	460	62	46	#	0.07	0.005	2	0.06	0.16	0.01	0.3	6.25	0.42969	954	61	977	24	1059	54	2.4	9.9
15JT11-30	81	1	1	#	0.06	0.005	0.9	0.07	0.1	0	0.1	9.9404	0.23715	618	14	624	35	665	95	1.0	7.1
15JT11-31	337	169	292	1	0.05	0.002	0.5	0.02	0.07	0	0.1	15.48	0.31151	403	8	406	12	409	60	0.7	1.4
15JT11-32	1386	373	903	2	0.05	0.002	0.4	0.02	0.05	0	0.3	19.531	0.61035	322	10	328	11	379	45	1.8	15.0
15JT11-33	351	202	391	1	0.06	0.003	0.5	0.03	0.06	0	0.3	15.773	0.42293	396	10	400	19	482	68	1.0	17.8
15JT11-35	607	397	779	1	0.05	0.002	0.4	0.02	0.06	0	0.2	16.892	0.39947	371	9	373	11	388	48	0.6	4.4
15JT11-36	116	48	79	2	0.06	0.005	0.5	0.04	0.07	0	0.1	15.314	0.51594	408	13	411	28	580	110	0.7	29.7
15JT11-37	170	74	135	1	0.05	0.003	0.5	0.03	0.06	0	0.1	15.898	0.35386	393	9	393	18	417	61	-0.1	5.7
15JT11-38	391	191	324	1	0.06	0.002	0.5	0.02	0.07	0	0.3	15.038	0.24874	415	7	419	11	435	36	1.0	4.6
15JT11-39	214	265	131	2	0.09	0.002	3	0.08	0.24	0.01	0.4	4.1374	0.08045	1395	25	1402	19	1457	25	0.5	4.3
15JT11-40	453	192	368	1	0.05	0.002	0.5	0.01	0.06	0	0.1	15.866	0.22402	394	5	396	10	430	39	0.5	8.4
15JT11-42	92	232	104	1	0.1	0.003	4	0.1	0.27	0.01	0.5	3.7216	0.08310	1534	30	1555	28	1619	28	1.4	5.3

Analysis	U	Pb	Th	U	207Pb		207Pb		206Pb		error	238U		206Pb		207Pb		207Pb	Error	Disc.[1]	Disc.[2]
	(ppm)	(ppm)	(ppm)	Th	206Pb	±2σ abs.	235U	±2σ abs.	238U	±2σ abs.	corr.	206Pb	±2σ abs.	238U	±2σ abs.	235U	±2σ abs.	206Pb	±2σ abs.	%	%
15JT11-43	469	191	346	1	0.05	0.002	0.5	0.02	0.06	0	0.3	15.873	0.37793	394	9	397	14	380	48	0.8	-3.6
15JT11-44	500	313	552	1	0.06	0.002	0.5	0.02	0.07	0	0.4	15.385	0.40237	406	10	408	13	446	37	0.5	9.0
15JT11-46	182	185	111	2	0.08	0.004	2	0.1	0.18	0.01	0.6	5.5249	0.15873	1072	29	1077	36	1205	57	0.5	11.0
15JT11-47	158	32	54	3	0.06	0.004	0.5	0.04	0.07	0	0.2	15.06	0.38558	414	10	419	25	522	96	1.2	20.7
15JT11-48	395	109	209	2	0.05	0.003	0.5	0.03	0.06	0	0.4	16.475	0.37997	380	9	383	20	416	69	0.8	8.6
15JT11-49	631	150	352	2	0.05	0.003	0.4	0.02	0.05	0	-0.1	19.455	0.56776	323	9	326	16	365	97	0.8	11.4
15JT11-50	158	37	67	2	0.05	0.003	0.5	0.04	0.06	0	0.4	16.026	0.53932	390	13	386	24	421	81	-1.0	7.4
15JT11-51	147	145	46	4	0.2	0.006	9	0.4	0.43	0.02	0.4	2.3256	0.08113	2302	69	2357	35	2404	42	2.3	4.2
15JT11-52	214	36	48	5	0.06	0.002	0.7	0.03	0.09	0	0.4	11.628	0.22985	532	10	533	15	566	37	0.2	6.0
15JT11-53	442	99	192	2	0.05	0.002	0.5	0.01	0.06	0	0.3	16.033	0.23650	390	6	391	9	418	31	0.3	6.7
15JT11-54	248	101	179	2	0.05	0.004	0.5	0.04	0.07	0	0.4	14.728	0.47718	423	13	419	26	454	83	-1.0	6.8
15JT11-55	142	67	139	1	0.06	0.005	0.4	0.04	0.05	0	0.0	18.657	0.55692	337	10	354	25	450	120	4.8	25.1
15JT11-56	121	24	48	3	0.05	0.005	0.4	0.03	0.05	0	0.1	18.797	0.45933	334	8	333	23	411	89	-0.4	18.6
15JT11-57	347	134	241	2	0.05	0.002	0.5	0.02	0.07	0	0.3	15.314	0.30487	408	8	408	13	440	42	0.1	7.4
15JT11-58	358	367	165	2	0.1	0.005	4	0.1	0.28	0.01	0.2	3.5714	0.16582	1589	67	1620	25	1648	32	1.9	3.6
15JT11-59	180	426	128	1	0.1	0.003	9	0.2	0.43	0.01	0.7	2.3288	0.04285	2302	35	2309	17	2324	19	0.3	0.9
15JT11-60	317	162	116	3	0.08	0.004	2	0.06	0.19	0.01	0.0	5.3792	0.16783	1099	31	1109	22	1119	33	0.9	1.8
15JT11-61	146	106	58	3	0.09	0.003	3	0.1	0.23	0	0.3	4.3535	0.08150	1333	22	1328	27	1359	39	-0.4	1.9
15JT11-62	557	162	372	2	0.05	0.003	0.4	0.02	0.06	0	0.2	18.018	0.55190	348	11	347	15	356	58	-0.3	2.2
15JT11-64	562	125	270	2	0.06	0.004	0.4	0.03	0.06	0	0.1	17.731	0.81736	354	16	368	17	488	88	3.8	27.5
15JT11-65	897	252	405	2	0.06	0.003	0.7	0.02	0.08	0	0.2	12.255	0.39047	506	15	511	15	546	43	1.0	7.3
15JT11-66	1227	387	820	1	0.05	0.002	0.4	0.01	0.06	0	0.4	17.637	0.40437	355	8	360	7	416	27	1.3	14.6
15JT11-67	263	38	91	3	0.05	0.002	0.3	0.02	0.05	0	0.5	21.692	0.51760	290	7	290	12	246	50	-0.1	-18.0
15JT11-68	266	503	245	1	0.1	0.005	4	0.2	0.27	0.01	0.0	3.7313	0.15315	1531	57	1567	34	1636	43	2.3	6.4
15JT11-69	339	113	179	2	0.05	0.003	0.5	0.04	0.07	0	0.9	15.083	0.45499	414	12	410	24	416	53	-1.0	0.5
15JT11-71	518	163	308	2	0.05	0.002	0.5	0.02	0.06	0	0.5	16.367	0.45537	382	10	383	12	438	38	0.3	12.8
15JT11-72	296	44	85	3	0.06	0.004	0.5	0.03	0.07	0	-0.2	15.456	0.43000	404	11	403	18	414	75	-0.2	2.4
15JT11-73	129	108	72	2	0.08	0.003	2	0.05	0.18	0	-0.2	5.4377	0.10941	1088	20	1081	18	1126	38	-0.6	3.4
15JT11-74	438	160	310	1	0.05	0.002	0.5	0.02	0.06	0	0.3	15.967	0.23709	392	6	389	11	412	42	-0.6	5.0
15JT11-75	269	129	157	2	0.06	0.003	0.9	0.04	0.11	0	0.0	9.3458	0.27077	655	18	657	19	724	64	0.3	9.5
15JT11-76	279	79	130	2	0.06	0.002	0.5	0.02	0.07	0	0.1	15.011	0.20053	416	5	411	11	442	43	-1.1	6.0
15JT11-77	210	33	60	4	0.06	0.003	0.5	0.02	0.07	0	0.0	15.198	0.27716	412	7	408	13	482	59	-0.9	14.6
15JT11-79	485	158	327	1	0.06	0.003	0.5	0.02	0.06	0	0.0	16.537	0.26254	379	6	380	14	459	48	0.4	17.5

Analysis	U	Pb	Th	U	207Pb		207Pb		206Pb		error	238U		206Pb		207Pb		207Pb	Error	Disc.[1]	Disc.[2]
	(ppm)	(ppm)	(ppm)	Th	206Pb	±2σ abs.	235U	±2σ abs.	238U	±2σ abs.	corr.	206Pb	±2σ abs.	238U	±2σ abs.	235U	±2σ abs.	206Pb	±2σ abs.	%	%
15JT11-80	318	176	368	1	0.05	0.003	0.4	0.03	0.06	0	0.4	17.065	0.46593	367	10	369	17	407	64	0.5	9.8
15JT11-83	122	61	41	3	0.07	0.003	2	0.06	0.18	0	0.0	5.7045	0.11715	1041	20	1036	23	1001	53	-0.5	-4.0
15JT11-84	486	113	213	2	0.06	0.003	0.5	0.03	0.06	0	-0.1	15.625	0.41504	400	10	405	19	489	88	1.2	18.2
15JT11-85	845	160	375	2	0.05	0.002	0.3	0.01	0.05	0	0.4	21.782	0.33686	289	4	290	9	326	51	0.3	11.2
15JT11-86	285	89	190	1	0.05	0.003	0.4	0.02	0.06	0	0.1	17.544	0.40012	357	8	359	15	415	58	0.5	13.9
15JT11-87	523	97	216	2	0.05	0.003	0.4	0.03	0.06	0	0.0	18.248	0.36630	344	7	342	19	368	80	-0.6	6.5
15JT11-88	347	77	164	2	0.05	0.004	0.4	0.02	0.06	0	0.0	17.452	0.70052	359	14	354	16	289	83	-1.4	-24.2
15JT11-89	654	346	640	1	0.06	0.003	0.5	0.03	0.06	0	0.1	15.699	0.64076	398	15	396	19	446	62	-0.5	10.8
15JT11-90	284	92	164	2	0.05	0.003	0.5	0.02	0.06	0	0.4	15.949	0.43243	392	10	386	16	391	39	-1.6	-0.3
15JT11-91	478	170	327	1	0.06	0.003	0.4	0.02	0.06	0	0.3	17.182	0.56093	365	12	366	14	459	69	0.3	20.5
15JT11-92	704	301	608	1	0.05	0.002	0.4	0.02	0.06	0	0.4	17.036	0.46435	367	10	367	11	389	43	-0.1	5.6
15JT11-93	390	116	237	2	0.05	0.005	0.4	0.03	0.06	0	0.1	17.241	0.53508	363	11	358	23	297	79	-1.4	-22.2
15JT11-95	479	188	130	4	0.08	0.002	2	0.09	0.19	0.01	0.6	5.152	0.19642	1143	40	1138	28	1146	20	-0.4	0.3
15JT11-96	266	46	95	3	0.05	0.003	0.4	0.02	0.06	0	0.3	17.953	0.30621	349	6	350	13	442	47	0.2	21.0
15JT11-97	1077	226	442	2	0.06	0.002	0.4	0.02	0.05	0	0.4	18.832	0.74478	333	13	333	12	406	61	0.0	18.0
15JT11-98	570	292	467	1	0.06	0.004	0.5	0.03	0.06	0	0.1	16.026	0.61637	390	15	394	20	481	99	1.0	18.9
15JT11-99	407	210	323	1	0.05	0.002	0.5	0.02	0.06	0	0.1	15.748	0.32240	397	8	398	12	433	53	0.3	8.4
15JT11-100	319	95	157	2	0.05	0.003	0.5	0.02	0.07	0	0.2	14.948	0.33515	417	9	413	15	422	47	-1.0	1.1
15JT11-101	405	413	404	1	0.06	0.002	0.9	0.02	0.11	0	0.1	9.1158	0.13296	671	9	672	13	702	33	0.2	4.4
15JT11-103	454	167	296	2	0.05	0.002	0.4	0.02	0.06	0	0.5	18.315	0.43607	343	8	343	12	378	47	0.1	9.4
15JT11-104	707	147	275	2	0.05	0.002	0.4	0.02	0.06	0	0.3	17.331	0.36044	362	8	361	12	383	50	-0.1	5.6
15JT11-105	568	124	223	2	0.05	0.002	0.4	0.01	0.06	0	0.0	17.544	0.33857	358	7	357	8	381	39	-0.1	6.2
15JT11-106	689	316	473	1	0.05	0.002	0.5	0.02	0.07	0	0.3	14.577	0.29750	428	8	425	10	458	37	-0.7	6.6
15JT11-107	472	116	201	2	0.05	0.002	0.4	0.02	0.06	0	0.7	16.807	0.84740	372	18	371	16	442	43	-0.3	15.8
15JT11-108	606	194	312	2	0.05	0.003	0.5	0.03	0.06	0	0.6	15.823	0.55079	395	13	390	23	389	56	-1.3	-1.5
15JT11-110	132	124	56	2	0.09	0.003	3	0.09	0.23	0	0.4	4.3141	0.07817	1343	22	1346	24	1357	31	0.2	1.0
15JT11-111	168	391	145	1	0.1	0.003	5	0.1	0.32	0.01	0.2	3.1706	0.07539	1772	38	1773	18	1816	32	0.1	2.4
15JT11-112	286	92	152	2	0.05	0.003	0.5	0.02	0.06	0	0.1	16.287	0.42441	386	10	382	15	406	67	-1.0	5.0
15JT11-113	280	48	49	6	0.06	0.005	0.9	0.06	0.1	0.01	0.0	9.5511	0.49261	642	31	645	31	695	61	0.5	7.6
15JT11-114	1422	403	858	2	0.05	0.002	0.4	0.01	0.05	0	0.1	20.08	0.48386	313	8	314	10	339	45	0.3	7.7
15JT11-115	214	162	68	3	0.1	0.002	4	0.07	0.27	0.01	0.3	3.6819	0.07592	1548	28	1547	15	1553	22	-0.1	0.3
15JT11-116	377	203	356	1	0.05	0.003	0.4	0.03	0.06	0	0.4	17.182	0.64950	364	13	364	18	411	49	0.0	11.4
15JT11-117	1471	264	529	3	0.05	0.002	0.4	0.01	0.06	0	0.3	17.889	0.51203	350	10	352	8	350	32	0.6	0.0

Analysis	U (ppm)	Pb (ppm)	Th (ppm)	U/Th	207Pb/206Pb	±2σ abs.	207Pb/235U	±2σ abs.	206Pb/238U	±2σ abs.	error corr.	238U/206Pb	±2σ abs.	206Pb/238U	±2σ abs.	207Pb/235U	±2σ abs.	207Pb/206Pb	Error ±2σ abs.	Disc.[1] %	Disc.[2] %
15JT11-118	188	41	62	3	0.06	0.003	0.5	0.03	0.06	0	0.1	15.773	0.34830	397	9	397	18	430	46	0.1	7.8
15JT11-119	493	62	119	4	0.05	0.003	0.4	0.02	0.06	0	-0.1	16.75	0.42086	374	9	374	14	395	66	0.1	5.4
15JT11-120	438	132	229	2	0.06	0.002	0.5	0.02	0.06	0	0.2	15.823	0.45065	397	11	395	10	424	45	-0.5	6.4
15JT11, experiment 5																					
15JT11-121	202	34	56	3	0.06	0.003	0.6	0.03	0.07	0	-0.2	14.045	0.35507	443	11	448	18	490	64	1.1	9.6
15JT11-122	381	59	47	7	0.07	0.001	1	0.04	0.15	0	0.8	6.6007	0.16556	909	21	915	18	931	23	0.7	2.4
15JT11-123	454	84	182	2	0.05	0.003	0.4	0.02	0.06	0	0.3	17.241	0.59453	364	12	366	14	395	59	0.5	7.8
15JT11-124	942	135	288	3	0.06	0.002	0.4	0.02	0.06	0	0.4	17.212	0.41474	364	9	369	11	388	41	1.3	6.1
15JT11-125	401	75	150	2	0.05	0.003	0.4	0.02	0.06	0	0.1	18.235	0.31588	344	6	348	12	377	77	1.1	8.7
15JT11-126	273	169	131	2	0.07	0.003	2	0.07	0.17	0.01	0.4	5.9844	0.17907	996	27	1007	25	1038	27	1.1	4.0
15JT11-127	148	149	78	2	0.09	0.003	3	0.09	0.24	0.01	0.4	4.1719	0.11487	1384	34	1394	24	1398	32	0.7	1.0
15JT11-128	143	74	46	3	0.07	0.002	2	0.08	0.18	0.01	0.8	5.6657	0.19581	1053	35	1056	27	1053	32	0.3	0.0
15JT11-130	112	85	41	2	0.1	0.004	4	0.1	0.27	0.01	0.2	3.7051	0.09747	1539	36	1547	32	1584	41	0.5	2.8
15JT11-131	258	114	180	1	0.06	0.004	0.5	0.04	0.07	0	0.6	15.106	0.86710	413	23	414	28	530	66	0.2	22.1
15JT11-132	526	120	255	2	0.05	0.002	0.4	0.02	0.06	0	0.2	17.483	0.39733	358	8	363	13	393	44	1.3	8.8
15JT11-134	449	250	224	2	0.08	0.003	2	0.06	0.18	0.01	0.1	5.4201	0.16157	1091	30	1094	18	1105	40	0.3	1.3
15JT11-135	531	219	626	2	0.06	0.002	0.5	0.02	0.06	0	0.4	15.748	0.37200	397	9	400	11	435	33	0.8	8.8
15JT11-136	474	101	246	2	0.05	0.002	0.4	0.02	0.06	0	0.3	18.149	0.39526	346	7	346	11	395	35	0.1	12.5
15JT11-137	553	117	108	6	0.07	0.003	1	0.05	0.15	0.01	0.4	6.5833	0.25137	911	33	917	21	914	38	0.7	0.3
15JT11-138	578	268	649	1	0.05	0.002	0.4	0.02	0.05	0	0.2	18.416	0.47482	343	9	347	12	404	65	1.2	15.1
15JT11-139	263	76	193	2	0.05	0.005	0.5	0.04	0.06	0	0.1	16.529	0.62837	378	14	378	28	583	95	0.0	35.2
15JT11-140	1363	313	885	2	0.05	0.003	0.4	0.02	0.06	0	0.0	17.953	0.51571	349	10	350	14	400	60	0.2	12.7
15JT11-141	494	146	373	2	0.05	0.002	0.4	0.02	0.06	0	0.3	17.794	0.47492	352	9	353	11	334	47	0.2	-5.4
15JT11-142	301	177	360	1	0.06	0.003	0.5	0.03	0.07	0	0.2	15.038	0.45226	415	12	420	18	448	56	1.2	7.4
15JT11-143	240	37	93	3	0.06	0.004	0.4	0.03	0.06	0	0.1	17.212	0.47399	364	10	369	20	496	65	1.4	26.6
15JT11-144	135	195	110	1	0.09	0.003	3	0.1	0.26	0.01	0.7	3.8971	0.14732	1471	50	1477	32	1556	28	0.4	5.5
15JT11-145	314	104	178	2	0.06	0.003	0.5	0.03	0.07	0	0.0	15.038	0.36181	415	10	413	18	463	53	-0.5	10.3
15JT11-147	178	69	54	3	0.07	0.002	2	0.05	0.16	0	0.3	6.3654	0.10535	941	14	939	19	1002	47	-0.2	6.1
15JT11-148	112	248	118	1	0.09	0.003	3	0.1	0.25	0.01	0.4	4.0032	0.11699	1436	38	1427	27	1447	30	-0.6	0.8
15JT11-149	204	37	37	6	0.06	0.002	0.9	0.03	0.1	0	0.3	9.6805	0.20617	634	13	631	19	669	38	-0.5	5.2
15JT11-150	535	191	335	2	0.05	0.004	0.5	0.04	0.07	0	0.3	14.793	0.61272	421	17	413	26	428	98	-1.9	1.6

Analysis	U (ppm)	Pb (ppm)	Th (ppm)	U Th	207Pb 206Pb	±2σ abs.	207Pb 235U	±2σ abs.	206Pb 238U	±2σ abs.	error corr.	238U 206Pb	±2σ abs.	206Pb 238U	±2σ abs.	207Pb 235U	±2σ abs.	207Pb 206Pb	Error ±2σ abs.	Disc.[1] %	Disc.[2] %
16JT11, experiment 5																					
16JT11-1	327	227	134	2	0.08	0.003	2	0.08	0.19	0.01	0.3	5.144	0.12701	1145	26	1129	28	1095	44	-1.4	-4.6
16JT11-2	1435	916	1448	1	0.06	0.002	0.5	0.01	0.07	0	0.4	14.409	0.37373	432	11	427	9	456	53	-1.2	5.3
16JT11-3	201	150	197	1	0.06	0.003	0.6	0.02	0.08	0	0.0	13.333	0.21333	466	7	458	16	466	50	-1.8	0.0
16JT11-5	619	209	149	4	0.08	0.003	2	0.07	0.16	0.01	0.5	6.3532	0.22604	942	31	965	26	1077	58	2.4	12.5
16JT11-6	372	117	185	2	0.05	0.002	0.5	0.02	0.07	0	0.3	15.175	0.36843	411	10	407	14	373	46	-1.1	-10.3
16JT11-7	338	148	117	3	0.07	0.001	2	0.03	0.16	0	0.3	6.435	0.11181	931	15	929	12	932	25	-0.2	0.1
16JT11-8	314	103	198	2	0.05	0.003	0.4	0.02	0.06	0	0.4	17.182	0.32475	364	7	365	15	389	53	0.2	6.3
16JT11-9	339	363	167	2	0.1	0.002	4	0.09	0.28	0.01	0.6	3.5474	0.07047	1600	28	1596	18	1615	20	-0.3	0.9
16JT11-10	355	208	415	1	0.05	0.003	0.4	0.03	0.06	0	0.3	16.835	0.36844	372	8	367	20	322	62	-1.4	-15.5
16JT11-11	628	355	319	3	0.07	0.002	1	0.06	0.15	0.01	0.7	6.734	0.21766	892	27	887	25	927	37	-0.6	3.8
16JT11-13	723	121	97	8	0.07	0.002	1	0.03	0.15	0	0.0	6.6756	0.17380	899	22	900	12	913	33	0.1	1.5
16JT11-14	384	324	214	2	0.08	0.002	2	0.04	0.2	0	0.4	4.995	0.06487	1176	14	1176	14	1213	24	0.0	3.1
16JT11-16	132	137	95	2	0.08	0.004	2	0.08	0.18	0.01	-0.1	5.5586	0.16376	1066	29	1065	28	1056	54	-0.1	-0.9
16JT11-17	51	128	92	1	0.08	0.004	2	0.09	0.18	0	0.0	5.5586	0.10197	1066	18	1118	29	1201	42	4.7	11.2
16JT11-18	717	26	21	#	0.07	0.002	2	0.06	0.18	0.01	0.8	5.6915	0.19436	1043	33	1045	20	1071	17	0.2	2.6
16JT11-19	119	257	112	1	0.1	0.005	5	0.3	0.32	0.01	0.6	3.0864	0.10479	1806	52	1828	46	1836	45	1.2	1.6
16JT11-20	180	351	210	1	0.09	0.004	3	0.08	0.23	0.01	-0.3	4.4248	0.11356	1313	31	1330	21	1338	45	1.3	1.9
16JT11-21	114	115	64	2	0.09	0.004	3	0.1	0.24	0.01	0.2	4.1186	0.12044	1401	37	1417	24	1384	30	1.1	-1.2
16JT11-23	227	63	54	5	0.07	0.004	1	0.07	0.15	0.01	0.1	6.5963	0.23931	910	31	927	30	914	63	1.8	0.4
16JT11-24	558	211	105	6	0.1	0.002	4	0.08	0.3	0.01	0.5	3.3445	0.06264	1686	28	1705	15	1682	15	1.1	-0.2
16JT11-26	913	482	1006	1	0.05	0.002	0.4	0.02	0.05	0	0.8	20.243	1.39320	310	21	319	17	334	54	2.8	7.2
16JT11-27	479	686	506	1	0.08	0.003	2	0.08	0.19	0.01	0.5	5.3419	0.16265	1106	31	1125	27	1109	45	1.7	0.3
16JT11-28	308	142	170	2	0.06	0.003	0.9	0.03	0.1	0	0.2	10.02	0.23092	613	14	628	15	649	56	2.4	5.5
16JT11-30	249	139	115	2	0.07	0.002	2	0.05	0.16	0	0.4	6.3452	0.14091	943	19	966	18	943	27	2.4	0.0
16JT11-35	753	590	1007	1	0.06	0.004	0.5	0.03	0.07	0	0.1	14.881	0.53146	419	15	435	18	494	58	3.7	15.2
16JT11-36	217	78	58	3	0.07	0.004	2	0.06	0.15	0	0.2	6.5876	0.17359	911	22	940	22	914	57	3.1	0.3
16JT11-39	341	738	357	1	0.1	0.002	4	0.07	0.27	0.01	0.4	3.7258	0.07218	1532	26	1564	15	1563	22	2.0	2.0
16JT11-41	363	358	253	1	0.07	0.003	2	0.06	0.18	0.01	0.5	5.6915	0.22675	1043	38	1066	23	1055	33	2.2	1.1
16JT11-42	439	276	181	2	0.08	0.003	2	0.07	0.19	0.01	0.6	5.2604	0.22414	1121	44	1158	24	1139	45	3.2	1.6
16JT11-44	307	494	346	1	0.07	0.002	2	0.06	0.17	0.01	0.6	5.9952	0.20487	994	31	1008	21	1020	34	1.4	2.5
16JT11-45	1025	263	199	4	0.07	0.002	2	0.07	0.17	0.01	0.6	5.787	0.25452	1027	41	1049	25	1065	29	2.1	3.6
16JT11-46	217	53	86	2	0.06	0.003	0.6	0.03	0.07	0	0.1	13.441	0.28905	462	10	473	17	530	54	2.2	12.8

Analysis	U	Pb	Th	U	207Pb		207Pb		206Pb		error	238U		206Pb		207Pb		207Pb	Error	Disc.[1]	Disc.[2]
	(ppm)	(ppm)	(ppm)	Th	206Pb	±2σ abs.	235U	±2σ abs.	238U	±2σ abs.	corr.	206Pb	±2σ abs.	238U	±2σ abs.	235U	±2σ abs.	206Pb	±2σ abs.	%	%
16JT11-49	769	1532	1090	1	0.08	0.003	2	0.08	0.19	0.01	0.4	5.1573	0.13565	1142	27	1157	25	1169	46	1.3	2.3
16JT11-51	99	247	86	1	0.1	0.005	5	0.2	0.32	0.01	0.2	3.1626	0.09202	1770	45	1784	36	1719	36	0.8	-3.0
16JT11-52	606	331	251	2	0.07	0.002	2	0.03	0.16	0	0.3	6.3776	0.13015	938	18	953	10	960	24	1.6	2.3
16JT11-54	759	210	138	4	0.08	0.003	2	0.2	0.2	0.01	0.9	4.9751	0.32177	1179	68	1183	59	1178	55	0.3	-0.1
16JT11-55	99	55	111	1	0.06	0.004	0.6	0.05	0.08	0	0.3	12.422	0.27777	499	11	497	28	630	80	-0.4	20.8
16JT11-57	308	212	389	1	0.06	0.002	0.7	0.03	0.08	0	0.1	11.947	0.25693	518	10	520	16	534	50	0.4	3.0
16JT11-58	78	100	109	1	0.07	0.007	2	0.1	0.16	0.01	-0.2	6.25	0.28516	956	41	953	53	930	110	-0.3	-2.8
16JT11-59	405	137	386	1	0.06	0.003	0.4	0.03	0.06	0	0.0	17.065	0.49506	367	11	371	20	385	76	1.1	4.7
16JT11-61	271	499	303	1	0.1	0.002	4	0.08	0.3	0.01	0.3	3.3636	0.05318	1677	23	1682	16	1705	22	0.3	1.6
16JT11-62	192	116	105	2	0.08	0.003	2	0.1	0.18	0	0.3	5.4171	0.11445	1092	21	1095	32	1125	54	0.3	2.9
16JT11-63	205	263	174	1	0.1	0.003	4	0.1	0.31	0.01	0.3	3.2457	0.05689	1730	27	1729	18	1750	22	-0.1	1.1
16JT11-64	263	83	195	2	0.06	0.003	0.5	0.03	0.07	0	0.3	14.245	0.32467	438	9	442	17	517	61	1.0	15.4
16JT11-65	181	47	135	2	0.06	0.004	0.5	0.04	0.07	0	0.2	15.06	0.47630	414	13	412	25	475	81	-0.5	12.8
16JT11-66	207	141	126	2	0.09	0.003	3	0.1	0.23	0.01	0.7	4.386	0.21160	1320	60	1318	40	1288	49	-0.2	-2.5
16JT11-67	55	187	72	1	0.1	0.006	4	0.2	0.28	0.01	0.0	3.5286	0.10583	1607	43	1608	44	1595	51	0.1	-0.8
16JT11-68	178	85	46	3	0.08	0.004	2	0.08	0.19	0.01	0.0	5.1414	0.13217	1145	27	1142	25	1089	61	-0.3	-5.1
16JT11-69	288	139	99	3	0.07	0.003	1	0.04	0.14	0	-0.1	6.9013	0.15241	872	18	872	17	876	39	0.0	0.5
16JT11-71	73	116	43	1	0.1	0.005	4	0.2	0.28	0.01	0.1	3.5461	0.12323	1610	46	1606	34	1635	49	-0.2	1.5
16JT11-72	296	78	102	2	0.06	0.003	0.5	0.02	0.06	0	0.3	15.625	0.36621	400	9	398	16	482	57	-0.5	17.0
16JT11-75	321	486	106	2	0.2	0.007	10	0.4	0.48	0.02	0.5	2.0833	0.10417	2520	100	2583	31	2680	22	2.4	6.0
16JT11-76	226	282	107	2	0.09	0.004	3	0.1	0.24	0.01	0.4	4.2052	0.13440	1375	40	1376	33	1459	41	0.1	5.8
16JT11-77	712	357	372	2	0.06	0.002	0.7	0.02	0.08	0	0.3	11.891	0.26863	520	11	525	13	566	43	1.0	8.1
16JT11-78	704	184	167	3	0.06	0.003	0.7	0.04	0.09	0	0.3	11.249	0.37959	549	18	545	21	597	62	-0.7	8.0
16JT11-79	779	186	262	2	0.06	0.004	0.5	0.03	0.07	0	0.2	15.504	0.60093	403	15	414	19	550	82	2.7	26.7
16JT11-80	730	593	904	1	0.05	0.003	0.5	0.02	0.06	0	0.1	16.556	0.54822	378	12	379	15	401	43	0.3	5.7
16JT11-81	486	331	202	2	0.07	0.003	2	0.07	0.17	0.01	0.4	5.7737	0.18001	1029	30	1030	27	1064	48	0.1	3.3
16JT11-82	431	11	7	#	0.07	0.003	1	0.06	0.14	0	0.4	7.0721	0.19006	853	22	851	26	869	36	-0.2	1.8
16JT11-83	600	175	121	#	0.06	0.002	1	0.05	0.12	0	0.8	8.6207	0.28983	707	23	707	26	733	45	0.0	3.5
16JT11-84	409	322	155	2	0.1	0.003	3	0.1	0.25	0.01	0.4	4.0306	0.11535	1428	36	1454	25	1536	44	1.8	7.0
16JT11-86	366	284	447	1	0.06	0.004	0.6	0.05	0.08	0	0.5	12.626	0.52609	491	20	497	28	531	55	1.2	7.5
16JT11-87	591	113	71	8	0.08	0.002	2	0.05	0.18	0.01	0.4	5.5036	0.14539	1076	26	1080	18	1126	31	0.4	4.4
16JT11-90	331	101	223	2	0.06	0.002	0.4	0.02	0.06	0	0.1	16.949	0.45964	369	10	369	13	452	43	-0.1	18.3
16JT11-91	168	372	207	1	0.1	0.006	5	0.1	0.33	0.01	-0.1	3.003	0.09920	1853	52	1866	26	1882	44	0.7	1.5

Analysis	U (ppm)	Pb (ppm)	Th (ppm)	U Th	207Pb 206Pb	±2σ abs.	207Pb 235U	±2σ abs.	206Pb 238U	±2σ abs.	error corr.	238U 206Pb	±2σ abs.	206Pb 238U	±2σ abs.	207Pb 235U	±2σ abs.	207Pb 206Pb	Error ±2σ abs.	Disc.[1] %	Disc.[2] %
16JT11-92	123	248	101	1	0.2	0.008	10	0.5	0.49	0.02	0.2	2.0492	0.08818	2576	94	2591	36	2617	35	0.6	1.6
16JT11-93	420	229	572	1	0.05	0.003	0.4	0.02	0.06	0	0.0	16.978	0.40355	369	9	376	14	417	49	2.0	11.6
16JT11-94	320	612	335	1	0.1	0.01	6	0.2	0.33	0.02	0.2	3.0395	0.22173	1830	120	1905	30	1991	58	3.9	8.1
16JT11-95	139	239	140	1	0.1	0.007	4	0.2	0.26	0.02	0.3	3.7879	0.22957	1509	84	1558	34	1638	53	3.1	7.9
16JT11-96	735	75	72	#	0.07	0.002	1	0.05	0.15	0.01	0.5	6.7522	0.24164	889	30	902	20	963	29	1.4	7.7
16JT11-98	672	338	614	1	0.05	0.005	0.4	0.04	0.06	0.01	0.3	17.036	1.50910	367	31	369	27	740	110	0.5	50.4
16JT11-100	1321	361	701	2	0.06	0.003	0.5	0.02	0.06	0	0.0	15.576	0.67934	401	17	414	12	488	59	3.1	17.8
16JT11-101	63	40	30	2	0.07	0.004	2	0.08	0.16	0	0.1	6.1805	0.16425	966	24	986	31	1027	64	2.0	5.9
16JT11-103	479	126	38	#	0.1	0.005	4	0.1	0.27	0.02	0.3	3.663	0.20126	1551	74	1580	24	1664	35	1.8	6.8
16JT11-104	181	270	51	3	0.2	0.01	10	0.4	0.45	0.03	0.3	2.2321	0.13453	2380	120	2403	40	2408	36	1.0	1.2
16JT11-105	478	276	207	2	0.06	0.003	0.9	0.03	0.1	0	0.1	9.8328	0.35773	624	22	646	14	732	36	3.4	14.8
16JT11-111	460	120	38	#	0.07	0.003	2	0.07	0.17	0.01	0.5	5.9809	0.17528	996	27	1012	25	1074	46	1.6	7.3
16JT11-113	239	475	125	1	0.1	0.004	4	0.1	0.28	0.01	0.3	3.56	0.12040	1594	48	1615	24	1655	34	1.3	3.7
16JT11-114	125	76	29	4	0.08	0.005	2	0.1	0.16	0	0.2	6.3857	0.17534	937	24	949	41	1024	88	1.3	8.5
16JT11, experiment 6																					
16JT11-115	296	79	129	2	0.06	0.003	0.5	0.02	0.06	0	0.3	16.502	0.35400	379	8	383	17	469	78	1.0	19.2
16JT11-117	827	740	1205	1	0.06	0.002	0.5	0.01	0.07	0	0.6	15.015	0.40581	416	11	416	9	437	33	-0.1	4.8
16JT11-118	741	168	125	6	0.07	0.002	2	0.04	0.16	0.01	0.2	6.3171	0.18756	947	26	944	15	940	27	-0.3	-0.7
16JT11-120	329	238	117	3	0.09	0.003	3	0.08	0.23	0.01	0.4	4.2992	0.18114	1347	51	1350	23	1391	35	0.2	3.2
16JT11-122	86	95	54	2	0.08	0.004	2	0.1	0.2	0.01	0.3	4.9432	0.13439	1187	29	1189	33	1179	56	0.2	-0.7
16JT11-123	1301	401	308	4	0.07	0.004	2	0.05	0.17	0.01	0.1	6.0132	0.24950	991	38	1017	20	1064	39	2.6	6.9
16JT11-126	457	291	409	1	0.05	0.002	0.5	0.02	0.07	0	0.6	14.599	0.31968	427	9	422	16	324	54	-1.2	-31.8
16JT11-127	195	270	82	2	0.2	0.007	10	0.4	0.49	0.02	0.4	2.0408	0.07497	2566	76	2611	30	2684	31	1.7	4.4
16JT11-128	223	100	195	1	0.06	0.005	0.5	0.04	0.06	0	-0.1	15.949	0.71223	392	17	402	30	551	76	2.5	28.9
16JT11-129	276	270	135	2	0.1	0.005	3	0.2	0.26	0.01	0.5	3.8911	0.19682	1474	67	1507	34	1596	33	2.2	7.6
16JT11-130	1114	405	786	1	0.06	0.003	0.5	0.02	0.07	0	0.3	14.728	0.41211	423	11	427	14	508	51	0.9	16.7
16JT11-131	601	100	192	3	0.05	0.002	0.5	0.02	0.07	0	0.3	15.504	0.33652	403	8	402	10	421	33	-0.2	4.3
16JT11-132	127	204	162	1	0.07	0.003	2	0.06	0.16	0	0.0	6.3211	0.12786	947	18	941	23	980	46	-0.6	3.4
16JT11-134	1200	786	1185	1	0.06	0.002	0.7	0.02	0.09	0	0.7	11.696	0.36934	528	16	528	14	554	25	0.0	4.7
16JT11-135	714	470	816	1	0.06	0.001	0.6	0.01	0.07	0	0.5	13.831	0.32522	450	10	450	9	453	38	0.1	0.7
16JT11-137	291	181	323	1	0.06	0.004	0.5	0.03	0.06	0	0.4	15.873	0.52910	393	13	405	19	510	99	3.0	22.9
16JT11-138	101	206	91	1	0.1	0.005	5	0.2	0.32	0.01	0.4	3.1626	0.09102	1770	45	1807	33	1890	39	2.0	6.3

Analysis	U	Pb	Th	U	207Pb		207Pb		206Pb		error	238U		206Pb		207Pb		207Pb	Error	Disc.[1]	Disc.[2]
	(ppm)	(ppm)	(ppm)	Th	206Pb	±2σ abs.	235U	±2σ abs.	238U	±2σ abs.	corr.	206Pb	±2σ abs.	238U	±2σ abs.	235U	±2σ abs.	206Pb	±2σ abs.	%	%
16JT11-139	198	106	88	2	0.07	0.002	2	0.05	0.16	0	0.1	6.1767	0.09919	967	15	965	20	977	40	-0.2	1.0
16JT11-142	1134	779	1550	1	0.06	0.002	0.6	0.03	0.07	0	0.8	13.624	0.59396	457	19	465	18	518	32	1.7	11.8
16JT11-143	137	81	58	3	0.09	0.005	2	0.1	0.21	0.01	0.3	4.8686	0.16592	1203	37	1246	37	1345	64	3.5	10.6
16JT11-145	96	52	39	3	0.08	0.006	2	0.1	0.18	0.01	0.1	5.711	0.22179	1040	37	1089	45	1171	91	4.5	11.2
16JT11-146	706	372	641	1	0.06	0.002	0.6	0.02	0.08	0	-0.1	13.369	0.23235	465	8	468	12	499	65	0.7	6.9
16JT11-148	49	62	42	1	0.08	0.004	2	0.1	0.2	0.01	0.3	4.8828	0.10729	1200	24	1202	33	1265	56	0.2	5.1
16JT11-149	591	230	480	1	0.05	0.003	0.5	0.02	0.06	0	0.1	16.181	0.41893	387	10	384	12	448	79	-0.7	13.7
16JT11-150	375	182	132	3	0.08	0.003	2	0.06	0.17	0	0.0	5.8858	0.13164	1011	21	1037	21	1108	58	2.5	8.8
16JT24, experiment 6																					
16JT24-1	122	83	153	1	0.06	0.005	0.4	0.03	0.06	0	0.1	17.794	0.34827	352	7	352	22	579	95	-0.1	39.2
16JT24-3	348	115	188	2	0.05	0.002	0.4	0.02	0.06	0	0.1	16.562	0.25509	378	6	373	13	421	42	-1.3	10.2
16JT24-6	153	124	75	2	0.07	0.003	2	0.06	0.17	0.01	0.4	5.9488	0.16279	1001	25	1008	26	1049	43	0.7	4.6
16JT24-7	353	127	193	2	0.05	0.002	0.5	0.02	0.06	0	0.2	15.65	0.26940	399	7	398	11	423	54	-0.3	5.6
16JT24-8	154	95	52	3	0.08	0.002	2	0.06	0.19	0	0.1	5.3447	0.09141	1105	18	1104	20	1142	33	-0.1	3.2
16JT24-9	254	165	221	1	0.06	0.002	0.6	0.02	0.07	0	0.0	13.661	0.22395	456	7	453	13	485	47	-0.6	6.1
16JT24-10	168	247	164	1	0.07	0.004	1	0.08	0.15	0	0.4	6.4683	0.15062	926	20	923	33	915	59	-0.3	-1.2
16JT24-12	322	75	53	7	0.07	0.002	1	0.05	0.15	0.01	0.4	6.734	0.21313	892	27	896	18	965	33	0.4	7.6
16JT24-13	115	128	38	4	0.08	0.005	2	0.1	0.18	0.01	0.5	5.6022	0.28247	1058	49	1107	44	1199	41	4.4	11.8
16JT24-14	20	50	31	1	0.08	0.007	2	0.2	0.19	0.01	-0.1	5.3735	0.17613	1099	33	1103	68	1170	100	0.4	6.1
16JT24-15	235	676	285	1	0.1	0.005	4	0.1	0.29	0.01	0.1	3.4771	0.06166	1629	26	1629	26	1672	34	0.0	2.6
16JT24-16	242	156	213	1	0.06	0.004	0.6	0.03	0.07	0	0.3	13.477	0.38143	462	12	462	22	541	94	0.0	14.6
16JT24-18	448	176	292	2	0.06	0.003	0.5	0.03	0.06	0	0.3	15.699	0.44360	398	11	401	19	435	59	0.7	8.5
16JT24-19	886	257	571	2	0.05	0.002	0.4	0.01	0.05	0	0.5	19.802	0.62739	318	10	318	10	395	44	-0.1	19.6
16JT24-20	111	180	83	2	0.09	0.002	3	0.08	0.26	0	0.2	3.8373	0.06332	1492	22	1492	19	1513	26	0.0	1.4
16JT24-21	79	91	42	2	0.1	0.005	4	0.2	0.27	0.01	0.2	3.7594	0.14133	1518	53	1526	34	1575	59	0.5	3.6
16JT24-22	236	648	374	1	0.08	0.003	2	0.08	0.17	0.01	0.4	5.7804	0.19379	1028	32	1047	27	1132	40	1.8	9.2
16JT24-23	51	111	41	1	0.1	0.004	5	0.2	0.32	0.01	0.1	3.0826	0.06557	1810	34	1804	30	1836	42	-0.3	1.4
16JT24-24	135	110	72	2	0.08	0.004	2	0.09	0.19	0.01	0.3	5.2493	0.14604	1123	29	1126	29	1154	43	0.3	2.7
16JT24-25	297	175	82	4	0.1	0.005	4	0.2	0.29	0.01	0.2	3.4965	0.09169	1621	38	1619	37	1668	35	-0.1	2.8
16JT24-28	319	41	32	#	0.07	0.003	2	0.09	0.17	0.01	0.7	5.8651	0.17200	1014	27	1011	33	1069	55	-0.3	5.1
16JT24-29	241	103	82	3	0.07	0.002	2	0.06	0.17	0	0.4	5.9242	0.14389	1005	23	1005	21	1006	38	0.0	0.1
16JT24-31	509	238	164	3	0.08	0.004	2	0.09	0.19	0.01	0.3	5.385	0.24069	1097	45	1092	33	1143	68	-0.5	4.0

Analysis	U	Pb	Th	U	207Pb		207Pb		206Pb		error	238U		206Pb		207Pb		207Pb	Error	Disc.[1]	Disc.[2]
	(ppm)	(ppm)	(ppm)	Th	206Pb	±2σ abs.	235U	±2σ abs.	238U	±2σ abs.	corr.	206Pb	±2σ abs.	238U	±2σ abs.	235U	±2σ abs.	206Pb	±2σ abs.	%	%
16JT24-32	33	135	74	0	0.09	0.006	3	0.2	0.24	0.01	0.3	4.158	0.12102	1388	37	1390	54	1423	63	0.1	2.5
16JT24-33	261	127	124	2	0.07	0.004	1	0.07	0.15	0	0.2	6.6357	0.18494	904	24	910	27	925	58	0.7	2.3
16JT24-34	468	162	311	1	0.06	0.003	0.5	0.02	0.07	0	0.4	15.244	0.48799	410	13	409	15	508	50	-0.2	19.3
16JT24-36	131	46	84	2	0.06	0.004	0.6	0.04	0.07	0	0.4	13.717	0.45160	454	15	464	22	524	66	2.2	13.4
16JT24-37	809	417	544	1	0.06	0.003	1	0.05	0.11	0	0.7	8.7719	0.30779	696	23	693	25	747	59	-0.4	6.8
16JT24-38	347	644	254	1	0.1	0.004	5	0.2	0.33	0.01	0.2	3.0497	0.07255	1828	38	1872	24	1924	31	2.4	5.0
16JT24-40	167	126	99	2	0.08	0.006	2	0.1	0.18	0.01	0.2	5.6465	0.29014	1050	50	1067	43	1176	74	1.6	10.7
16JT24-41	425	32	26	#	0.07	0.003	1	0.05	0.14	0	0.4	7.0274	0.20741	857	23	858	20	899	36	0.1	4.7
16JT24-42	119	98	73	2	0.07	0.004	2	0.07	0.17	0.01	0.0	5.9916	0.17232	994	27	991	26	1003	91	-0.3	0.9
16JT24-43	992	317	637	2	0.05	0.002	0.5	0.02	0.06	0	0.5	16.667	0.41667	376	9	378	16	422	58	0.6	11.0
16JT24-44	236	530	259	1	0.1	0.005	4	0.2	0.27	0.01	0.2	3.663	0.14759	1557	54	1561	34	1634	40	0.3	4.7
16JT24-45	402	67	127	3	0.06	0.003	0.5	0.02	0.06	0	0.2	15.873	0.40312	394	10	396	15	484	61	0.5	18.6
16JT24-48	528	319	155	4	0.1	0.004	4	0.2	0.26	0.01	0.5	3.861	0.17889	1482	62	1536	35	1643	38	3.5	9.8
16JT24-50	623	213	328	2	0.05	0.002	0.4	0.02	0.06	0	0.4	17.036	0.49337	368	10	371	13	415	52	0.8	11.3
16JT24-53	481	47	24	#	0.08	0.003	2	0.1	0.18	0.01	0.6	5.5835	0.24628	1061	43	1095	40	1168	56	3.1	9.2
16JT24-54	219	164	232	1	0.05	0.003	0.5	0.03	0.06	0	0.6	16.026	0.43660	390	11	389	19	458	62	-0.3	14.8
16JT24-55	135	71	31	4	0.09	0.006	3	0.2	0.25	0.01	0.4	4.0323	0.21137	1424	67	1425	43	1494	44	0.1	4.7
16JT24-56	190	146	45	4	0.1	0.004	4	0.1	0.29	0.01	-0.1	3.453	0.07154	1639	30	1679	25	1726	36	2.4	5.0
16JT24-57	885	1479	554	2	0.1	0.003	4	0.1	0.27	0.01	0.5	3.7065	0.12364	1539	46	1588	21	1671	22	3.1	7.9
16JT24-58	78	147	59	1	0.09	0.007	3	0.2	0.22	0.01	0.1	4.4843	0.20109	1299	54	1292	57	1316	80	-0.5	1.3
16JT24-59	203	232	136	1	0.07	0.003	1	0.06	0.15	0.01	0.2	6.8074	0.20853	883	25	881	27	954	67	-0.2	7.4
16JT24-60	161	73	40	4	0.07	0.003	2	0.07	0.16	0	0.4	6.1237	0.15375	975	23	973	28	1010	48	-0.2	3.5
16JT24-62	903	257	339	3	0.06	0.003	0.5	0.03	0.06	0	0.1	15.65	0.41634	399	10	400	19	436	52	0.2	8.5
16JT24-63	785	290	377	2	0.06	0.002	0.5	0.03	0.07	0	0.7	14.556	0.57207	428	16	428	19	455	45	0.0	5.9
16JT24-64	53	25	11	5	0.08	0.01	2	0.3	0.2	0.01	0.1	4.9875	0.19652	1177	42	1175	89	1210	100	-0.2	2.7
16JT24-65	74	74	40	2	0.07	0.007	2	0.2	0.17	0.01	0.5	5.7837	0.25423	1027	41	1024	68	1080	120	-0.3	4.9
16JT24-66	278	112	65	4	0.07	0.004	2	0.07	0.16	0	0.3	6.3412	0.15682	944	22	942	27	1014	59	-0.2	6.9
16JT24-68	156	70	65	2	0.07	0.004	1	0.06	0.12	0.01	0.3	8.5397	0.47402	713	37	716	28	816	80	0.4	12.6
16JT24-70	211	105	56	4	0.08	0.006	2	0.1	0.2	0.01	0.0	4.89	0.21042	1198	47	1201	39	1286	74	0.2	6.8
Discarded analyses																					
16JT27-3	319	b.d.	b.d.	2	0.06	0.007	0.1	0.02	0.02	0	0.5	63.613	3.19680	101	5	123	12	620	190	18.2	83.8
16JT27-4	378	b.d.	b.d.	2	0.05	0.004	0.4	0.03	0.06	0	0.1	17.762	0.69407	353	14	364	19	396	72	3.0	10.9

Analysis	U	Pb	Th	U	207Pb		207Pb		206Pb		error	238U		206Pb		207Pb		207Pb	Error	Disc.[1]	Disc.[2]
	(ppm)	(ppm)	(ppm)	Th	206Pb	±2σ abs.	235U	±2σ abs.	238U	±2σ abs.	corr.	206Pb	±2σ abs.	238U	±2σ abs.	235U	±2σ abs.	206Pb	±2σ abs.	%	%
16JT27-7	528	b.d.	b.d.	4	0.07	0.003	2	0.05	0.16	0.01	0.7	6.3331	0.33290	945	46	1001	16	1035	41	5.6	8.7
16JT27-8	366	b.d.	b.d.	2	0.08	0.003	2	0.05	0.18	0.01	0.4	5.4437	0.25188	1087	46	1141	16	1180	29	4.7	7.9
16JT27-11	1559	b.d.	b.d.	8	0.05	0.003	0.1	0.01	0.02	0	-0.2	59.809	2.71860	107	5	111	5	206	53	3.3	48.1
16JT27-12	1853	b.d.	b.d.	2	0.05	0.002	0.1	0.01	0.02	0	0.2	64.185	2.51300	100	4	107	4	205	64	6.6	51.4
16JT27-22	1800	111	78	#	0.07	0.003	2	0.04	0.17	0.01	0.4	5.8789	0.25575	1012	41	1012	14	1064	44	0.0	4.9
16JT27-23	2184	309	2035	1	0.05	0.003	0.1	0.01	0.02	0	0.0	59.382	3.20890	108	6	108	4	177	50	-0.1	39.2
16JT27-26	2163	276	2024	1	0.05	0.003	0.1	0.01	0.02	0	0.3	64.433	3.03070	99	5	99	6	280	66	-0.1	64.5
16JT27-33	2136	445	802	3	0.06	0.002	0.5	0.01	0.07	0	0.1	14.925	0.60147	418	16	423	9	446	35	1.1	6.3
16JT27-37	1	79	2	0	0.8	0.1	60	8	0.55	0.1	0.5	1.8182	0.33058	2800	420	4100	140	4860	120	31.7	42.4
16JT27-46	2054	138	749	2	0.05	0.002	0.1	0	0.02	0	0.1	61.539	2.49940	104	4	105	3	293	70	1.4	64.5
16JT27-49	978	b.d.	b.d.	2	0.06	0.003	0.5	0.02	0.06	0	0.6	16.695	0.86399	379	17	381	13	418	63	0.5	9.3
16JT27-50	1591	b.d.	b.d.	1	0.06	0.002	0.5	0.01	0.06	0	0.6	16.667	0.66667	375	14	384	7	478	56	2.3	21.5
16JT27-51	333	b.d.	b.d.	1	0.07	0.003	2	0.03	0.16	0.01	0.2	6.2696	0.22799	954	32	951	12	1004	41	-0.3	5.0
16JT27-52	1393	b.d.	b.d.	1	0.05	0.003	0.1	0.01	0.02	0	0.4	64.433	2.49100	99	4	100	4	206	46	0.7	51.8
16JT27-53	280	3341	b.d.	5	0.07	0.004	2	0.06	0.16	0.01	0.0	6.3654	0.27552	941	38	935	27	882	76	-0.6	-6.7
16JT27-54	1109	>9000	b.d.	1	0.06	0.002	0.8	0.01	0.1	0	0.3	10.537	0.39973	585	21	584	8	651	28	-0.2	10.1
16JT27-59	1733	778	6536	1	0.05	0.003	0.1	0.01	0.02	0	0.9	56.148	2.33290	114	5	115	5	248	58	1.4	54.1
16JT27-61	1374	245	104	3	0.09	0.003	3	0.06	0.21	0.01	0.8	4.7619	0.21088	1234	52	1275	17	1312	38	3.2	5.9
16JT27-63	469	69	28	3	0.09	0.004	3	0.08	0.21	0.01	0.4	4.8333	0.20791	1212	47	1299	24	1353	36	6.7	10.4
16JT27-64	94	32	13	1	0.09	0.004	3	0.06	0.23	0.01	0.0	4.279	0.17577	1353	50	1401	16	1514	39	3.4	10.6
16JT27-65	363	172	54	1	0.1	0.004	4	0.1	0.29	0.01	0.7	3.4722	0.16879	1630	67	1689	20	1814	42	3.5	10.1
16JT27-66	811	42	61	3	0.05	0.003	0.4	0.02	0.05	0	0.2	18.868	0.89000	333	15	349	12	397	41	4.6	16.1
16JT27-67	186	15	6	6	0.1	0.004	3	0.07	0.25	0.01	0.2	3.9984	0.15348	1439	49	1504	15	1589	35	4.3	9.4
16JT27-69	1226	14	68	3	0.05	0.004	0.1	0.01	0.02	0	-0.2	67.935	3.04600	94	4	104	6	299	98	9.3	68.5
16JT27-85	1144	371	790	2	0.06	0.003	0.5	0.03	0.06	0	0.2	17.123	0.43981	366	9	391	18	552	64	6.5	33.8
16JT27-86	832	416	474	2	0.07	0.003	1	0.04	0.11	0.01	0.2	9.3633	0.39452	654	26	735	21	959	64	11.0	31.8
16JT27-90	917	40	57	#	0.1	0.002	3	0.06	0.18	0	0.8	5.5432	0.10140	1069	18	1293	18	1665	20	17.3	35.8
16JT27-91	283	130	171	2	0.06	0.003	0.7	0.03	0.08	0	0.0	12.18	0.20770	508	9	533	16	627	47	4.6	18.9
16JT27-119	1817	534	1154	2	0.06	0.003	0.5	0.02	0.06	0	0.7	16.181	0.78550	386	18	387	16	421	45	0.3	8.3
16JT27-122	511	246	327	2	0.08	0.007	0.7	0.07	0.07	0	0.3	14.948	0.80436	417	22	557	42	1210	170	25.1	65.5
16JT27-127	2074	125	557	3	0.05	0.002	0.1	0.01	0.02	0	0.2	55.897	1.49980	114	3	115	5	239	61	0.2	52.2
16JT27-128	5	7	1	4	0.4	0.2	4	2	0.09	0.05	0.1	10.989	5.55490	550	250	1460	440	3830	200	62.3	85.6
16JT27-132	4113	432	2236	2	0.05	0.002	0.1	0	0.02	0	0.2	61.013	1.78680	105	3	104	3	161	42	-0.5	34.9

Analysis	U	Pb	Th	U	207Pb		207Pb		206Pb		error	238U		206Pb		207Pb		207Pb	Error	Disc.[1]	Disc.[2]
	(ppm)	(ppm)	(ppm)	Th	206Pb	±2σ abs.	235U	±2σ abs.	238U	±2σ abs.	corr.	206Pb	±2σ abs.	238U	±2σ abs.	235U	±2σ abs.	206Pb	±2σ abs.	%	%
16JT27-134	1943	468	b.d.	1	0.06	0.002	0.5	0.01	0.07	0	0.4	15.314	0.30487	408	8	409	9	411	33	0.2	0.8
16JT27-136	3664	952	b.d.	1	0.06	0.003	0.5	0.03	0.06	0	0.3	15.674	0.44221	399	11	412	18	548	86	3.2	27.2
16JT27-140	3437	480	b.d.	2	0.06	0.003	0.5	0.02	0.06	0	0.1	16.26	0.58166	385	14	387	13	430	75	0.5	10.5
16JT27-143	5072	178	b.d.	2	0.06	0.004	0.2	0.01	0.02	0	0.6	52.632	4.43210	121	10	141	13	589	51	14.2	79.5
15JT10-14	93	45	27	2	0.06	0.006	0.6	0.05	0.07	0	0.0	13.532	0.34791	460	12	497	33	750	82	7.4	38.7
15JT10-28	512	279	407	1	0.06	0.002	0.6	0.02	0.07	0	0.3	15.083	0.31849	414	8	458	12	639	59	9.6	35.2
15JT10-37	138	207	46	3	0.1	0.004	6	0.2	0.32	0.01	0.6	3.1516	0.08244	1780	42	1949	24	2141	28	8.7	16.9
15JT10-45	56	78	27	2	0.1	0.004	5	0.2	0.32	0.01	0.2	3.1056	0.05208	1799	26	1795	27	1799	33	-0.2	0.0
15JT10-48	37	44	30	1	0.2	0.02	2	0.1	0.07	0	0.4	14.085	0.61496	442	18	1102	46	2883	63	59.9	84.7
15JT10-49	353	97	224	2	0.06	0.003	0.4	0.02	0.06	0	0.5	17.606	0.40295	356	8	374	17	452	63	4.8	21.2
15JT10-50	578	127	279	2	0.06	0.002	0.5	0.02	0.06	0	0.5	18.116	0.42664	347	8	377	11	571	53	8.1	39.3
15JT10-54	643	164	492	1	0.06	0.002	0.3	0.01	0.04	0	0.4	26.316	0.76177	240	7	290	9	656	40	17.2	63.4
15JT10-57	498	247	475	1	0.06	0.002	0.5	0.01	0.06	0	0.0	16.584	0.27502	377	6	418	9	633	36	9.7	40.4
15JT10-60	200	64	129	2	0.07	0.003	0.5	0.03	0.06	0	0.5	16.529	0.40981	378	9	437	19	755	67	13.4	49.9
15JT10-62	546	542	240	2	0.1	0.002	4	0.06	0.28	0	0.4	3.6127	0.05743	1575	23	1645	11	1746	16	4.3	9.8
15JT10-64	13	7	3	4	0.1	0.006	5	0.3	0.33	0.01	0.4	2.994	0.10757	1854	58	1839	54	1855	63	-0.8	0.1
15JT10-65	739	285	551	1	0.06	0.002	0.5	0.02	0.06	0	0.3	15.699	0.32038	398	8	420	13	506	54	5.3	21.4
15JT10-73	115	185	77	1	0.1	0.002	6	0.1	0.36	0.01	0.3	2.8161	0.04124	1958	25	1955	15	1956	21	-0.2	-0.1
15JT10-74	208	42	98	2	0.05	0.002	0.4	0.02	0.06	0	0.0	17.346	0.25876	361	5	363	12	416	53	0.5	13.1
15JT10-82	1022	292	816	1	0.06	0.002	0.4	0.02	0.05	0	0.8	18.904	0.57175	332	10	366	14	639	33	9.2	48.0
15JT10-83	72	233	95	1	0.1	0.003	7	0.2	0.37	0.01	0.3	2.6702	0.04421	2049	29	2141	20	2235	21	4.3	8.3
15JT10-84	469	152	374	1	0.06	0.003	0.5	0.03	0.07	0	0.3	15.083	0.47774	413	13	429	17	485	53	3.7	14.8
15JT10-88	1388	402	988	1	0.07	0.002	0.5	0.01	0.06	0	0.3	17.829	0.31150	352	6	434	6	899	34	19.0	60.9
15JT10-93	191	87	154	1	0.05	0.003	0.5	0.02	0.06	0	0.2	15.699	0.24645	398	6	394	16	420	49	-1.0	5.3
15JT10-99	184	95	142	1	0.06	0.004	0.5	0.03	0.07	0	0.2	15.504	0.36056	403	9	406	23	433	77	0.7	6.9
15JT10-110	124	392	119	1	0.1	0.003	9	0.1	0.42	0.01	0.2	2.3646	0.03355	2273	27	2307	13	2324	17	1.5	2.2
15JT10-113	255	113	217	1	0.06	0.002	0.5	0.02	0.07	0	0.2	15.456	0.23889	405	6	420	14	473	49	3.6	14.4
15JT10-119	353	79	193	2	0.06	0.004	0.5	0.04	0.06	0	0.2	17.212	0.47399	364	10	380	28	452	77	4.2	19.5
15JT10-120	1136	489	1047	1	0.06	0.002	0.6	0.02	0.06	0	0.1	16.234	0.36895	386	8	450	10	748	54	14.4	48.5
15JT10-123	270	139	249	1	0.07	0.003	0.6	0.03	0.06	0	0.2	16.978	0.31708	370	7	463	17	1003	60	20.1	63.1
15JT10-126	1714	369	985	2	0.08	0.003	0.4	0.01	0.04	0	0.8	28.653	1.97040	223	15	316	11	1126	79	29.4	80.2
15JT10-127	596	134	295	2	0.05	0.002	0.4	0.02	0.06	0	0.3	17.637	0.34216	356	7	359	11	383	35	1.0	7.2

Analysis	U	Pb	Th	U	207Pb		207Pb		206Pb		error	238U		206Pb		207Pb		207Pb	Error	Disc.[1]	Disc.[2]
	(ppm)	(ppm)	(ppm)	Th	206Pb	±2σ abs.	235U	±2σ abs.	238U	±2σ abs.	corr.	206Pb	±2σ abs.	238U	±2σ abs.	235U	±2σ abs.	206Pb	±2σ abs.	%	%
15JT10-128	1329	253	550	2	0.06	0.003	0.5	0.02	0.06	0	0.0	16.75	0.44892	374	10	403	13	552	55	7.2	32.3
15JT10-130	80	177	78	1	0.1	0.004	5	0.1	0.29	0.01	0.1	3.427	0.08104	1653	35	1788	21	1928	47	7.6	14.3
15JT10-131	1047	526	1215	1	0.06	0.001	0.5	0.02	0.05	0	0.8	19.157	0.44039	328	7	381	12	666	35	13.9	50.8
15JT10-133	1790	196	631	3	0.06	0.002	0.4	0.01	0.05	0	0.5	19.763	0.50774	320	8	358	10	572	37	10.6	44.1
15JT10-135	129	36	87	2	0.05	0.004	0.4	0.03	0.06	0	-0.1	17.331	0.48058	361	10	361	18	529	78	-0.1	31.7
15JT10-136	568	305	419	1	0.1	0.007	1	0.07	0.07	0	0.3	15.385	0.33136	406	9	718	33	1844	91	43.5	78.0
15JT10-139	1931	355	1160	2	0.06	0.002	0.4	0.02	0.04	0	0.9	22.727	0.92975	278	11	331	15	706	31	16.0	60.6
15JT10-141	178	75	162	1	0.06	0.003	0.5	0.03	0.06	0	0.1	15.798	0.27453	396	7	415	19	500	58	4.7	20.9
15JT10-143	262	75	127	1	0.06	0.004	0.5	0.03	0.06	0	0.3	15.773	0.62196	396	15	402	20	486	76	1.5	18.5
15JT10-145	1730	574	567	1	0.06	0.002	0.4	0.02	0.06	0	0.3	17.153	0.52958	365	11	368	13	396	46	0.8	7.8
15JT10-149	726	175	166	1	0.06	0.004	0.5	0.03	0.06	0	0.4	17.953	0.77357	349	15	377	24	553	60	7.4	36.9
15JT10-150	402	509	83	2	0.2	0.003	9	0.3	0.38	0.02	0.9	2.6596	0.11317	2048	75	2343	35	2591	16	12.6	21.0
15JT11-3	768	492	261	3	0.1	0.002	4	0.1	0.29	0.01	0.5	3.4614	0.09345	1636	39	1684	20	1719	19	2.9	4.8
15JT11-7	869	70	58	#	0.09	0.009	2	0.4	0.15	0.01	0.8	6.4935	0.46382	921	59	1070	110	1370	210	13.9	32.8
15JT11-12	1177	282	724	2	0.05	0.002	0.4	0.02	0.06	0	0.5	18.018	0.48697	348	9	361	12	408	47	3.5	14.6
15JT11-19	163	87	78	2	0.07	0.005	2	0.07	0.15	0.01	0.1	6.6578	0.39007	901	49	950	28	1062	61	5.2	15.2
15JT11-21	1071	352	750	1	0.06	0.003	0.5	0.02	0.06	0	0.4	16.393	0.88686	382	20	407	14	522	52	6.1	26.8
15JT11-25	195	33	61	4	0.07	0.006	0.5	0.06	0.05	0.01	0.8	18.727	2.41970	335	42	413	39	880	110	18.9	61.9
15JT11-34	365	136	257	1	0.05	0.003	0.5	0.02	0.06	0	0.3	16	0.35840	391	9	395	17	440	59	1.0	11.2
15JT11-41	382	144	253	1	0.06	0.002	0.5	0.02	0.07	0	0.2	15.038	0.24874	415	6	417	10	445	35	0.6	6.8
15JT11-45	492	240	121	4	0.1	0.002	3	0.09	0.19	0.01	0.6	5.1733	0.14452	1138	29	1309	26	1615	27	13.1	29.5
15JT11-63	446	369	191	3	0.1	0.002	3	0.1	0.21	0.01	0.9	4.7619	0.20862	1238	49	1381	37	1575	22	10.4	21.4
15JT11-70	660	119	265	3	0.05	0.003	0.4	0.02	0.05	0	0.3	18.904	0.46455	333	8	331	13	318	51	-0.5	-4.6
15JT11-78	253	420	202	1	0.1	0.003	3	0.09	0.24	0	0.2	4.1754	0.06625	1384	20	1483	21	1633	26	6.7	15.2
15JT11-81	656	406	287	2	0.08	0.002	2	0.06	0.17	0.01	0.5	5.7241	0.17366	1038	29	1078	21	1190	37	3.7	12.8
15JT11-82	554	155	289	2	0.06	0.003	0.5	0.02	0.07	0	0.0	15.456	0.54944	404	14	428	13	585	41	5.6	30.9
15JT11-94	295	85	150	2	0.05	0.002	0.5	0.02	0.06	0	0.2	16.051	0.41223	389	9	390	12	413	49	0.2	5.7
15JT11-102	567	563	305	3	0.1	0.002	3	0.08	0.23	0.01	0.6	4.3048	0.10007	1345	28	1481	20	1691	18	9.2	20.5
15JT11-109	455	84	135	3	0.06	0.005	0.3	0.03	0.04	0	0.2	25.253	0.63769	250	7	297	19	764	97	15.7	67.2
15JT11-129	375	178	358	1	0.06	0.002	0.5	0.02	0.06	0	0.5	16.447	0.48693	380	11	381	14	405	53	0.3	6.2
15JT11-133	2430	220	659	4	0.06	0.003	0.4	0.01	0.05	0	0.2	20.08	0.76612	313	12	319	8	411	41	1.8	23.8
15JT11-146	1549	304	746	2	0.05	0.003	0.4	0.02	0.05	0	0.4	18.975	1.04420	331	17	325	16	383	50	-1.8	13.6

Analysis	U (ppm)	Pb (ppm)	Th (ppm)	U Th	207Pb 206Pb	±2σ abs.	207Pb 235U	±2σ abs.	206Pb 238U	±2σ abs.	error corr.	238U 206Pb	±2σ abs.	206Pb 238U	±2σ abs.	207Pb 235U	±2σ abs.	207Pb 206Pb	Error ±2σ abs.	Disc.[1] %	Disc.[2] %
16JT11-4	937	665	394	2	0.08	0.003	2	0.05	0.2	0.01	0.4	5.0582	0.13560	1163	28	1154	18	1165	28	-0.8	0.2
16JT11-12	140	117	78	2	0.07	0.003	2	0.07	0.17	0.01	0.1	5.7438	0.15836	1038	25	1036	24	1052	57	-0.2	1.3
16JT11-15	2924	809	1604	2	0.05	0.001	0.5	0.01	0.06	0	0.7	15.848	0.35162	394	9	395	9	382	21	0.1	-3.2
16JT11-22	1235	764	1542	1	0.06	0.001	0.5	0.01	0.07	0	0.3	15.504	0.28844	403	8	413	7	446	24	2.5	9.6
16JT11-25	678	305	454	2	0.06	0.002	0.7	0.04	0.08	0	0.7	12.24	0.58428	506	23	517	23	532	33	2.1	4.9
16JT11-29	461	321	621	1	0.06	0.002	0.5	0.01	0.07	0	0.2	15.038	0.31658	415	8	429	9	462	38	3.3	10.1
16JT11-31	383	106	201	2	0.05	0.003	0.5	0.02	0.06	0	0.1	17.094	0.49675	367	10	380	10	363	47	3.4	-1.1
16JT11-32	266	40	72	3	0.06	0.002	0.6	0.02	0.07	0	0.3	14.144	0.32010	440	10	457	13	499	45	3.6	11.7
16JT11-33	280	1389	377	1	0.2	0.007	10	0.3	0.47	0.02	0.2	2.1097	0.08012	2497	81	2636	24	2679	24	5.3	6.8
16JT11-34	1296	89	49	#	0.09	0.004	3	0.1	0.21	0.01	0.5	4.7349	0.21074	1235	50	1312	27	1379	28	5.9	10.4
16JT11-37	330	202	310	1	0.06	0.004	0.7	0.04	0.08	0	0.2	12.674	0.46585	493	19	512	23	565	46	3.7	12.7
16JT11-38	147	210	107	1	0.09	0.004	3	0.2	0.24	0.01	0.5	4.2373	0.09157	1365	27	1429	36	1417	42	4.5	3.7
16JT11-40	388	541	423	1	0.07	0.003	1	0.04	0.14	0.01	0.0	6.93	0.21611	868	25	920	18	985	35	5.7	11.9
16JT11-43	389	112	180	2	0.06	0.002	0.6	0.01	0.07	0	0.2	14.124	0.27929	441	9	455	10	504	37	3.1	12.5
16JT11-47	702	119	188	4	0.06	0.002	0.6	0.02	0.08	0	0.8	12.788	0.50693	485	19	498	14	518	27	2.6	6.4
16JT11-48	561	497	937	1	0.06	0.001	0.5	0.02	0.07	0	0.7	14.641	0.36442	425	11	437	11	450	32	2.7	5.6
16JT11-50	483	108	194	2	0.06	0.002	0.6	0.03	0.08	0	0.4	12.771	0.29360	486	11	497	19	535	51	2.2	9.2
16JT11-53	200	385	113	1	0.2	0.006	10	0.4	0.52	0.02	0.4	1.9157	0.05505	2708	63	2731	26	2753	38	0.8	1.6
16JT11-56	191	144	103	2	0.09	0.003	3	0.08	0.25	0.01	0.0	4.0486	0.08687	1422	27	1425	20	1424	27	0.2	0.1
16JT11-60	3677	1910	6330	1	0.06	0.002	0.5	0.02	0.06	0	0.6	16.584	0.66005	377	15	404	13	598	37	6.7	37.0
16JT11-70	2339	1664	2977	1	0.06	0.002	0.4	0.01	0.06	0	0.2	16.892	0.57067	371	12	375	8	420	50	1.1	11.7
16JT11-73	1671	667	1020	1	0.06	0.001	0.5	0.01	0.07	0	0.4	14.837	0.28617	422	8	423	8	478	26	0.4	11.8
16JT11-74	1790	295	395	4	0.06	0.003	0.5	0.03	0.07	0	0.5	14.245	0.50730	437	15	443	19	493	44	1.4	11.4
16JT11-85	525	496	589	1	0.06	0.002	0.8	0.04	0.1	0	0.3	10.515	0.34277	585	18	588	21	618	68	0.5	5.3
16JT11-88	195	218	415	0	0.06	0.007	0.5	0.05	0.07	0.01	-0.2	15.337	1.08210	407	28	434	32	600	160	6.2	32.2
16JT11-89	3614	1246	2689	1	0.06	0.003	0.4	0.02	0.06	0	0.4	17.953	0.99920	349	19	360	13	493	56	3.1	29.2
16JT11-97	1363	199	332	4	0.06	0.005	0.5	0.04	0.06	0	0.3	17.212	0.91835	364	19	428	27	760	110	15.0	52.1
16JT11-99	336	395	197	2	0.1	0.006	3	0.2	0.26	0.02	0.4	3.8462	0.34024	1470	110	1494	52	1633	69	1.6	10.0
16JT11-102	194	196	101	2	0.09	0.004	3	0.09	0.24	0.01	0.1	4.2035	0.13782	1375	41	1394	24	1431	43	1.4	3.9
16JT11-106	177	62	78	2	0.05	0.002	0.4	0.02	0.06	0	0.3	17.699	0.37591	355	7	368	14	397	52	3.7	10.7
16JT11-107	990	318	318	2	0.06	0.002	0.6	0.01	0.07	0	0.0	14.205	0.28248	438	9	452	7	474	30	3.1	7.6
16JT11-108	163	93	31	4	0.09	0.006	3	0.2	0.24	0.01	0.2	4.2017	0.17654	1377	53	1395	42	1464	40	1.3	5.9

Analysis	U (ppm)	Pb (ppm)	Th (ppm)	U Th	207Pb 206Pb	±2σ abs.	207Pb 235U	±2σ abs.	206Pb 238U	±2σ abs.	error corr.	238U 206Pb	±2σ abs.	206Pb 238U	±2σ abs.	207Pb 235U	±2σ abs.	207Pb 206Pb	Error ±2σ abs.	Disc.[1] %	Disc.[2] %
16JT11-109	248	211	63	3	0.09	0.004	3	0.08	0.24	0.01	0.2	4.2212	0.14255	1369	42	1388	21	1441	40	1.4	5.0
16JT11-110	157	2	1	#	0.08	0.003	2	0.06	0.2	0.01	0.2	5.0813	0.13168	1158	28	1173	18	1214	37	1.3	4.6
16JT11-112	25	52	15	1	0.1	0.01	3	0.4	0.17	0.01	0.4	5.9702	0.27088	997	42	1390	100	2030	160	28.3	50.9
16JT11-116	671	302	398	2	0.06	0.002	0.7	0.02	0.08	0	0.4	11.933	0.31328	519	13	515	13	519	33	-0.8	0.0
16JT11-119	253	140	64	4	0.08	0.002	2	0.06	0.18	0	0.3	5.4915	0.10856	1078	20	1154	20	1323	32	6.6	18.5
16JT11-121	490	70	79	6	0.06	0.002	0.8	0.02	0.1	0	0.4	10.384	0.31271	593	17	591	13	630	39	-0.3	5.9
16JT11-124	844	299	441	2	0.06	0.002	0.5	0.02	0.07	0	0.4	14.577	0.25500	427	7	425	10	438	46	-0.6	2.4
16JT11-125	339	476	206	2	0.09	0.003	3	0.09	0.26	0.01	0.4	3.8911	0.09236	1474	31	1472	21	1478	27	-0.1	0.3
16JT11-133	1695	271	1044	2	0.06	0.003	0.4	0.02	0.05	0	0.4	18.382	0.57445	341	10	355	17	506	50	3.9	32.6
16JT11-136	1077	323	667	2	0.06	0.002	0.4	0.02	0.06	0	0.4	17.182	0.50188	366	10	367	12	421	37	0.2	13.0
16JT11-140	128	153	72	2	0.1	0.004	5	0.2	0.3	0.01	0.2	3.319	0.06499	1697	29	1746	31	1826	30	2.8	7.1
16JT11-141	151	172	89	2	0.1	0.003	4	0.2	0.28	0.01	0.5	3.5461	0.10311	1601	41	1622	34	1643	25	1.3	2.6
16JT11-144	240	369	154	2	0.1	0.003	6	0.1	0.34	0.01	0.4	2.9369	0.04485	1888	25	1982	14	2067	21	4.7	8.7
16JT11-147	282	328	250	1	0.08	0.002	2	0.08	0.18	0	0.6	5.6657	0.12198	1047	21	1053	28	1104	37	0.6	5.2
16JT24-2	3033	443	1003	3	0.05	0.002	0.3	0.02	0.05	0	0.8	22.321	0.94667	283	12	297	16	433	38	4.7	34.6
16JT24-4	111	47	66	2	0.06	0.004	0.6	0.03	0.07	0	0.0	13.459	0.34417	462	11	460	22	490	89	-0.4	5.7
16JT24-5	2833	117	191	#	0.06	0.001	0.5	0.01	0.07	0	0.7	15.152	0.32140	412	9	411	9	433	23	-0.2	4.8
16JT24-11	909	826	367	3	0.09	0.002	3	0.07	0.22	0.01	0.6	4.5106	0.12818	1290	33	1356	20	1453	31	4.9	11.2
16JT24-17	174	186	118	2	0.07	0.003	1	0.06	0.15	0.01	0.1	6.5062	0.19049	922	25	925	23	961	45	0.3	4.1
16JT24-26	349	152	128	3	0.09	0.005	1	0.1	0.09	0.01	0.8	11.534	0.94454	535	42	760	51	1484	61	29.6	63.9
16JT24-27	448	89	89	5	0.07	0.003	1	0.07	0.14	0	0.4	6.9204	0.19157	870	22	869	28	959	60	-0.1	9.3
16JT24-30	65	45	40	2	0.07	0.005	2	0.1	0.16	0.01	0.1	6.0939	0.22281	979	33	962	40	964	86	-1.8	-1.6
16JT24-35	233	120	189	1	0.06	0.005	0.7	0.06	0.08	0	0.5	12.24	0.52435	506	21	561	35	748	91	9.8	32.4
16JT24-39	540	218	200	3	0.08	0.004	2	0.1	0.18	0.01	0.6	5.7045	0.21152	1041	36	1120	39	1312	73	7.1	20.7
16JT24-46	170	71	75	2	0.1	0.02	0.8	0.2	0.06	0	0.3	15.576	0.67934	401	17	623	87	1550	310	35.6	74.1
16JT24-47	1059	336	499	2	0.2	0.004	7	0.3	0.29	0.01	0.8	3.413	0.15143	1656	65	2118	37	2619	24	21.8	36.8
16JT24-49	2610	455	417	6	0.08	0.007	0.6	0.04	0.06	0	0.2	17.986	0.84105	349	16	458	22	1190	150	23.8	70.7
16JT24-51	109	203	46	2	0.2	0.008	10	0.5	0.43	0.02	0.5	2.3148	0.09109	2310	78	2413	46	2491	31	4.3	7.3
16JT24-52	9	107	21	0	0.7	0.07	20	3	0.2	0.03	0.8	5.1282	0.76266	1180	170	3050	160	4769	73	61.3	75.3
16JT24-61	332	195	86	4	0.09	0.006	3	0.3	0.23	0.01	0.7	4.4053	0.25229	1336	74	1369	63	1458	74	2.4	8.4
16JT24-67	1501	633	1032	1	0.06	0.003	0.5	0.03	0.06	0	0.4	15.848	0.77858	394	19	400	19	493	57	1.5	20.1
16JT24-69	292	236	153	2	0.09	0.004	3	0.1	0.22	0.01	0.6	4.6512	0.23797	1253	58	1301	30	1459	46	3.7	14.1

Analysis	U (ppm)	Pb (ppm)	Th (ppm)	U/Th	207Pb/206Pb	±2σ abs.	207Pb/235U	±2σ abs.	206Pb/238U	±2σ abs.	error corr.	238U/206Pb	±2σ abs.	206Pb/238U	±2σ abs.	207Pb/235U	±2σ abs.	207Pb/206Pb	Error ±2σ abs.	Disc.[1] %	Disc.[2] %
16JT24-71	135	59	73	2	0.06	0.007	0.7	0.09	0.08	0	0.5	12.18	0.48958	509	20	513	59	550	150	0.8	7.5
16JT24-72	162	96	93	2	0.06	0.003	0.9	0.05	0.1	0	0.3	9.6805	0.28114	636	18	640	28	700	78	0.6	9.1

Notes: Disc. 1, <1.2 Ga; Disc. 2, >1.2 Ga. b.d. = below detection

APPENDIX B – Concordia diagrams

Sample 16JT11

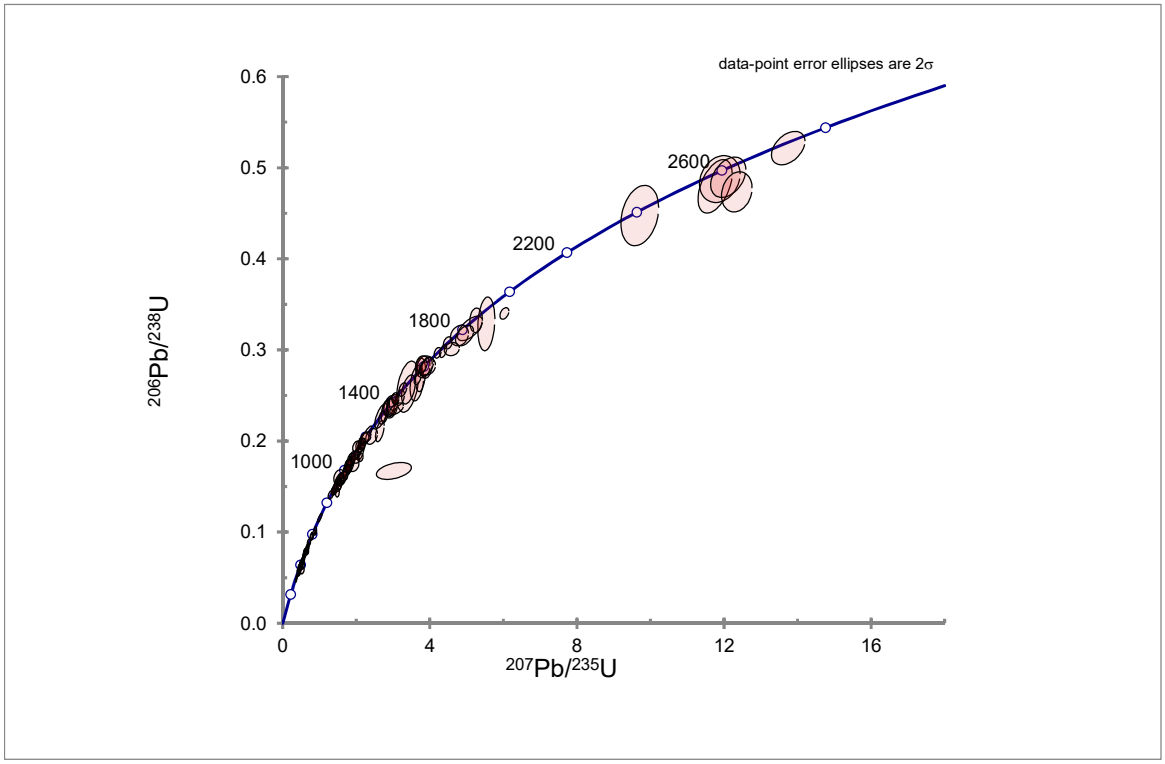


Fig. 12. Concordia diagram of all analyses in modern river sand sample 16JT11. The scale is 0 to 3000 Ma.

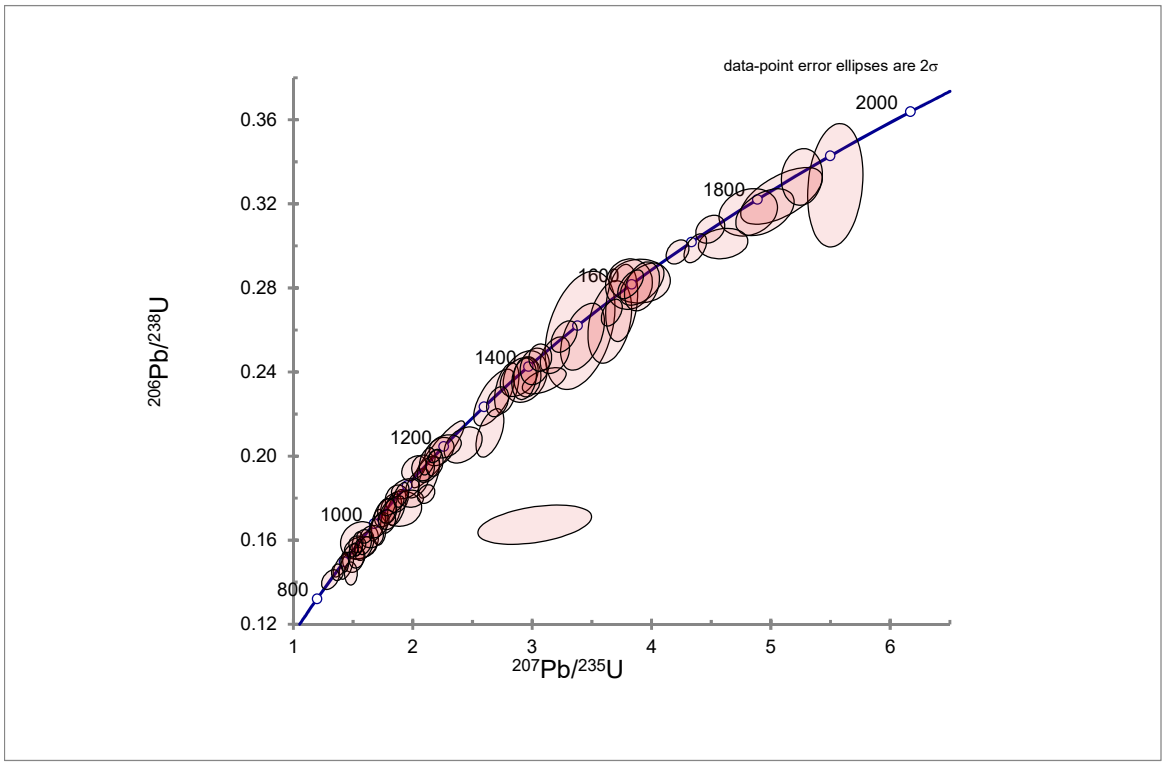


Fig. 13. Concordia diagram of analyses in modern river sand sample 16JT11 on a 2.0-0.8 Ga scale.

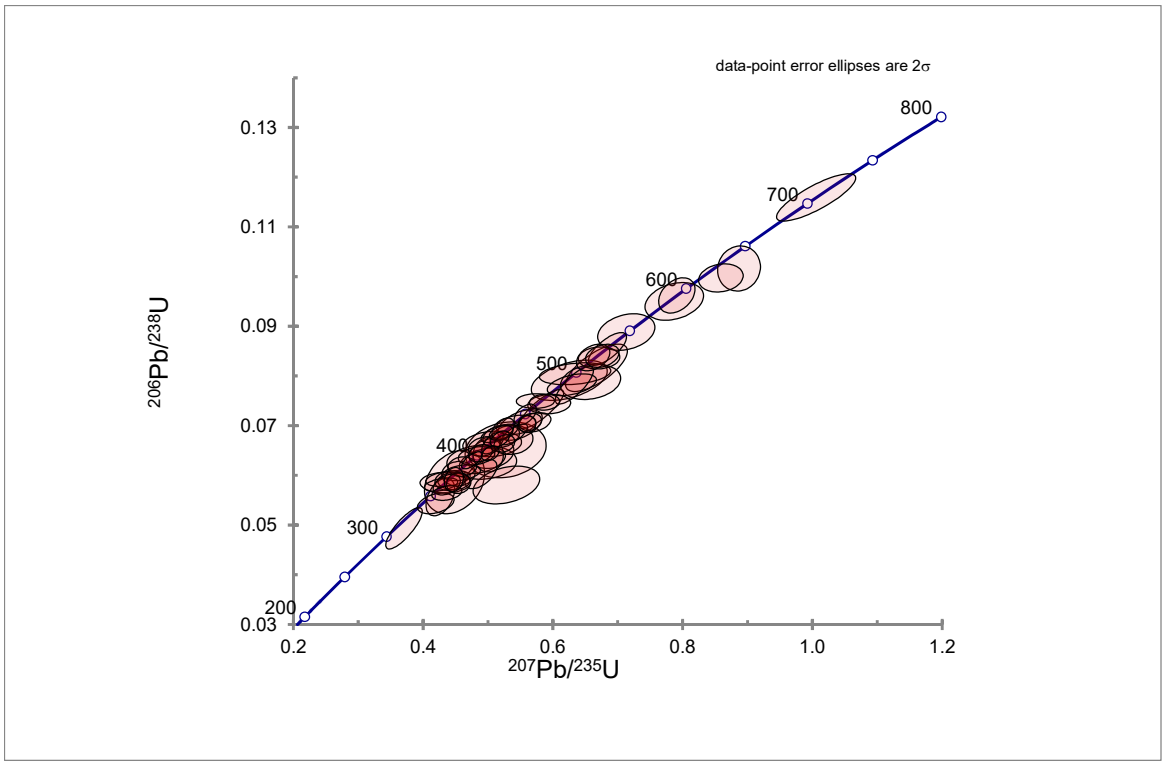


Fig. 14. Concordia diagram of analyses in modern river sand sample 16JT24 on a 800-200 Ma scale.

Sample 16JT24

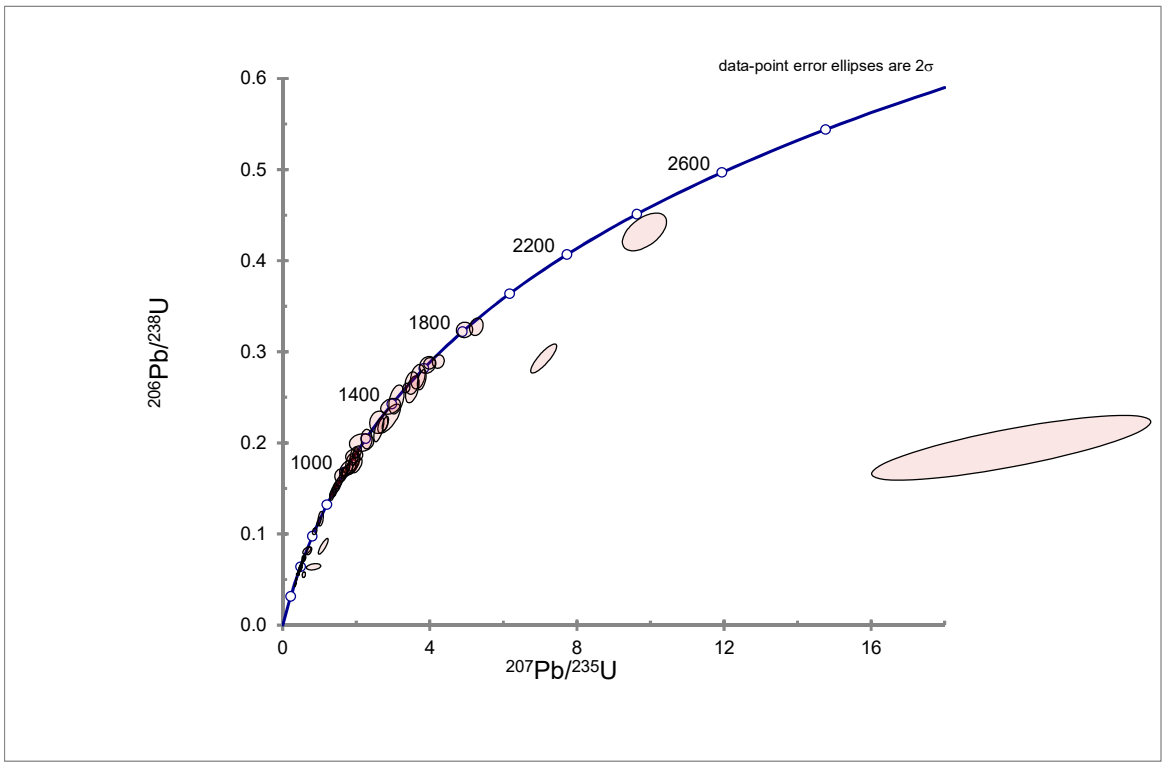


Fig. 15. Concordia diagram of all analyses in modern river sand sample 16JT11. The scale is 0 to 3000 Ma.

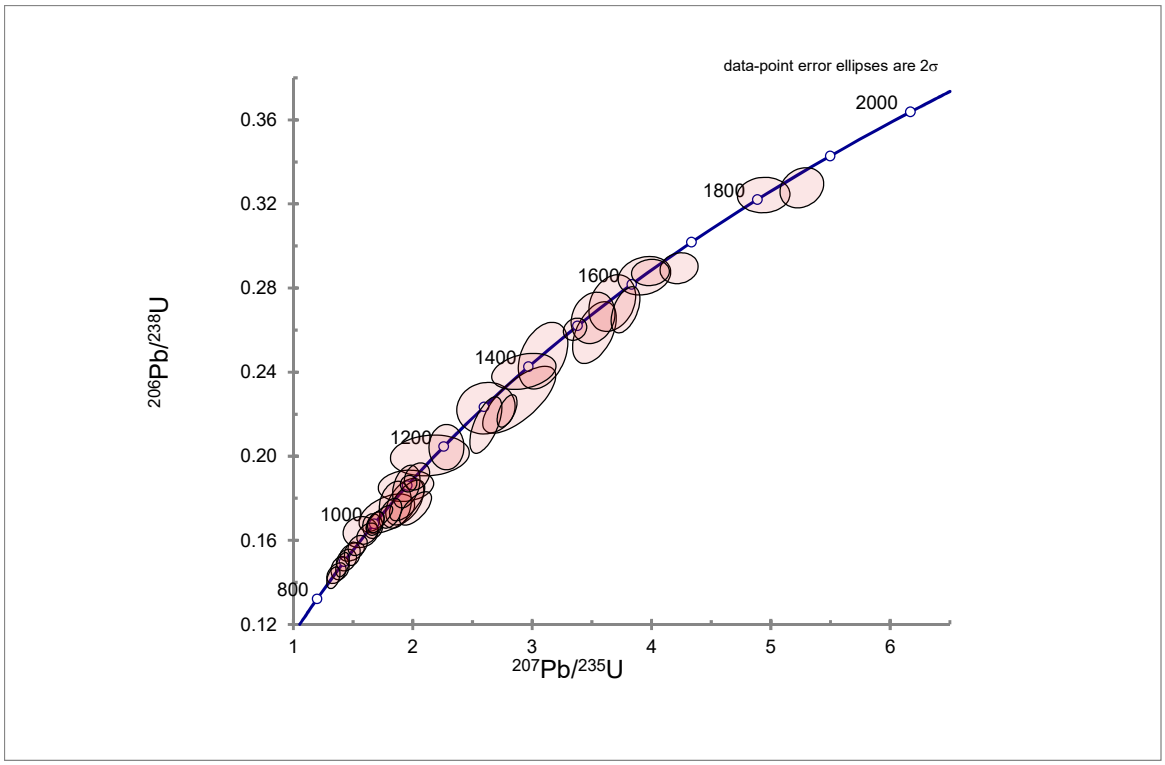


Fig. 16. Concordia diagram of analyses in modern river sand sample 16JT24 on a 2.0-0.8 Ga scale.

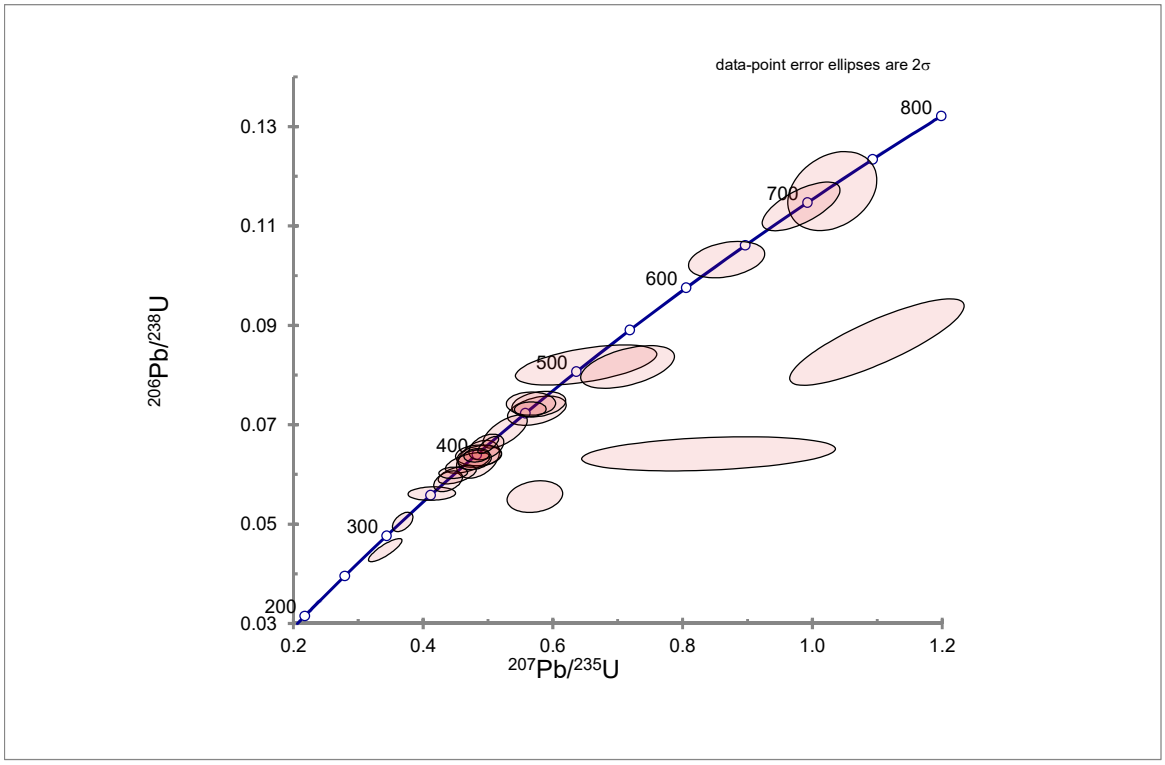


Fig. 17. Concordia diagram of analyses in modern river sand sample 16JT24 on a 800-200 Ma scale.

Sample 16JT27

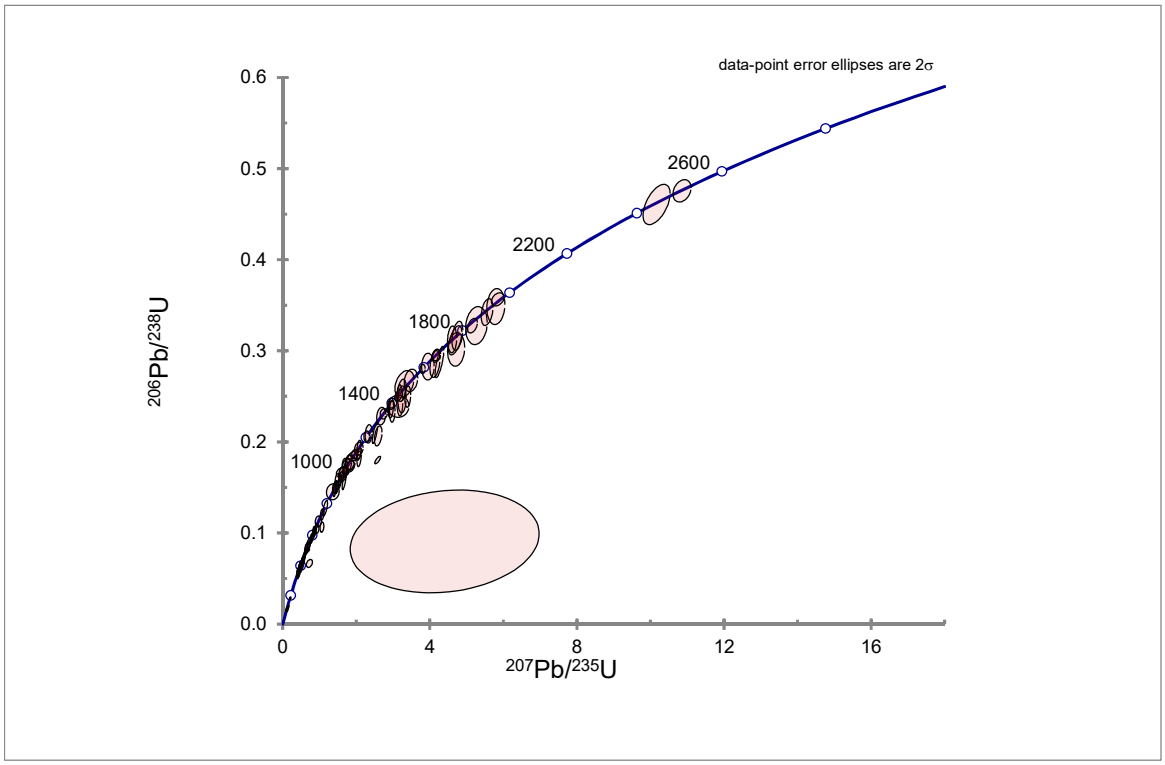


Fig. 18. Concordia diagram of all analyses in modern river sand sample 16JT27. The scale is 0 to 3000 Ma.

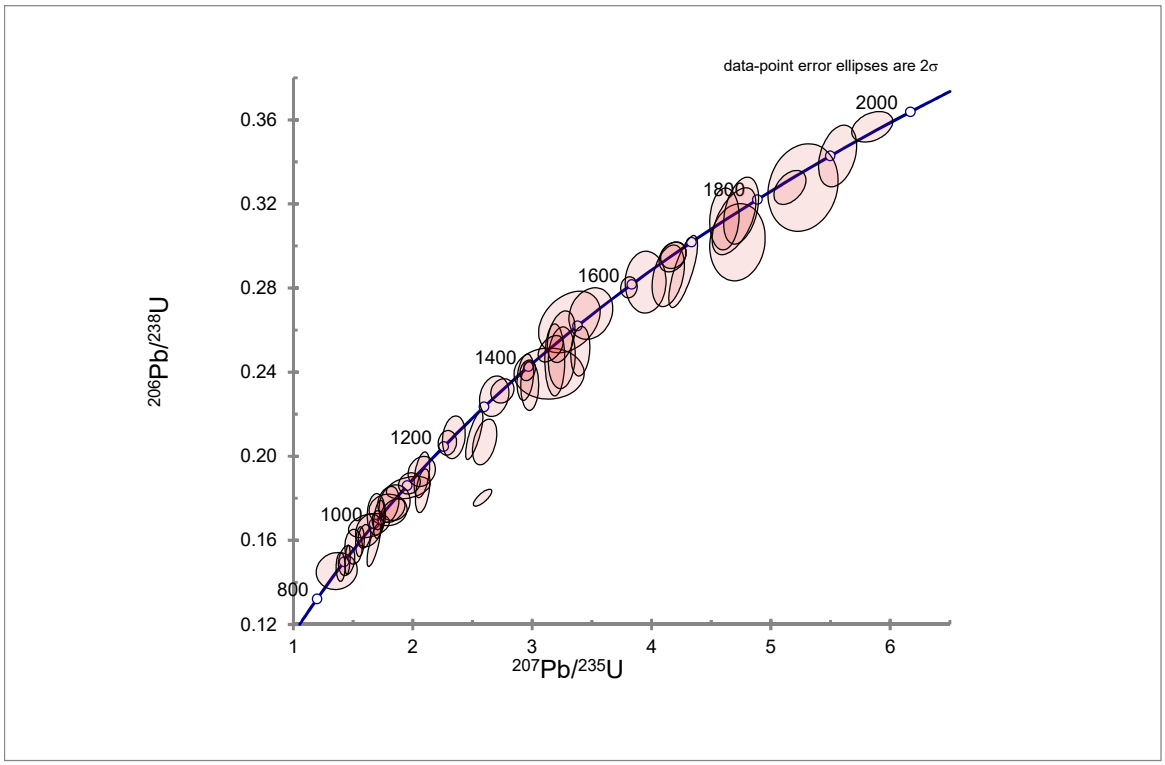


Fig. 19. Concordia diagram of analyses in modern river sand sample 16JT27 on a 2.0-0.8 Ga scale.

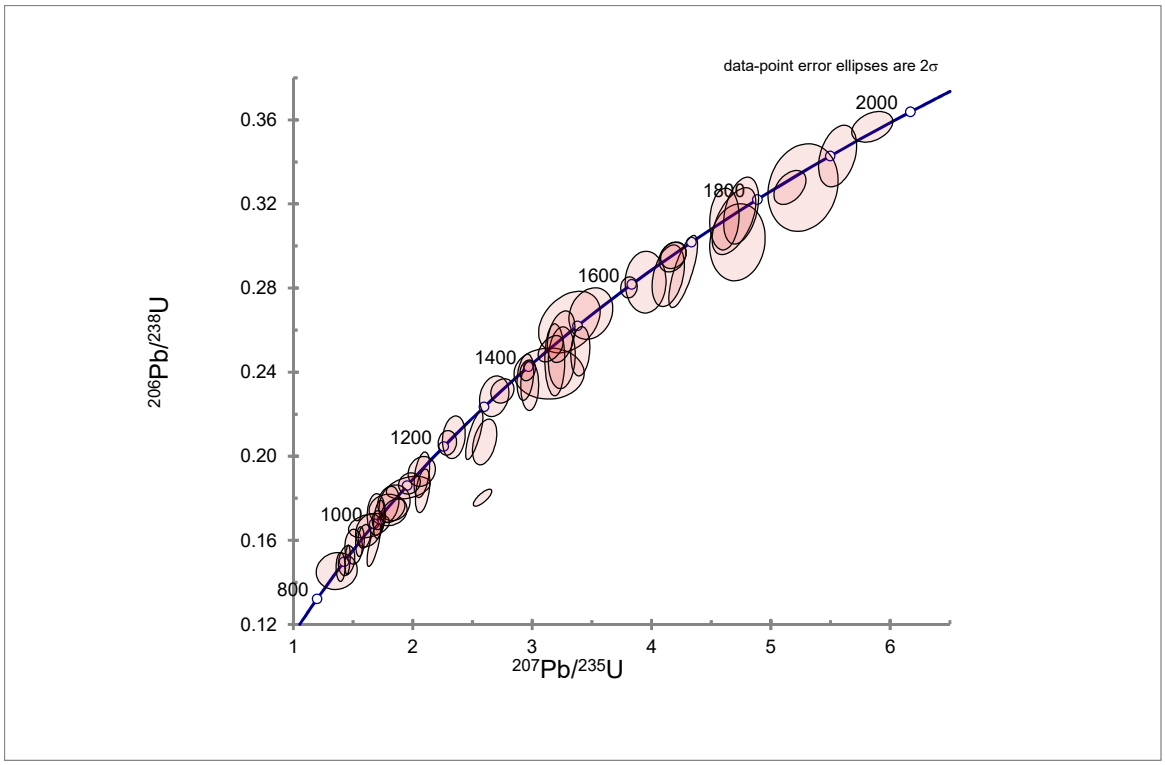


Fig. 20. Concordia diagram of analyses in modern river sand sample 16JT27 on a 800-200 Ma scale.

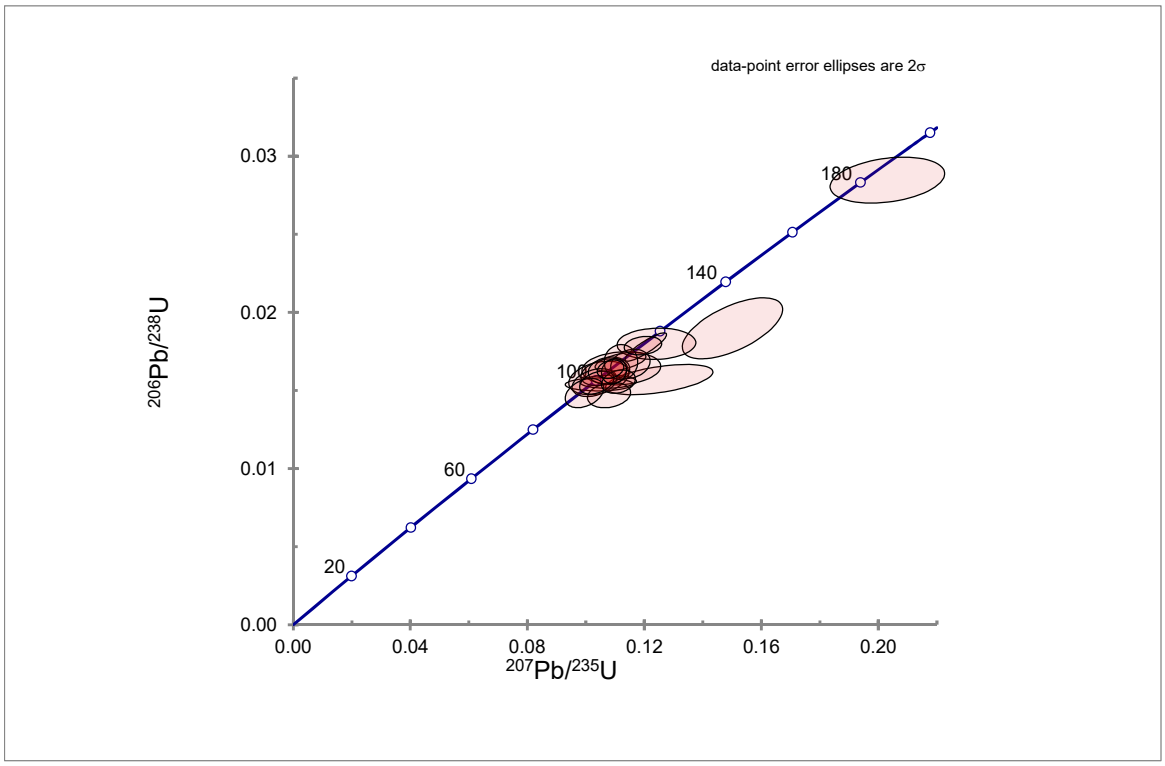


Fig. 21. Concordia diagram of analyses in modern river sand sample 16JT27 on a 200-0 Ma scale

Sample 15JT10

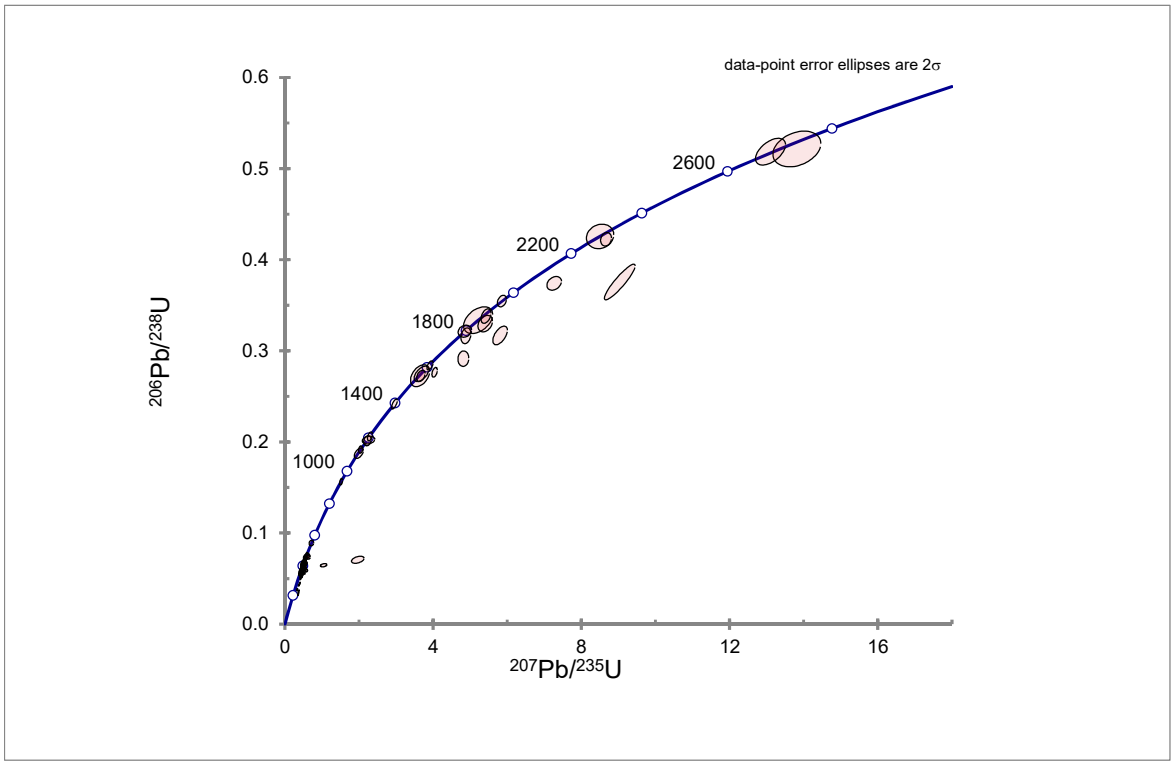


Fig. 22. Concordia diagram of all analyses in detrital rock *in-situ* sample 15JT10. The scale is 0 to 3000 Ma.

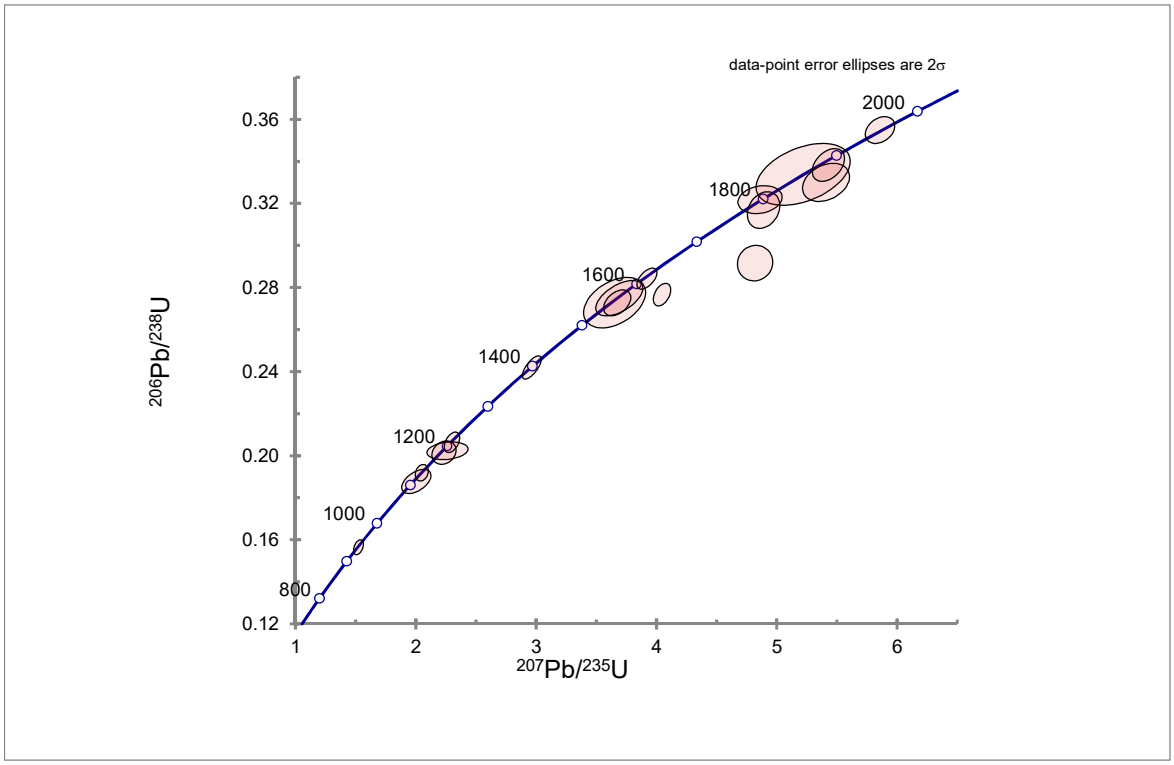


Fig. 23. Concordia diagram of analyses in detrital rock *in-situ* sample 15JT10 on a 2.0-0.8 Ga scale.

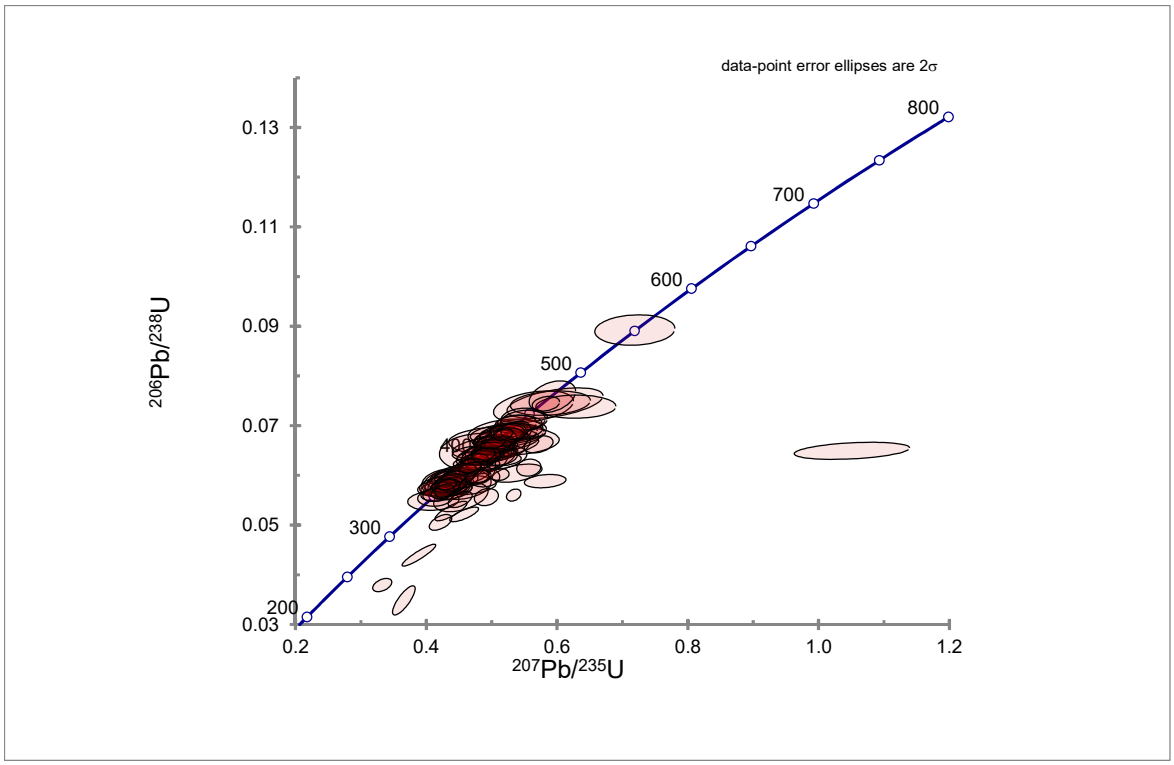


Fig. 24. Concordia diagram of analyses in detrital rock *in-situ* sample 15JT10 on a 800-200 Ma scale.

Sample 15JT11

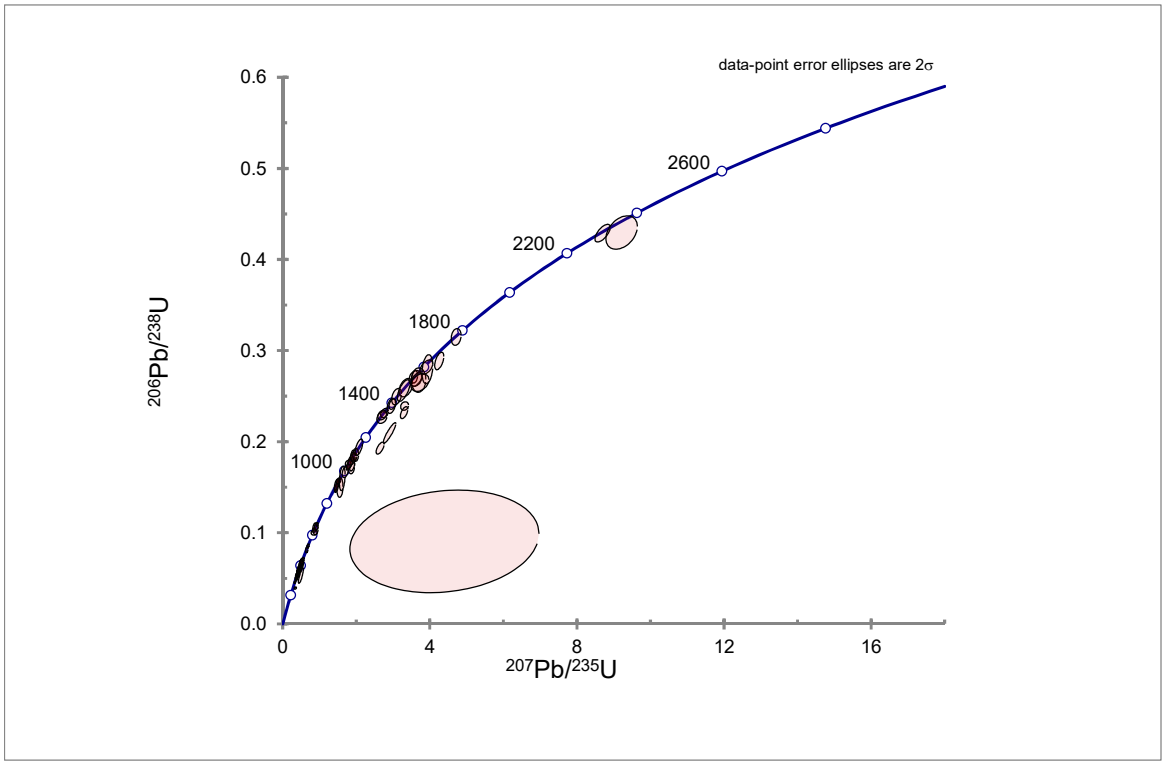


Fig. 25. Concordia diagram of all analyses in detrital rock *in-situ* sample 15JT11. The scale is 0 to 3000 Ma.

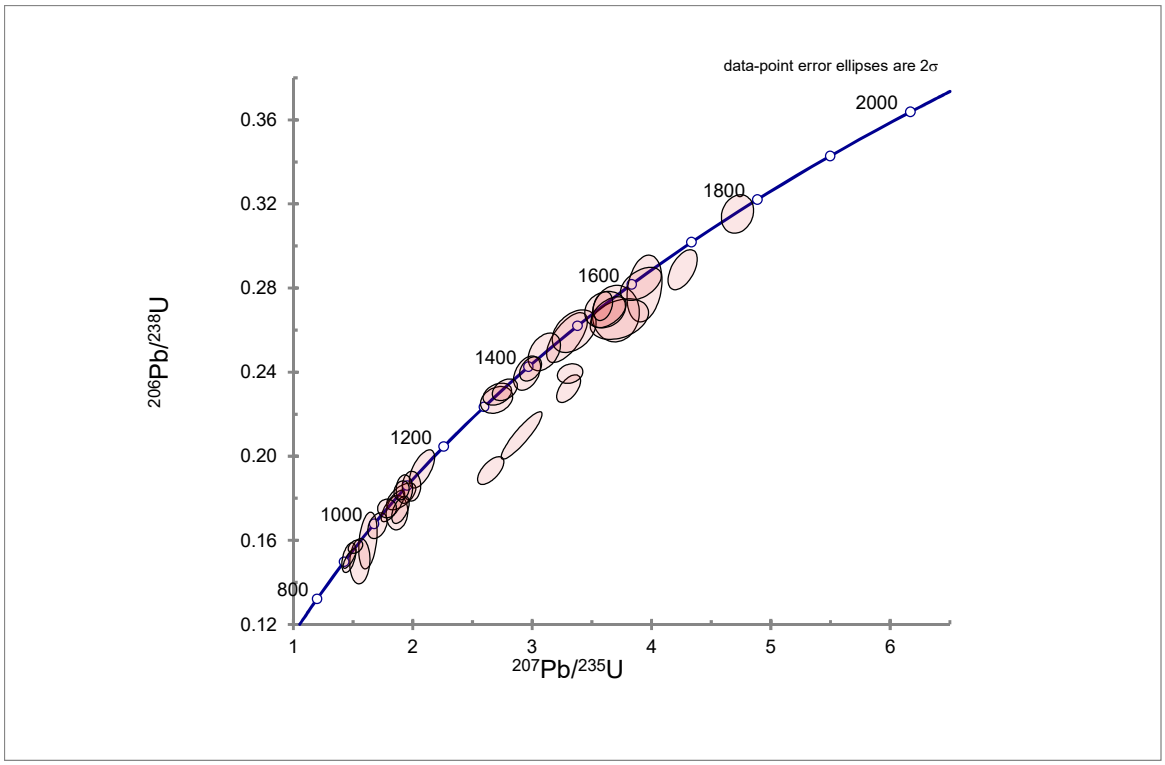


Fig. 26. Concordia diagram of analyses in detrital rock *in-situ* sample 15JT11 on a 2.0-0.8 Ga scale.

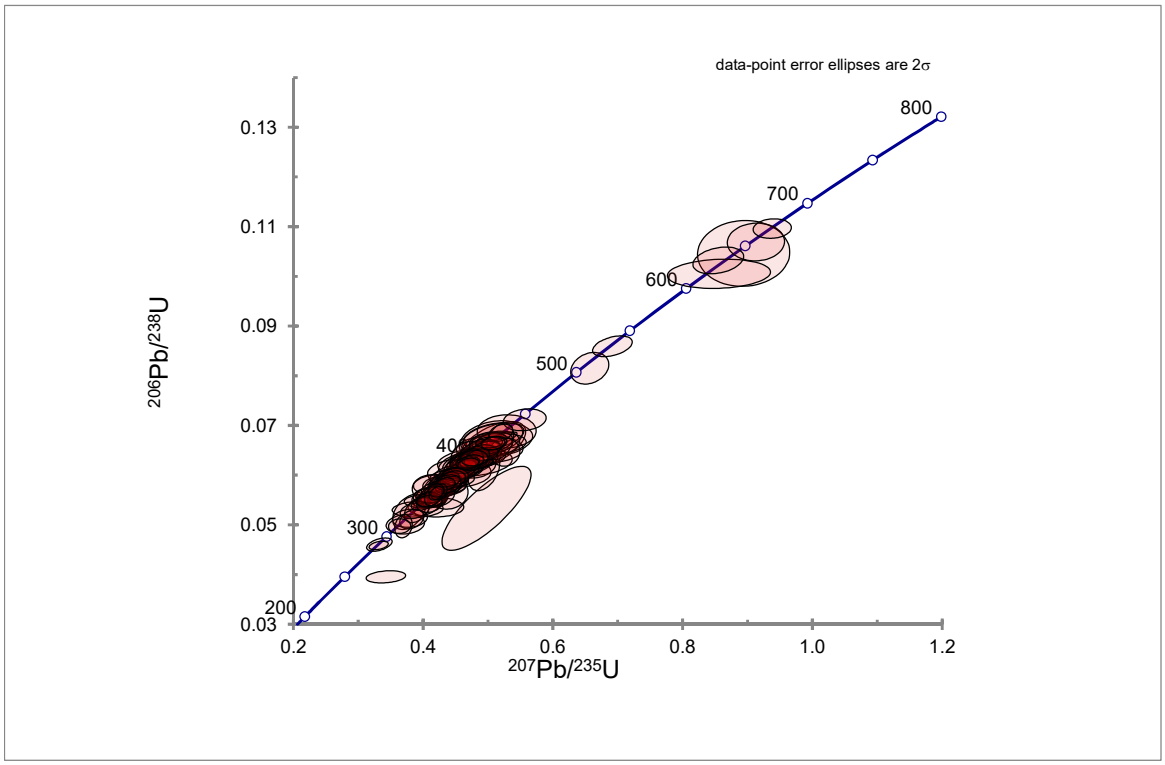


Fig. 27. Concordia diagram of analyses in detrital rock *in-situ* sample 15JT11 on a 800-200 Ma scale.

APPENDIX C - Calculated sample ages

	Accepted analyses	MDA (Ma) ±2σ	No. Peaks	Min. age grain (Ma) ±2σ	Max. age grain (Ma) ±2σ	Age peaks (Ma) ±2σ	No. Analyses
15JT10	110/150	364.9 ± 2.1	1	345 ± 10	2706 ± 56	399.4 ± 3.1	n=18
15JT11	129/149	289.7 ±3.7	1	289.4 ± 4.4	2404 ± 42	400.1 ± 2.5	n=18
16JT11	104/150		3	310 ± 21	2684 ± 31	404.7 ± 61	n=9
						938 ± 9.9	n=11
						1620 ± 23	n=18
16JT24	52/71		3	317.7 ± 9.6	1924 ± 31	398 ± 5.6	n=6
						1016 ± 17	n=9
						1662 ± 14	n=5
16JT27	109/150		2	95 ± 4.9	2539 ± 40	100.4 ± 2.7	n=5
						390.7 ± 3.5	n=18